THE ~~NEW METHOD OF~~ COMPUTATION OF RADIATION HEAT TRANSFER. ~~IN COMBUSTION CHAMBERS~~

by

NIPULKUMAR G. SHAH

BSc ARCS

Thesis submitted for the degree of

Doctor of Philosophy

in the Faculty of Engineering of the

University of London.

1979

Department of Mechanical Engineering,

Imperial College of Science and Technology,

London. SW7 2BX

Dedicated to my late father

ACKNOWLEDGEMENTS

Firstly I would sincerely like to thank Dr. F.C. Lockwood for his excellent supervision throughout the various stages of the development of this project. His experience of the practical difficulties involved with using various types of methods in everyday usage and industry has been especially helpful. Further I would like to thank Dr. J. Gibb of the C.E.G.B. for taking a keen interest as well as providing some very valuable analytic and Monte Carlo solutions. I would also like to thank Dr. D. Lucas and Dr. T. Collins of the British Gas Corporation for their interest and useful criticisms of the work.

I would also like to thank the British Gas Corporation for providing me with the financial support for 3½ years.

Finally I would like to thank Miss C. Maxwell for typing this thesis and our papers, Miss M. Smith for doing the corrections and Mrs. J. Hill for tracing the figures.

ABSTRACT

A six flux method first proposed by De Marco and Lockwood (1974) has been improved by varying the surfaces of integration. Some simple recommendations for improving the predictions for the cartesian and cylindrical co-ordinate systems are proposed after examining one-dimensional test cases. Further investigation of the flux method revealed a shortcoming, which affects all other flux methods as well, and this is thoroughly explored.

A completely new and exact method to solve the transport equation has been proposed. It has several marked advantages over other methods which make it especially useful in practical applications. It is tested against the results of a large number of standard solutions which are available in the literature for cartesian and cylindrical geometries. The method has been extended to include scattering and non-gray systems.

List of Contents

			Page
NOMENCLATURE			1
CHAPTER 1	Introduction		6
1.1	Preamble		6
1.2	Basic definitions and Equations		6
	1.2.1	The Transport Equation	7
	1.2.2	The Net Radiative Heat Flux	8
	1.2.3	Boundary Conditions	9
	1.2.4	The Energy Conservation Equation	10
1.3	Existing Methods for the Calculation of Radiation Transfer		11
	1.3.1	Analytical Approaches	11
	1.3.2	The Electric Circuit Analogy	12
	1.3.3	The Monte-Carlo Method	12
	1.3.4	The Zone Method	12
	1.3.5	Flux Methods or Differential Approximations	13
CHAPTER 2	Consideration of the Value of Analytical Treatments		17
2.1	Value of Analytic Solutions		17
2.2	Some Analytic Solutions		17
	2.2.1	One-Dimensional Cartesian Geometry with Specified Constant Interior Source	18
	2.2.2	One-Dimensional Cartesian Geometry with Constant Interior Temperature	20
	2.2.3	Two-Dimensional Cartesian Geometry; in the Form of a Rectangle, Cold Black Walls with Constant Interior Temperature	22

Page

2.2.4 Some useful Sources for Zone and Monte Carlo Solutions 23

CHAPTER 3. The Present Flux Method in Cartesian Co-Ordinates 25

3.1 Formuation 25

3.1.1 Choice of Series 25

3.1.2 The Surfaces of Integration 26

3.1.3 Derivation of the Flux Equations 28

3.1.4 Heat Flux and Energy Conservation Equations 31

3.1.5 Boundary Conditions 32

3.2 One-Dimensional Cartesian Validation Studies and some Recommendations for the Parameters 33

3.2.1 One-Dimensional Optically Thick Solution 33

3.2.2 One-Dimensional Optically Thin Solution 36

3.2.3 One-Dimensional Test Case with Constant Interior Source 37

3.2.4 One-Dimensional Cartesian Test Case with Constant Interior Temperature 44

3.2.5 Two-Dimensional Cartesian Test Case with Constant Interior Temperature 48

CHAPTER 4. The Present Flux Model in Cylindrical Coordinates 50

4.1 Formulation 50

4.1.1 Transformation of Radiative Transport Equation to Cylindrical Coordinates 51

4.1.2 Derivation of the Flux Equations 53

4.1.3 Boundary Conditions 54

4.1.4 Relation Between Sources and Temperatures 58

4.2 Validation Studies in Cylindrical Coordinates 59

4.2.1 One-Dimensional Solution for an Infinite Cylinder with Black Walls and Constant Source Inside 59

Page

4.2.2 One-Dimensional Solutions for an Infinitely Long Set of Co-Axial Cylinders with Constant Source Inside 62

CHAPTER 5. A Principal Failing of the Flux Model and Suggested Remedies 67

5.1 The Relation of the Integration Surface Parameters to Other Quantities 67

5.1.1 The Relation Between the Surface Integration Parameters and Mean Free Path Lengths 67

5.1.2 The Relations of the Integration Surface Parameters and the Intensity Distribution 70

5.2 A Principle Failing and a Suggested Remedy 75

5.2.1 A Principle Failing 75

5.2.2 The Boundary Layer Remedy 79

5.2.3 Application of Boundary Layer Remedy 80

CHAPTER 6. A New Discrete Transfer Method for the Calculation of Radiative Transfer 86

6.1 Description of the Basic Method 86

6.1.1 Limitations of Other Methods 86

6.1.2 Some Terminology 87

6.1.3 Basic Features of the Discrete Transfer Method 88

6.1.4 Boundary Conditions and Evaluation of the Fluxes 90

6.1.5 Recovering the Sources 91

6.2 The Computer Code and Advantages of the Method 94

6.2.1 Storage Organisation 94

6.2.2 The Computation Procedure 94

6.2.3 Principal Advantages of the Discrete Transfer Method 97

Page

CHAPTER 7 Validation of the Discrete Transfer (DT) Method 98

7.1 Cartesian Geometries 98

7.1.1 One-Dimensional Cartesian with Prescribed Temperatures 98

7.1.2 One-Dimensional Cartesian Geometry with Sources Prescribed 98

7.1.3 Two-Dimensional Cartesian Geometry with Temperatures Prescribed 105

7.1.4 Three-Dimensional Cartesian Geometry with Temperatures Prescribed 110

7.1.5 Three-Dimensional Cartesian Geometry with Sources Prescribed 115

7.2 Axi-Symmetric Geometries 126

7.2.1 An Infinite Cylinder with Prescribed Temperatures 126

7.2.2 An Infinite Cylinder with Uniform Heat Generation Inside 126

7.2.3 Two Infinitely Long Co-Axial Cylinders Sandwiching Gas at Prescribed Temperatures 129

7.2.4 Two Infinitely Long Co-Axial Cylinders with Prescribed Uniform Heat Generation 132

7.2.5 Finite Cylinders 132

7.2.6 Finite Cylinder with Varying Temperatures and Absorption Coefficient 138

7.3 Application to Determination of View Factors 145

7.3.1 Usage 145

		Page
CHAPTER 8	Scattering and Non-Gray Systems	146
8.1	Inclusion of Scattering in the Discrete Transfer Method	146
	8.1.1 Basic Equations	146
	8.1.2 Validation for One-Dimensional Parallel Plate Case	148
8.2	Calculation of Radiative Transfer in an Isotropically Scattering Medium with Gas and Particles at Different Temperatures	151
8.3	Method of Solution for Non-Gray Problems	152
CHAPTER 9	Conclusions and Future Recommendations	156
9.1	Conclusions	156
9.2	Future Recommendations	158
APPENDIX A2.1	Analytic solution of rectangular enclosure with cold black walls	160
APPENDIX A3.1	Integration over the surface surrounding the positive x axis	164
APPENDIX A3.2	The one-dimensional optically thick solution	167
APPENDIX A3.3	The one-dimensional optically thin solution	170
APPENDIX A3.4	Solution of flux equations in one dimension with prescribed constant source	172
APPENDIX A4.1	Solution of the present model for an infinitely long cylinder with black walls and a constant heat source inside	174
APPENDIX A4.2	Solution by the present model for infinitely long pair of co-axial cylinders with constant internal source	177

Page

APPENDIX A5.1 Derivation of new boundary conditions for black walls with interior temperatures prescribed 180

APPENDIX A5.2 One-dimensional solution for constant temperature gas using boundary layers 183

APPENDIX A5.3 Derivation of new boundary conditions for black walls with internal sources prescribed 185

REFERENCES 187

NOMENCLATURE

Symbol	Description	Equation of First Appearance
A	constant of integration	2.2.11
A_1, A_2, A_3	coefficients of the Taylor's series expansion for the intensity distribution	3.1.1
a	length of rectangular enclosure	2.2.20
B_1, B_2, B_3	coefficients of the Taylor's series expansion for the intensity distribution	3.1.1
b	width of a rectangular enclosure	2.2.20
$b(\underline{\Omega}' \cdot \underline{\Omega})$	as defined by	8.1.3
C_1	as defined by	3.1.10
C_2	as defined by	3.1.11
C_3	as defined by	3.1.12
D_0, D_1	terms of a Taylor's series expansion	3.2.14
d	followed by another symbol, is the usual elemental increase of another symbol used in calculus	1.2.1
$d\Omega$	$\sin\theta \, d\theta \, d\phi$	A3.1.4
E_n	as defined by	1.3.2
I	intensity	1.2.1
I_+	intensity going out in the positive direction	1.2.3
I_-	intensity going out in the negative direction	1.2.3
I_n	intensity on entry to the n^{th} cell	6.1.2

Symbol	Description	Equation of First Appearance
I_r	intensity before the ray impinges the wall	6.2.1
I_1	as defined by	2.2.18
I_2	as defined by	2.2.19
I_0	intensity leaving the wall	6.1.4
i,j,k	unit normals in cartesian coordinate directions	3.1.23
J_0, K_0, Ki_2	standard Bessel functions	2.2.20
K, K_g	absorption coefficient of gas	1.2.1
K_S	scattering coefficient	8.1.2
L	distance between two walls	2.2.1
L'	dimensionless distance between two walls	
L(z)	as defined near	2.2.20
ℓ,m,n	direction cosines	
$N_\theta N_\phi$	number of subdivisions of θ and ϕ	
$\hat{n}$	unit normal to a surface	1.2.2
P	point under consideration, near	3.1.1
$P(\underline{\Omega}.\underline{\Omega}')$	probability function for scattering	8.1.2
Q	as defined by eq. 2.2.3	2.2.1
Q*	as defined by	3.2.20
Q**	as defined by	3.2.22
Q_S	as defined by eq. 2.2.24	2.2.1
Q_S^*	as defined by	3.2.24
q	net flux	1.2.2

Symbol	Description	Equation of First Appearance
q_+	positive flux	1.2.3
	(flux through 2π solid angle around $\hat{n}$)	1.2.3
q_-	negative flux	1.2.4
	(flux through 2π solid angle around $-\hat{n}$)	1.2.4
R	outer radius	Fig. 7.18
r,θ,z	polar coordinates	4.1.3
r',θ',z'	direction cosines	4.1.8
r'',θ'',z''	surfaces of integration	4.2.4
r_Q,θ_Q,z_Q	as defined by	4.1.30
		4.1.33
		4.1.3
r_1	inner radius	4.2.5
r_2	outer radius	4.2.5
S	source (heat generation per unit volume)	1.2.7
S_n	source in the n^{th} cell	6.1.6
S_T	total source	8.1.1
s	distance	1.2.1
s'	distance defined by eq. 8.1.4	8.1.1
T	temperature	1.2.1
T_c	temperature at the centre	4.2.4
T_g	temperature of gas	2.2.11
$T_{g,i}$	temperature of gas in the i^{th} cell	6.1.8
T_W	temperature of wall	1.2.6
T_0	temperature of gas near a wall	3.2.17
T_1,T_2	temperature of walls 1 and 2	2.2.2
u	as defined in A2.1.8	2.2.20

Symbol	Description	Equation of Appearance
u_0	as defined in A2.1.8	2.2.20
X,x	distance from wall 1	1.3.1
X',Y',Z'	direction cosines as shown in fig. 3.1	3.1.1
X",Y",Z"	as shown in fig. 3.2	3.1.4,3.1.5 3.1.6
X_n	stretched dimensionless distance	3.2.13
X_Q	as defined by	3.1.27
x,y,z	distance along cartesian co-ordinate axis	3.1.2
x_n	small distance from a wall	3.2.13
x_w	point on the wall	3.2.13

Greek Symbols

α	as defined by	3.2.9
γ	an arbitrary constant	5.1.1
δ	optically thin distance	5.2.1
$\varepsilon,\varepsilon_W$	emissivity of wall	1.2.6
$\varepsilon_1,\varepsilon_2$	emissivity at walls 1 and 2	2.2.1
θ,ϕ	azimuthal angles	6.2.1
$\theta,\hat{\theta},\theta',\theta'',\theta_Q$	see r	
θ^*	as defined by	3.2.25
θ_S^*	as defined by	3.2.26
$\theta(KX)$	as defined in 2.2.5	2.2.2.
$\theta_S(KX)$	as defined in 2.2.6	2.2.2

Symbol	Description	Equation of First Appearance
σ	Stefan Boltzmann constant	1.2.1
τ	optical distance	2.2.16
τ_0	optical diameter	4.2.4
ϕ	dimensionless ratio - also see	4.2.5
$\Omega, \underline{\Omega}$	solid angle	1.2.2
ω	defined by	3.1.5

Subscripts

g	refers to the properties of gas
p	refers to the properties of the particle
W_1, W_2	refers to property at walls 1 and 2 respectively
3,4,5,6	properties at walls 3,4,5,6 respectively

CHAPTER 1

INTRODUCTION

1.1 Preamble

Recent market trends in the economics of the world's fuels have increased the demand for accurate, reliable and general combustion chamber prediction models. Now while there have been significant advances in the development of predicticn procedures for the flow and chemical reaction (see Abou-Ellail et al (1978) for example), the development of prediction methods for the thermal radiation has lagged behind.

The scale of the flow problem may be measured in terms of the number of partial differential equations which have to be solved namely: three momentum equations; at least three turbulence equations; one equation for a mixing parameter; at least one species equation; one equation for energy conservation; and yet additional equations for the carbon particles if the fuel is oil or pulverized coal. All this is before radiation is even considered. For these 12 plus variables a very coarse finite difference grid subdivision of the combustion chamber of say 10 x 10 x 10 grid nodes results in a storage requirement in excess of 12 K. It is evident that forthe thermal radiation we require a model which makes low demands on storage, is computationally economic and possesses reasonable accuracy.

The treatment of thermal radiation as distinct from the flow, in an enclosure is complicated by the fact that the radiation passing a given point originates at points throughout the gas (Hottel and Sarofim, (1967), Deissler (1964)). According to Maxwell's classical electromagnetic theory, radiant energy travels in the form of electromagnetic waves;

however according to Plank's hypothesis it travels in the form of discrete photons(Ozisik, (1973)). While neither of these separate concepts fits all the physical facts, each has its merits (Sparrow and Cess, (1966)). The analysis of thermal radiation is further complicated because "the usual exact formulation of the radiation interchange in an enclosure containing an absorbing-emitting non-isothermal gas by the use of integral equations becomes so complex, even after such simplifying assumptions as gray gases and gray surfaces, that a solution becomes prohibitively tedious" (Prelmutter and Howell (1964B)).

1.2 Basic Definitions and Equations

1.2.1 The Transport Equation

This thesis is throughout confined to a gray gas in non-scattering system-excepting Chapter 8 where a method is described for removing these restrictions. As a ray traverses an absorbing medium, the energy of the ray is both diminished by absorption and augmented by emission. The fundamental quantity which usually forms the basis in radiative transfer studies is the intensity, defined as the amount of radiant energy transmitted by the ray in any given direction per unit area normal to the ray, per unit solid angle per unit time. It is usually denoted by the symbol I (see Chandrasekhar (1960) for example).

For a ray travelling distance ds through a medium at temperature T and of absorption coefficient K, the change in the intensity dI, assuming Kirchoff's Law holds, is given by (Ozisik (1973), for example)

$$\frac{dI}{ds} = - KI + \frac{K\sigma T^4}{\pi} \tag{1.2.1}$$

where σ is the Stefan-Boltzmann constant. The first term on the right hand side is the absorption term and the second is the emission one.

The above equation often appears in the literature using the del notation (Richter (1974) for example); but this practice can be misleading because the del operator in these works is assigned a special ~~meaning~~ use as opposed to the standard del notation found in mathematics. (see Section 4.1.1).

1.2.2 The Net Radiative Heat Flux

The net radiative heat flux $\underline{q}$ is defined by

$$\underline{q} = \int_{4\pi} I(\underline{\Omega}.\underline{\hat{n}})\, d\Omega \qquad (1.2.2)$$

where intensity I is in the direction $\underline{\Omega}$ and $\hat{n}$ is the unit normal to the surface (see fig. 1.1). The integration is over the whole solid angle 4π and determines the net flow of radiative energy normal to the surface per unit time and per unit area.

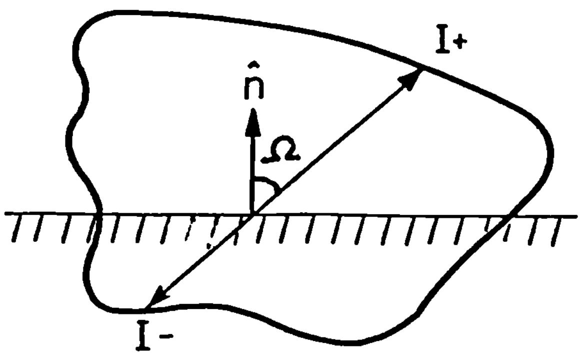

Fig. 1.1 Intensity in direction Ω at a wall with normal $\hat{n}$

Similarly, the quantities q_+ and q_- may be defined as follows:

$$q_+ = \int_{2\pi} I_+(\underline{\Omega}.\underline{\hat{n}})\, d\Omega \qquad (1.2.3)$$

$$q_- = \int_{2\pi} I_-(\underline{\Omega}.\underline{\hat{n}})d\Omega \qquad (1.2.4)$$

where I, $\underline{\Omega}$ and $\underline{\hat{n}}$ are as before. The integration in the case of q_+ is over the hemisphere which accounts for all the rays leaving the surface (I_+). Similarly the integration in the case of q_- is over the hemisphere which accounts for all the rays incident on the surface (I_-). The sign convention used here is the same as that used by Ozisik (1973) in his eqns. (1.132) to (1.133b). Subtracting eq. (1.2.4) from eq. (1.2.3) gives:

$$q = q_+ - q_- \qquad (1.2.5)$$

1.2.3 Boundary Conditions

It is possible to derive boundary conditions for a quite general wall, but for validation purposes, we deal with gray lambert surfaces only. A gray lambert surface is here defined as a surface that emits an intensity distribution sufficiently near to independence of angle of emission, so as to make the cosine-law assumption an acceptable simplification. (Hottel and Sarofim, (1967)). Some of the flux arriving at the wall is reflected back into the chamber and this is augmented by the emission due to the temperature of the wall. Equating the wall fluxes gives:

$$q_+ = (1-\varepsilon)q_- + \sigma\varepsilon T_W^4 \qquad (1.2.6)$$

where q_+ and q_- are defined in section 1.2.2 and ε and T_W are the emissivity and the temperature of the wall respectively. The wall is assumed to be opaque; that is the transmitted component is assumed to be zero. This relationship is commonly found in the literature (see Heaslet and Warming, (1964) for example).

1.2.4 The Energy Conservation Equation

Usually in a complete prediction procedure for combustion chambers, the temperatures are prescribed and we need to calculate the sources due to radiative transfer. For theoretical purposes the reverse is more convenient.

Defining the source S as the amount of heat generation per unit volume and for a system in thermal equilibrium in the absence of conduction and convection effects, the total amount of heat generation inside an enclosure must be equal to the total amount of heat radiated through the walls, that is:

$$\nabla \underline{q} = S \tag{1.2.7}$$

The flux $\underline{q}$ is defined by eq. (1.2.2). Using the definition of divergence, eq. (1.2.7) can be rewritten as

$$\int_{\text{enclosure}} \underline{q}\,d\underline{A} = \int_{\text{volume}} S\,dv \tag{1.2.8}$$

Thus in theory we can now calculate the heat fluxes through the walls and the sources or sinks (negative sources) inside the chamber if temperatures are prescribed (or vice versa).

Sometimes intensity distributions may also be of interest although most researchers seem to ignore them once the relevant equations are derived. However, some very useful insight into the problem has been gained by looking at intensity distrbutions as we shall see in Chapter 5.

1.3 Existing Methods for the Calculation of Radiation Transfer

1.3.1 Analytical Approaches

In order to solve for the heat fluxes with temperatures prescribed, it is usual to proceed in the following manner. The transport equation (eq. 1.2.1) is first integrated along each ray, giving an integral involving temperatures and exponentials (described in more detail in section 6.1). After substituting the boundary conditions, the intensity is further integrated weighted with the direction cosines over a whole solid angle 4π in order to obtain the fluxes (see Chandrasekhar, (1960) for example). This leads to rather complicated Bessel functions and integrals (see section 2.2.3).

On the other hand if sources are prescribed, the transport equation for one dimensional case integrates to (see Goulard and Goulard, 1960 for example):

$$\sigma T^4(Kx) = \frac{q+W1}{2} E_2(Kx) + \frac{q-W2}{2} E_2(KL-Kx) + \frac{S}{4K}$$

$$+ \frac{1}{2} \int_0^{KL} \sigma T^4(Ky) E_1(|Kx-Ky|)\ d(Ky) \qquad (1.3.1)$$

where

$$E_n(x) = \int_0^1 e^{\left(-\frac{x}{\mu}\right)} \mu^{n-2}\ d\mu \qquad (1.3.2)$$

This expression leads to rather complex integrals. Some of these are tabulated in (Chandrasekhar and Elbert (1952)). The complexity of these equations can be appreciated by studying the one-dimensional solutions of Heaslet and Warming (1964). Further analytical work has also been carried out by Viskanta (1966) and Kourganoff (1963) and others.

1.3.2 The Electric Circuit Analogy

The transport equation integrated over 4π solid angle can be rephrased in a form that suggests an analogy with an electric circuit composed of resistances, voltage sources and current sources. This was first discussed by Oppenheim (1956). Further details can be found in various texts (see Sparrow and Cess (1966) for example). The electric analogue is not widely used these days.

1.3.3 The Monte Carlo Method

This is a statistical approach based on random number generator facility of the computer. Representative rays, typically no more than 9 for economic reasons, are fired in random directions. The required quantities are then evaluated as each ray crosses the enclosure. By taking enough rays any degree of accuracy is achievable, but systematic errors can occur as existing tests to determine the randomness of the generated numbers are not always sufficient. Prelmutter and Howell (1964A,B) have used this method extensively.

1.3.4 The Zone Method

In the Zone Method, the walls and the interior of the enclosure are divided into zones (surfaces and volumes) of finite size. 'Direct exchange areas' also, referred to as view factors, are defined which are a measure of the exchange occurring between zone pairs when no reflections occur. For simple geometries these values have been tabulated

(Hottel and Sarofim (1967) for example). The exchange between each zone pair is then calculated using the integrated form of the transport equation (eq. 1.2.1). In general, the procedure results in n simultaneous equations for each zone where n is the total number of zones, and leads to a simultaneous system with a $n^2 \times n^2$ matrix. All the view factors between each pair of zones have to be stored along with this large matrix. Provided the zone size is fine enough this numerical method is probably capable of the better accuracy than the Monte Carlo procedure, simply because one can never be sure of the accuracy of the random number generator. The Zone Method has nonetheless some serious drawbacks, for example the fact that view factors for some awkward geometries are not readily available,or the frequent need for uneconomically fine grids, and these have been studied by many researchers (Drake and Eckert (1959) for example). Another principle drawback is the size of the matrix that needs to be solved. Various special methods and "short cuts" to reduce the size for particular cases have been developed, but for general applications, this method proves expensive in terms of computational economy, with perhaps a few isolated exceptions. Nevertheless it is a useful method to compute solutions for test case geometries in order to validate new methods.

1.3.5 Flux Methods or Differential Approximations

Flux methods are also known as differential approximations. The basic idea behind most flux methods is to separate the directional dependence from the spacial dependence of the intenstiy. Hence the integro-differential equation reduces to a system of differential equations. Although the mathematics may appear to be rather different, broadly all flux methods can be classed under two categories: the continuous and the discontinuous types.

Examples of the continuous type include spherical harmonics, momentum etc. see Fig. (1.2).

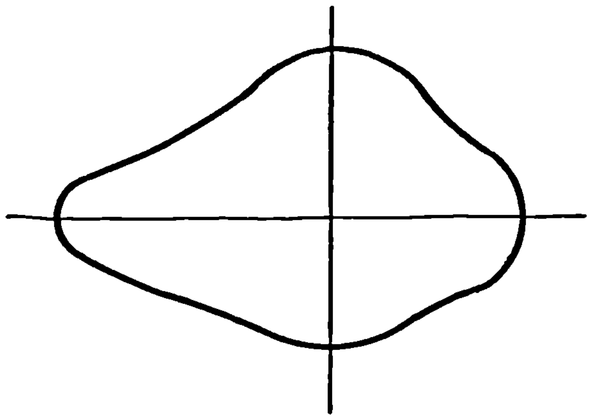

Fig. 1.2 Typical intensity distribution solution of a continuous type flux method

Perhaps one of the simplest continuous approximations is the 'diffusion' or the 'Rosseland' (1936) approximation. Here the intensity distribution is assumed to be isotropic. This approximation gives good results for optically thick limits and has become one of the standard tests for any model. The optically thick result for flux obtained by this method is

$$q = - \frac{4}{3K} \frac{d(\sigma T^4)}{dx} \tag{1.3.3}$$

where x is measured from a boundary wall.

The Rosseland approximation has been modified in many different ways (see Deissler, (1964) for example). If the transfer equation is considered in the integrated form Eq.(1.3.1), then the kernals that appear under the integrations may be expressed as a series of exponentials. This method is known as the exponential kernal approximation (Krook (1955). A similar approach, but where the series is approximated by spherical harmoinc kernals, is known as the spherical harmonics method (see Siddall, (1974) for example). In general one can assume any series expansion for the intensity in various kernals and then multiply the transport equation by each kernal and integrate to yield a set of first order interconnected differential equations. Such formulations are known as the moment methods (Chandrasekhar, (1960) for example). Some modifications to this approach are reported by Olfe (1967) all of which can still be classed as continuous flux methods.

Examples of discontinuous methods include the 2, 4 and 6 flux methods of the Spalding (1972) and Gosman and Lockwood (1973), type discrete ordinate models etc. see fig. 1.3.

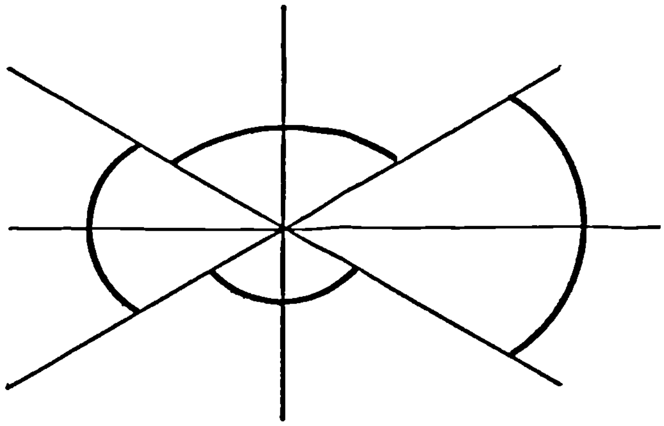

Fig. 1.3 Typical intensity distribution solution of a discontinuous type flux method

The Eddington approximation (1960) is perhaps one of the earliest of these type. The Schuster (1905) and Schwarzchild (1906) approximations are also along similar lines. Gosman and Lockwood (1973) have also developed models based on the assumption of uniform intensity value within equal discrete solid angles. Richter (1974) has gone a step further by allowing the solid angles to vary. In the discrete ordinate method used by Truelove (1976) in addition to uniform intensities in certain solid angles, weighted intensities are summed when the fluxes and sources in the chamber are calculated.

Both the continuous and the discontinuous flux models finally yield a set of first order differential equations (hence the term differential approximations). In principal the number of equations equals the number of terms retained in the series expansion or the number of fluxes considered. For some methods this can be easily reduced to a lower number of higher order differential equations. The more the number of equations, the more are the number of coefficients to be stored per node. In other words we have in general a three-dimensional matrix to store for each coefficient. A model where we only need to store half the coefficients through the solution of second order, rather than first order, differential equations has obvious merit. Although still higher order differential equations would reduce the storage problems, the actual solution procedures are more cumbersome in practice.

It is worthy of note that certain expansions will 'fit' certain situations better simply because of the nature of solution. Hence methods that work in certain co-ordinate systems may not necessarily perform equally well in other systems.

CHAPTER 2

CONSIDERATION OF THE VALUE OF ANALYTICAL TREATMENTS

2.1 Value of Analytic Solutions

When new general, usually numerical, models are created they have to be systematically tested. Usually a few very simple cases are studied even though most models with reasonable assumptions are bound to work, say, for the one-dimensional cartesian case with constant source. Conclusions are then made regarding other co-ordinate systems and more dimensions. However what works for a one-dimensional cartesian geometry will not necessarily work for the cylindrical transformation or indeed even a two-dimensional cartesian geometry. Now even one-dimensional validation can be further subdivided into two groups, namely, one with the sources specified and the other with temperatures specified. Therefore the range of test cases that may have to be studied is potentially enormous.

A thorough study would entail calculating for each possible permutation, a 'Zone' solution and then comparing with the solution obtained from the test model. But this often proves tedious and expensive of computer time and the accuracy sought by a particular analyst may not be of the same importance as that of the user. For instance, for a particular method the temperature predictions may be bad, but flux predictions may be excellent. Hence for some specific users, this method may be ideal whilst those interested in temperatures only, may not find the method so useful.

An attempt has been made in the following section to collect together useful analytic solutions. Some of these are readily available while some may be new. Also, in section 2.2.4, some useful sources of Zone and Monte Carlo solutions are mentioned. Further analytic solutions are also presented in Chapter 7.

2.2 Some Analytic Solutions

2.2.1 One-Dimensional Cartesian Geometry with Specified Constant Interior Source

This is probably one of the most well documented cases. Much credit must be given to Heaslet and Warming (1964) since, although there had been a considerable quantity of related and previous analytical work, these authors have managed to avoid the need for awkward tabulated functions.

Consider two infinitely long parallel walls 1 and 2 at temperatures T_1 and T_2 with emissivities ε_1 and ε_2 respectively. The walls are distance L apart and having a constant source S per unit volume and a constant absorption coefficient K inside. Then the flux at wall 1 is given by the following expression, Heaslet and Warming (1964), eq. 18)

$$q_{W1} = \frac{(\sigma T_{W1}^4 - \sigma T_{W2}^4)Q - \frac{S}{K}[Q_S + KL(\frac{1}{\varepsilon_2} - 1)Q]}{1 + (\frac{1}{\varepsilon_1} + \frac{1}{\varepsilon_2} - 2)Q} \qquad (2.2.1)$$

and the temperature at any point distance x from wall 1 is given by (Heaslet and Warming (1964), eq. 17),

$$\sigma T_1^4 - \sigma T_2^4 = \frac{(\sigma T_1^4 - \sigma T_2^4)[\theta(KX) + (\frac{1}{\varepsilon_2} - 1)Q]}{1 + (\frac{1}{\varepsilon_1} + \frac{1}{\varepsilon_2} - 2)Q} + \frac{S}{K}\{\theta_S(KX) +$$

$$\frac{[Q_S(\frac{1}{\varepsilon_1} + \frac{1}{\varepsilon_2} - 2) - (\frac{1}{\varepsilon_2} - 1)KL]\,\theta(KX) + (\frac{1}{\varepsilon_2} - 1)(KL - Q_S) + KL(\frac{1}{\varepsilon_1} - 1)(\frac{1}{\varepsilon_2} - 1)Q\}}{1 + (\frac{1}{\varepsilon_1} + \frac{1}{\varepsilon_2} - 2)Q} \qquad (2.2.2)$$

where
$$Q = 1-2\int_0^{KL} \theta(Kx)E_2(Kx)d(Kx) \tag{2.2.3}$$

$$Q_S = 2\int_0^{KL} \theta_S(Kx)E_2(Kx)d(Kx) \tag{2.2.4}$$

$$\theta(Kx) = \frac{1}{2}E_2(Kx) + \frac{1}{2}\int_0^{KL} \theta(Ky)E_1(Kx-Ky)d(Ky) \tag{2.2.5}$$

$$\theta_S(Kx) = \frac{1}{4} + \frac{1}{2}\int_0^{KL} \theta_S(Ky)E_1(|Kx-Ky|)d(Ky) \tag{2.2.6}$$

and
$$E_n(x) = \int_0^1 \exp(-\frac{x}{\mu})\mu^{n-2}\, d\mu \tag{2.2.7}$$

The above relations are very complicated and need theory for special X and Y functions described by Chandrasekhar and Elbert (1952) for their evaluation. However, Θ and Θ_S can be represented by two fairly simple sets of curves: Fig. 3.4 and Fig. 3.5; Q is given by the table (3.2); Q_S can be approximated to a good accuracy by:

$$Q_S = \frac{KL}{2} \tag{2.2.8}$$

and further good approximations for θ and θ_S are

$$\theta(KX) = \frac{-\frac{3}{4}(KX - KL) + \frac{1}{2}}{1 + \frac{3}{4}KL} \tag{2.2.9}$$

and

$$\theta_S(KX) = -\frac{3}{8}[(KL)^2 - K^2XL] + \frac{KL}{4} + \frac{3}{8} \tag{2.2.10}$$

. These results and graphs have been derived after much mathematical manipulation and are well presented in Heaslet and Warming (1964). (These are also presented in fig. 3.4 and fig. 3.5)

Further results and graphs for different emissivities are also presented in the same paper. These results constitute a good base for judging models, but of course this one case alone is not sufficient.

For two and three dimensional validation, and for interior sources prescribed, we have to resort to Zone solutions. Again for a thorough study, various optical thicknesses coupled with various values for wall emissivities have to be considered.

2.2.2 One-Dimensional Cartesian Geometry With Constant Interior Temperature

We have so far emphasized source prescribed problems. This is not surprising since, while detailed information about intensity at every point is relatively unimportant and impossible to store economically, fluxes are easy to compare. Therefore the transport equation (eq. 1.3.1) is more often utilised for analytic solutions. Hence it is mathematically more tempting to look for solutions for situations where the source is zero.

However, in the present flow programmes at Imperial College, temperatures are prescribed and the radiation sources have to be evaluated. This class of situations has not received enough attention by researchers of analytic solutions.

As an initial example of an analytically tractable prescribed-temperature problem, consider two infinitely long parallel black walls 1 and 2 at temperatures T_1 and T_2 respectively. The walls are distance L apart and have isothermal gas at T_g with absorption coefficient K. The transport equation eq. (1.2.1) may be integrated along the ray to yield:

$$I = \frac{\sigma T_g^4}{\pi} + Ae^{-KS} \tag{2.2.11}$$

where A is a constant of integration. Hence, for rays emerging from black wall 1 at X = 0, the intensity from eq. (2.2.11) at distance x from the wall is given by

$$I_+ = \frac{\sigma T_g^4}{\pi}(1 - e^{-\frac{Kx}{\cos\theta}}) + \frac{\sigma T_1^4}{\pi} e^{-\frac{Kx}{\cos\theta}} \tag{2.2.12}$$

where θ is the angle of the ray with the X axis. Similarly for rays emerging from the black wall 2 at x = L, the intensity as deduced from eq. (2.2.11) at distance x from the first wall is

$$I_- = \frac{\sigma T_g^4}{\pi}(1 - e^{\frac{K(L-x)}{\cos}}) + \frac{\sigma T_2^4}{\pi} e^{\frac{K(L-x)}{\cos}} \tag{2.2.13}$$

Substituting the values of intensities from eqs. (2.2.12) and (2.2.13) into the definitions for q_+ and q_- (eq. 1.2.3. and eq. 1.2.4) respectively, the following solutions may be derived,

$$q_+ = \sigma T_g^4 \left[1 - 2E_3(Kx)\right] + \sigma T_1^4 \, 2E_3(Kx) \tag{2.2.14}$$

and

$$q_- = \sigma T_g^4 \left[1 - 2E_3(Kx - KL)\right] + \sigma T_2^4 \, 2E_3(Kx-KL) \tag{2.2.15}$$

where E_3 is defined by eq. (2.2.7). Hence the flux out of wall 2 is given by

$$q_{W2} = (\sigma T_g^4 - \sigma T_1^4) \left[1 - 2E_3(KL)\right] + \sigma T_1^4 - \sigma T_2^4 \tag{2.2.16}$$

and flux out of wall 1 is

$$-q_{W1} = (\sigma T_g^4 - \sigma T_2^4) \left[1 - 2E_3(KL)\right] + \sigma T_2^4 - \sigma T_1^4 \tag{2.2.17}$$

Tables exist for E_3 hence the flux solutions for various values of optical thicknesses can be evaluated.

For situations with non black walls with emissivities ε_1 and ε_2 respectively, a similar approach is followed except that σT_1^4 is replaced by I_1, say and σT_2^4 is replaced by I_2. Then using eqs. (2.2.14) and (2.2.15) and applying the boundary condition (1.2.6), we get the following two simultaneous equations in I_1 and I_2

$$I_2 = (1-\varepsilon_1)\{\sigma T_g^4 [1 - 2E_3(KL)] + I_1 2E_3(KL)\} + \varepsilon_1 \sigma T_1^4 \qquad (2.2.18)$$

and

$$I_1 = (1 - \varepsilon_2)\{\sigma T_g^4 [1 - 2E_3(KL)] + I_2 2E_3(KL)\} + \varepsilon_2 \sigma T_2^4 \qquad (2.2.19)$$

The values of I_1 and I_2 can be evaluated . So the flux out of walls 1 and 2 is given by eq. (2.2.17) and eq. (2.2.16) with σT_1^4 and σT_2^4 replaced I_1 and I_2 respectively.

The above analysis brings to light the usefulness of the terms q_+ and q_- which in the past have been utilised only in so far as formulating the boundary conditions was concerned.

2.2.3 Two-Dimensional Cartesian Geometry; in the form of a rectangle, cold balck walls with constant interior temperature

The solution presented in this section has been provided by Gibb (1977) in a private communication. Adopting a similar approach to that of the last section, the sphere of analytical solutions can now be expanded to other geometries.

Consider a rectangular box with dimensions a by b and infinitely long in the third direction. The walls are all black and at $0^{o}K$. The enclosed gas is at a constant temperature T_g and has an absorption coefficient K. Then, from appendix (A2.1), the flux from a point distance x from the centre of wall length a is given by

$$\frac{q}{\sigma T_g^4} = \frac{2}{\pi} \int_{-\frac{Ka}{2}}^{\frac{Ka}{2}} L(|u-u_0|) - L \{[(u-u_0)^2 + K^2b^2]^{\frac{1}{2}} \}du \qquad (2.2.20)$$

where u_0 = KX and $L(Z) = K_0(Z) - K_{i_2}(Z)$. Here K_0 is the modified K Bessel function of order zero, and K_{i_2}, the twicerepeated integral of K_0. These functions are usually available on computers. Hence eq. (2.2.20) can be evaluated to a good accuracy using a simple numerical quadrature technique. An example for a square of unity opitical thickness has been presented by Lockwood and Shah (1978).

2.2.4 Some Useful Sources for Zone and Monte Carlo Solutions

The generalisation of analytical solutions beyond what has been described in this Chapter is, both mathematically and quantatively, too difficult to handle.

DeMarco and Lockwood (1974), and Lockwood and Shah (1976) have employed some three-dimensional Monte Carlo solutions provided by Gibb and Jenner (1974) for a model testing. Two further three-dimensional zone solutions are presented by Truelove (1976). Analytical solutions for two-dimensional problems with different boundary conditions are presented in Breig and Crosbie (1974).

For one-dimensional axisymmetric, cylindrical problems, Monte Carlo solutions can be found in Deissler (1964) and Prelmutter and Howell (1964). A Monte Carlo solution for an infinite cylinder has been presented by Cess (1966). For two-dimensional axisymmetric problems, a number of zone solutions are presented by Bartelds (1976). A Monte Carlo solution has also been provided by Gibb (1974) and is presented in Chapter 7. Further Zone solutions for specialised axisymmetric geometries can be found in Selcuk, Siddall and Beer (1976). While this list is not exhaustive, it forms a reasonably wide base for evaluation of radiative transfer models.

CHAPTER 3

THE PRESENT FLUX METHOD IN CARTESIAN COORDINATES

3.1 Formulation

3.1.1 Choice of Series

As for most physical problems, once the mathematical representation has been formulated, a numerical solution is derived by calculating values at given and convenient points and assuming that the intermediate values can be approximated by some simple smocth function. For scalars, one value per point is required, and for vectors, three values per point. Here the intensity has different values in different directions and these values may not necessarily be related. In general, therefore values for all discrete directions at every point need to be stored, as a consequence of this consideration some assumption about the intensity distribution has to be imposed to allow the economic solution of the transport equation. Since the intensity depends on direction, for a point p, we choose to expand the Taylor's series along the direction cosines in the following way:

$$I = A_1X' + A_2Y' + A_3Z' + B_1X'^2 + B_2Y'^2 + B_3Z'^2 \qquad (3.1.1)$$

where A_1, A_2, A_3, B_1, B_2 and B_3 are spacial coefficients independent of direction, and X', Y' and Z' are direction cosines in the i, j and k directionsrespectively (see fig. 3.1). More generally X', Y' and Z' may be replaced by ℓ, m, and n for a general orthogonal coordinate system. DeMarco (1974A) uses a similar series with a slightly different notation.

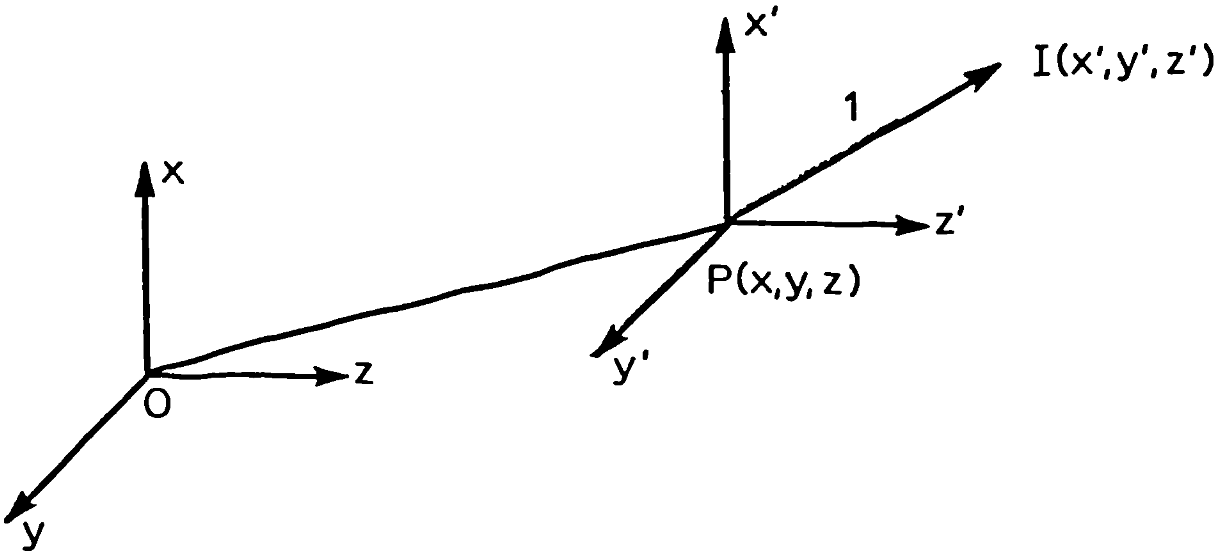

Fig. 3.1 The cartesian coordinate system

Notice that the constant term has been dropped from eq. (3.1.1). This is because the sum of squares of direction cosines equals unity, so when B_1,B_2 and B_3 are all equal we obtain the constant term. The cross terms have also been dropped to limit the number of parameters, and as will be shown later, neglecting the cross terms reduces the system from the expected six first order one to a three second order one so that only three of the six parameters need to be stored.

3.1.2 The Surfaces of Integration

Consider a sphere of unit radius with centre at point P (fig. 3.2) and a plane, passsing through a point (X", 0,0) whose normal is the positive X axis. The smaller surface of the sphere obtained by the intersection of the plane is considered for integration. The value of X" lies between 0 and +1. The corresponding surface for the negative

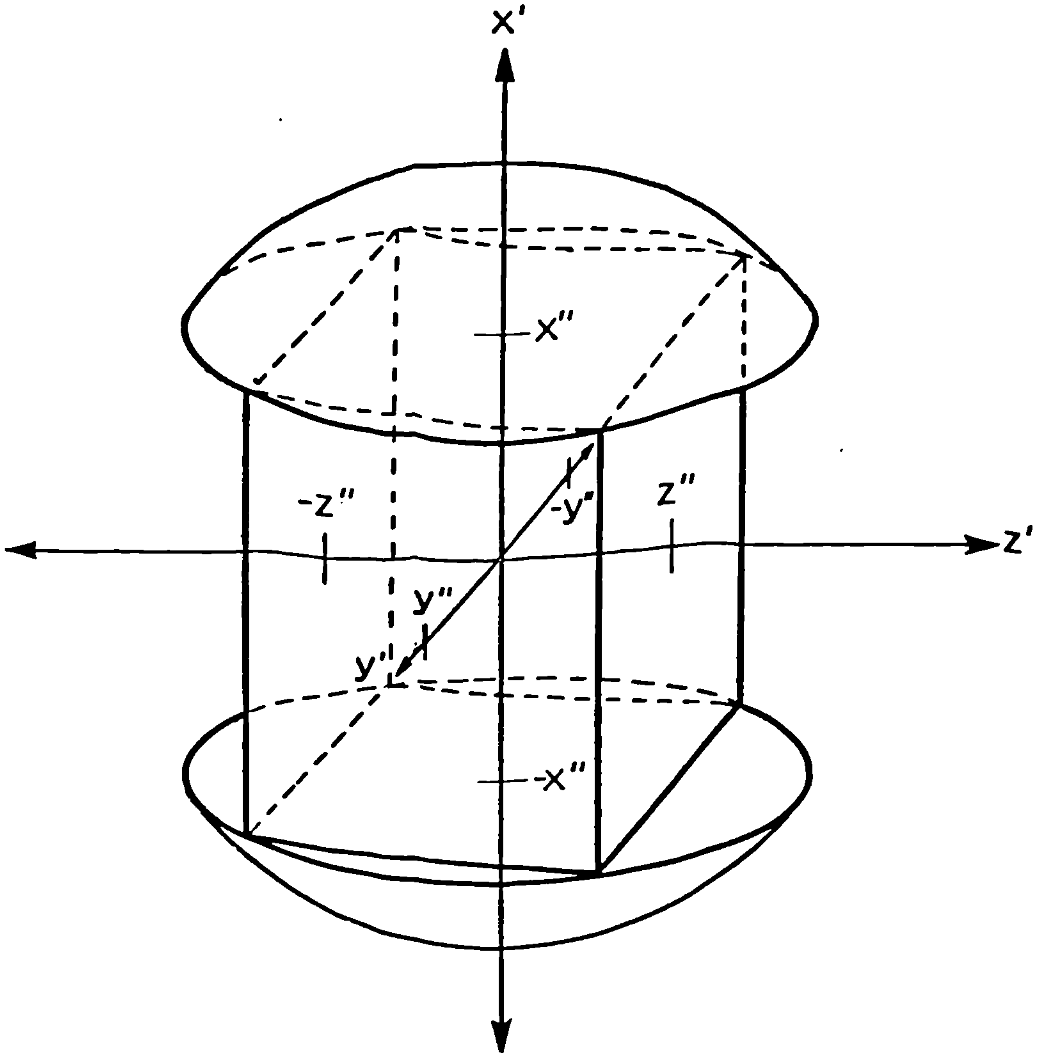

Fig. 3.2 The integration surfaces

direction is restricted to be the intersection with the sphere of the plane which passes through (-X", 0,0) and whose normal is the negative X axis. This restriction is imposed in order to keep the number of parameters small and also to obtain a compact set of final equations. The remaining pairs of surfaces are obtained in a similar fashion by fixing Y" and Z". In DeMarco's (1974) works, the values of X", Y" and Z" are all zero. For many problems the magnitude of the radiation intensity in some directions may be very much more significant than in others. It is expected that the solutions can be improved by varying, in an appropriate way the relative sizes of these surfaces of integration.

From the economic point of view, it is to be hoped that a satisfactory formulation will not necessitate a complicated set of three-dimensional tables of recommendations for the values of X", Y" and Z". A simple formulation is sought.

3.1.3 Derivation of the Flux Equations

For a Cartesian coordinate system, the transport equation, eq. (1.2.1), can for a particular ray, be rewritten in the form:

$$\frac{\partial}{\partial x}(I.X') + \frac{\partial}{\partial y}(I.Y') + \frac{\partial}{\partial z}(I.Z') = -KI + \frac{K\sigma T^4}{\pi} \qquad (3.1.2)$$

where X', Y' and Z' are the direction cosines of the ray and (I.X'), (I.Y'), (I.Z') implies the components of intensity on X, Y and Z axis for the ray. The remaining symbols have their usual meanings.

The series for I (3.1.1) is next substituted in the above form to yield:

$$\frac{\partial}{\partial x}\left[A_1 X'^2 + A_2X'Y' + A_3X'Z' + B_1X'^3 + B_2X'Y'^2 + B_3X'Z'^2\right]$$

$$+ \frac{\partial}{\partial y}\left[A_1X'Y' + A_2Y'^2 + A_3Y'Z' + B_1Y'X'^2 + B_2Y'^3 + B_3Y'Z'^2\right]$$

$$+ \frac{\partial}{\partial z}\left[A_1X'Z' + A_2Y'Z' + A_3Z'^2 + B_1X'^2Z' + B_2Y'^2Z' + B_3Z'^3\right]$$

$$= -K\left[A_1X' + A_2Y' + A_3Z' + B_1X'^2 + B_2Y'^2 + B_3Z'^2\right] + \frac{K\sigma T^4}{\pi} \qquad (3.1.3)$$

Six integrations are now performed on eq. (3.1.3) over the surfaces described in section 3.1.2 above to yield a set of six first order partial differential equations. The integrations are shown in Appendix A3.1. Similar integrations also occur in DeMarco's thesis (1974), but only for the special case where X" = Y" = Z" = 0. After further inverting of the matrix, the following set of 1st order equations may be derived:

$$-\frac{1}{K(1-X''^2)}\frac{\partial}{\partial x}\{(1-X''^2)C_1\} = A_1 \tag{3.1.4}$$

$$-\frac{1}{K(1-Y''^2)}\frac{\partial}{\partial y}\{(1-Y''^2)C_2\} = A_2 \tag{3.1.5}$$

$$-\frac{1}{K(1-Z''^2)}\frac{\partial}{\partial z}\{(1-Z''^2)C_3\} = A_3 \tag{3.1.6}$$

$$-\frac{1}{(1-X''^3)}\frac{\partial}{\partial x}[(1-X''^3)A_1] = KB_1 - \frac{K\sigma T^4}{\pi} \tag{3.1.7}$$

$$-\frac{1}{(1-Y''^3)}\frac{\partial}{\partial y}[(1-Y''^3)A_2] = KB_2 - \frac{K\sigma T^4}{\pi} \tag{3.1.8}$$

$$-\frac{1}{(1-Z''^3)}\frac{\partial}{\partial z}[(1-Z''^3)A_3] = KB_3 - \frac{K\sigma T^4}{\pi} \tag{3.1.9}$$

where C_1, C_2 and C_3 are defined as follows:

$$C_1 = \frac{1+X''^2}{2}B_1 + \frac{1-X''^2}{4}B_2 + \frac{1-X''^2}{4}B_3 \tag{3.1.10}$$

$$C_2 = \frac{1-Y''^2}{4}B_1 + \frac{1+Y''^2}{2}B_2 + \frac{1-Y''^2}{4}B_3 \tag{3.1.11}$$

$$C_3 = \frac{1-Z''^2}{4}B_1 + \frac{1-Z''^2}{4}B_2 + \frac{1+Z''^2}{2} B_3 \tag{3.1.12}$$

As stated earlier, a simple recommendation for the parameters X", Y" and Z" is sought. One particular simplification is to let the parameters vary with respect to the optical thickness only. In this case eqs. (3.1.4) to (3.1.9) can be re-stated more simply as follows:

$$-\frac{\partial C_1}{K\partial x} = A_1 \tag{3.1.13}$$

$$-\frac{\partial C_2}{K\partial y} = A_2 \tag{3.1.14}$$

$$-\frac{\partial C_3}{K\partial z} = A_3 \tag{3.1.15}$$

$$-\frac{\partial}{\partial x}A_1 = KB_1 - \frac{K\sigma T^4}{\pi} \tag{3.1.16}$$

$$-\frac{\partial}{\partial y}A_2 = KB_2 - \frac{K\sigma T^4}{\pi} \tag{3.1.17}$$

$$-\frac{\partial}{\partial z}A_3 = KB_3 - \frac{K\sigma T^4}{\pi} \tag{3.1.18}$$

These are the same as eqs. (3) to (8) in Lockwood and Shah (1976). The parameters are included in the definitionsof C_1, C_2 and C_3.

For calculations of radiative transfer using the present model, values of C_1, C_2 and C_3 only need be stored. The other coefficients are easily calculated when needed. The simple form of this system, especially eqs. (3.1.13) to (3.1.18) is due to the particular form of the assumed series (eq. (3.1.1)).

3.1.4 Heat Flux and Energy Conservation Equations

The net heat flux is defined in Chapter 1, eq. (1.2.2). After substituting the present variables, we obtain:

$$\underline{q} = \int_{4\pi} I(X',Y',Z').(X',Y',Z')\left(\frac{Y'dX-X'dY}{1-Z'^2}\right)dZ' \qquad (3.1.19)$$

On substitution of the series (3.1.1) this reduces to

$$\underline{q} = \frac{4\pi}{3}(A_1,A_2,A_3) \qquad (3.1.20)$$

Similarly the following expression can be derived, using the definition (1.2.3), for q_+ in the positive x direction,

$$q_+ = \left(\frac{2\pi}{3}A_1 + \frac{B_1}{2} + \frac{B_2}{4} + \frac{B_3}{4}\right) \qquad (3.1.21)$$

The expression for q_- is similar to eq. (3.1.21) except that the coefficient of A_1 is negative. For the flux at a black wall, at temperature T_W, and normal in the positive x direction, we can use

$$q = \frac{2\pi}{3}A_1 - \frac{B_1}{2} - \frac{B_2}{4} \quad \frac{B_3}{4} + \frac{\sigma T_W^4}{\pi} \qquad (3.1.22)$$

as a better estimate than the expression given by eq. (3.1.20), since the positive component of q is only that emmited by the temperature of the wall. We shall usually use eq. (3.1.20) unless otherwise specified.

Here again the choice of the series has helped to reduce eq. (3.1.19) to the simple form of eq. (3.1.20).and eq. (3.1.21).

The energy conservation equation eq. (1.2.7) is presented in Chapter 1. For the Cartesian coordinates it reduces to:

$$\frac{d}{dx}(\underline{q}.\underline{i}) + \frac{d}{dy}(\underline{q}.\underline{j}) + \frac{d}{dz}(\underline{q}.\underline{K}) = S \tag{3.1.23}$$

Substituting the series and using eqs. (3.1.4), (3.1.5) and (3.1.6), the energy conservation equation may be rewritten as:

$$\frac{1}{K(1-X''^2)}\frac{\partial}{\partial x}\{(1-X''^2)C_1\} + \frac{1}{K(1-Y''^2)}\frac{\partial}{\partial y}\{(1-Y''^2)C_2\}$$

$$+ \frac{1}{K(1-Z''^2)}\frac{\partial}{\partial z}\{(1-Z''^2)C_3\} = -\frac{3}{4\pi}S \tag{3.1.24}$$

If for a particular problem the temperature field is prescribed, then (3.1.24) is used to calculate the sources. If however sources are prescribed, then for a Cartesian system and, for constant X", Y" and Z", eq. (3.1.24) reduces to

$$\frac{K}{3}(B_1 + B_2 + B_3) - \frac{K\sigma T^4}{\pi} = -\frac{S}{4\pi} \tag{3.1.25}$$

3.1.5 Boundary Conditions

The boundary condition for a lambert surface is defined in Chapter 1 (eq. 1.2.6). Substituting the Taylor's series assumption (3.1.1) for expressions q_+ and q_- (eq. 3.1.21) we obtain:

$$(1-\varepsilon_W)\left(-\frac{2A_1}{3}+\frac{B_1}{2}+\frac{B_2}{4}+\frac{B_3}{4}\right)+\frac{\varepsilon_W\sigma T_W^4}{\pi}=\frac{2}{3}A_1X_Q+C_1 \qquad (3.1.26)$$

where
$$X_Q = \left(\frac{1-X''^3}{1-X''^2}\right) \qquad (3.1.27)$$

The above equation holds for a wall whose normal is parallel to the positive X axis. For the wall whose normal aligns with the negative negative X axis, eq. (1.2.6) reduces to:

$$(1-\varepsilon_W)\left(\frac{2A_1}{3}+\frac{B_1}{2}+\frac{B_2}{4}+\frac{B_3}{4}\right)+\frac{\varepsilon_W\sigma T_W^4}{\pi}=-\frac{2}{3}A_1X_Q+C_1 \qquad (3.1.28)$$

Similar expressions can be easily derived for the other two coordinate directions by rotating the variables cyclicaly.

3.2 One-Dimensional Cartesian Validation Studies and Some Recommendations for the Parameters

3.2.1 One-Dimensional Optically Thick Solution

The system described in section 3.1 is a general three-dimensional geometry. We choose to commence testing its validity from the starting point of simpler geometries. As explained earlier, a major validation problem is the lack of analytical solutions and also the enormous number of test cases that need to be studied.

Again a single recommendation for X" for each optical thickness is sought. For one dimensional gray system, the eqs. (3.1.13) to (3.1.18) reduce to:

$$A_1 = -\frac{1}{K}\frac{\partial C_1}{\partial X} \qquad (3.2.1)$$

$$A_2 = 0 \tag{3.2.2}$$

$$A_3 = 0 \tag{3.2.3}$$

$$-\frac{1}{K}\frac{d^2C_1}{dX^2} = -KB_1 + \frac{K\sigma T^4}{\pi} \tag{3.2.4}$$

$$B_2 = \frac{\sigma T^4}{\pi} \tag{3.2.5}$$

$$B_3 = \frac{\sigma T^4}{\pi} \tag{3.2.6}$$

The definition for C_1 remains the same as eq. (3.1.10) and the boundary conditions (3.1.26) and (3.1.28) reduce to

$$\frac{2}{3K}\left(\frac{1+X_Q}{\varepsilon_1} - 1\right)\frac{dC_1}{dX} + \frac{\sigma T_1^4}{\pi} = \frac{C_1}{\varepsilon_1} - \left(\frac{1}{\varepsilon_1} - 1\right)\left(\frac{B_1}{2} + \frac{B_2}{4} + \frac{B_3}{4}\right) \tag{3.2.7}$$

at wall 1 and at wall 2,

$$-\frac{2}{3K}\left(\frac{1+X_Q}{\varepsilon_2} - 1\right)\frac{dC_1}{dX} + \frac{\sigma T_2^4}{\pi} = \frac{C_1}{\varepsilon_2} - \left(\frac{1}{\varepsilon_2} - 1\right)\left(\frac{B_1}{2} + \frac{B_2}{4} + \frac{B_3}{4}\right) \tag{3.2.8}$$

Considering first the limit of an optically thick system, it is convenient to define a non-dimensional parameter α and a length scale parameter ϕ such that:

$$K = \frac{1}{\alpha\phi} \quad \text{and} \quad X = \frac{x}{\phi} \tag{3.2.9}$$

Now $\alpha \to o$ implies $KL \to \infty$. The eqs. (3.2.2), (3.2.3), (3.2.5) and (3.2.6) remain as before. Eq. (3.2.4) reduces to:

$$\alpha\frac{d^2C_1}{dX^2} = \frac{1}{\alpha}\left(B_1 - \frac{\sigma T^4}{\pi}\right), \tag{3.2.10}$$

and the boundary condition (3.2.7) becomes

$$\frac{2\alpha}{3}\left(\frac{1+X_Q}{\varepsilon_1} - 1\right)\frac{dC_1}{dX} + \frac{\sigma T_1^4}{\pi} = \frac{C_1}{\varepsilon_1} - \left(\frac{1}{\varepsilon_1} - 1\right)\left(\frac{B_1}{2} + \frac{B_2}{4} + \frac{B_3}{4}\right) \qquad (3.2.11)$$

Eq. (3.2.8) can be similarly transformed. In the limit as $\alpha \to o$, eq. (3.2.4) reduces to:

$$B_1 = \frac{\sigma T^4}{\pi} \qquad (3.2.12)$$

The solution does not depend on the value of the parameter X_Q''(hence X"). Also the solution does not involve the boundary condition. This is because we have a typical singular perturbation problem in which the boundary condition only influences a boundary layer of thickness $O(\alpha)$. The complete solution is therefore composed of inner and outer components of which eq. (3.2.12) constitutes the outer solution.

To obtain the inner solution at a point x_n whose distance from x_W, a point on the boundary, is of order α, it is necessary to stretch the coordinate x, given by

$$X_n = \frac{(x_n - x_W)}{\phi\alpha} \qquad (3.2.13)$$

Further C_1 is also expanded in Taylor's series defined as follows:

$$C_1 = D_o + \alpha D_1 + \ldots . \qquad (3.2.14)$$

Substituting eq. (3.2.13) into eq. (3.2.4) to magnify the dimensions and equating terms of order zero, we obtain (eq. A3.2.5):

$$\frac{d^2 D_o}{dX_n^2} = B_1 - \frac{\sigma T^4}{\pi} \qquad (3.2.15)$$

The dimensions in the boundary condition eq. (3.2.11) are similarly stretched and we solve the flux equations. Referring to appendix A3.2. The net flux is given by eq. (A3.2.4)

$$\underline{q} = -\frac{4\sigma}{3K}\frac{dT^4}{dX} \tag{3.2.16}$$

The above result is also known as diffusion approximation or Rosseland (1936) approximation. The temperature slip near the wall is (refer to appendix eq. A3.2.14):

$$\sigma T_o^4 - \sigma T_W^4 = \frac{1}{2}\left(\frac{1+X_Q}{\varepsilon_1} - 1\right)q_1 + \frac{1}{2}\left(1 + \frac{X''^2}{\varepsilon_1}\right)\frac{d^2(\sigma T^4)}{dX_n^2} \tag{3.2.17}$$

where T_o is the temperature adjacent to the wall and q_1 is the flux out of the wall. The Diessler's temperature jump at the boundary (Diessler, 1964) is obtained by simply putting X" = 0(X_Q = 1). Using this is a boundary condition, he concludes that the diffusion approximation solution is improved for comparatively low values of optical thicknesses. It is hoped that by specifying relatively simple recommendations for values of X", still more accurate results will be possible.

3.2.2 One-Dimensional Optically Thin Solution

For an optically thin system, it is convenient to define a non-dimensional parameter α and a length scale parameter ϕ such that:

$$K = \frac{\alpha}{\phi} \quad \text{and} \quad X = \frac{x}{\phi} \quad \text{i.e.} \quad L' = \frac{L}{\phi} \tag{3.2.18}$$

Now as $\alpha \to o$ implies KL $\to$ o. C_1 is expanded in Taylor's series from in a similar manner to eq. (3.2.14). As before, we substitute these new variables into eq. (3.2.4) and the boundary condition (3.2.7) and solve the resulting equations(refer to appendix A3.3). The net flux is given by eq. (A3.3.13); substituting X" = 0.0, the net flux out of wall is given by

$$q_{W_1} = \frac{\sigma T_2^4 - \sigma T_1^4}{(\frac{1}{\varepsilon_1} + \frac{1}{\varepsilon_2} - 1)} \tag{3.2.19}$$

This is the standard optically thin solution (see Ozisik (1973), for instance).

We conclude from the preceeding results that for optically thin limits, the recommendation for X" is 0.0. While the net flux for optically thick limit does not depend on the value of X", which is what we would expect.

3.2.3 One-Dimensional Test Case with Constant Interior Source

The analytical solution for this test case has been presented in section 2.2.1 and also by Heaslet and Warming (1964). In the present analysis the value of the parameter X" is assumed to vary with the optical thickness only. Therefore eqs. (3.2.1) to (3.2.6) and eq. (3.1.25) together with the boundary conditions (3.2.7) and (3.2.8) are used. More generally, the flux equations (3.1.4) to (3.1.9) should be used for the analysis.

Consider two infinitely long parallel walls 1 and 2, with emissivities ε_1 and ε_2 and at temperatures T_1 and T_2 respectively. The walls are distance L apart and the gas inside has a uniform absorption coefficient K and a uniform heat source S. Then the wall fluxes are given by (refer to appendix A3.4):

$$q_{W_1} = q_{W_2} - \frac{S}{L} = \frac{(\sigma T_1^4 - \sigma T_2^4)Q^* - LS\{(\frac{1}{\varepsilon_2} - 1)Q^{**} - \frac{1}{2}\}}{1 + (\frac{1}{\varepsilon_1} + \frac{1}{\varepsilon_2} - 2)Q^{**}} \tag{3.2.20}$$

where

$$Q^* = \frac{1}{X_Q + \frac{3}{4}KL} \qquad (3.2.21)$$

$$Q^{**} = \left(\frac{1+X_Q}{2}\right)Q^* \qquad (3.2.22)$$

and where X_Q is defined by eq. (3.1.27). Comparing eq. (3.2.20) with the analytic solution, eq. (2.2.1), it is evident that the recommended values of X_Q and therefore of X" should be chosen by comparing the analytic values of Q with either the expression for Q* or Q** depending on whether the wall temperatures, emissivities or the heat sources are of predominant interest. There is, however, not much difference between Q* and Q**. In order to keep to a simple recommendation, we choose to use the expression for Q* from eq. (3.2.20) and the analytical value of Q (table 3.2) on the left-hand side in order to solve for X_Q and hence X" for various values of optical thicknesses. Hence, we get a set of recommendations for X_Q for these values of optical thickness; recorded in table 3.1 which yield exact fluxes for one-dimensional problems with prescribed source. The corresponding values of X" (evaluated using a Newton-Raphson technique) are also presented in table 3.1. The intermediate values of X" can be evaluated using Fig. 3.3 or using a simple linear interpolation. For values of optical thickness greater than 3.0 the recommended values of X_Q and X" are 1.066 and 0.291 respectively.

If the value of X_Q is assumed to be unity (X" = 0), both eq. (3.2.21) and eq. (3.2.22) reduce to:

$$Q^* = \frac{1}{1 + \frac{3}{4}KL} \qquad (3.2.23)$$

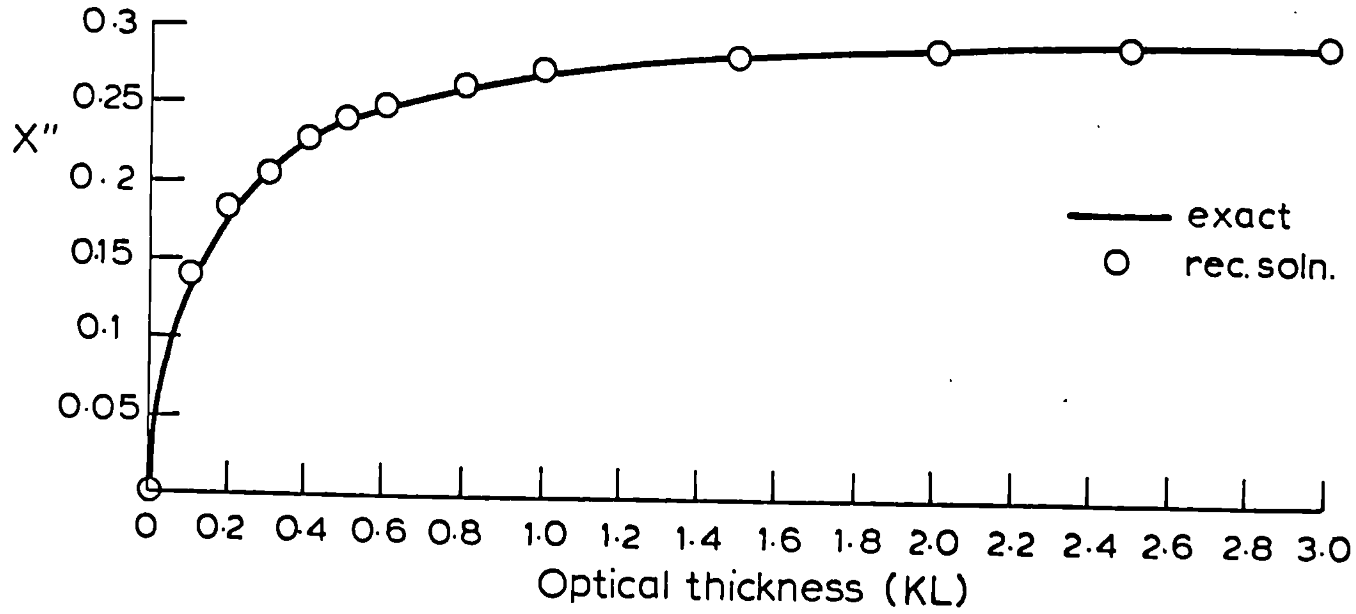

Fig. 3.3 Recommendation of X" for various optical thicknesses

τ	X_Q	X''
0.0	1.0	0.0
0.1	1.017	0.139
0.2	1.028	0.181
0.3	1.035	0.1207
0.4	1.041	0.224
0.5	1.045	0.237
0.6	1.049	0.247
0.8	1.054	0.261
1.0	1.058	0.271
1.5	1.062	0.282
2.0	1.064	0.287
2.5	1.065	0.290
3.0	1.066	0.291

Table 3.1 The recommended values for X_Q and X'' for various optical thicknesses for one-dimensional Cartesian geometry with sources prescribed.

This is a good approximation to the analytical solution (Table 3.2), with a maximum error of 3.4%. Of course the percentage errors are reduced to zero for the recommended values of X_Q from Table 3.1

KL	Q	Q*	$\frac{(Q^*-Q)1.00}{Q}$
0.0	1.0	1.0	0
0.1	0.9157	0.9303	1.6
0.2	0.8491	0.8695	2.4
0.3	0.7934	0.8163	2.9
0.4	0.7458	0.7672	3.2
0.5	0.7040	0.7272	3.3
0.6	0.6672	0.6896	3.4
0.8	0.6046	0.6250	3.4
1.0	0.5532	0.5714	3.3
1.5	0.4572	0.4706	3.0
2.0	0.3900	0.4000	2.6
2.5	0.3401	0.3478	2.3
3.0	0.3016	0.3077	0.4

Table 3.2 Comparison of flux model solution (*) for $X_Q = 1$ with exact solution for one-dimensional radiation

Considering now the solution for the temperature distribution between the plates, we note from appendix A3.4 (eq. A3.4.9) that

$$Q^*_S = \frac{KL}{2} \tag{3.2.24}$$

This does not depend on the values of the parameters.

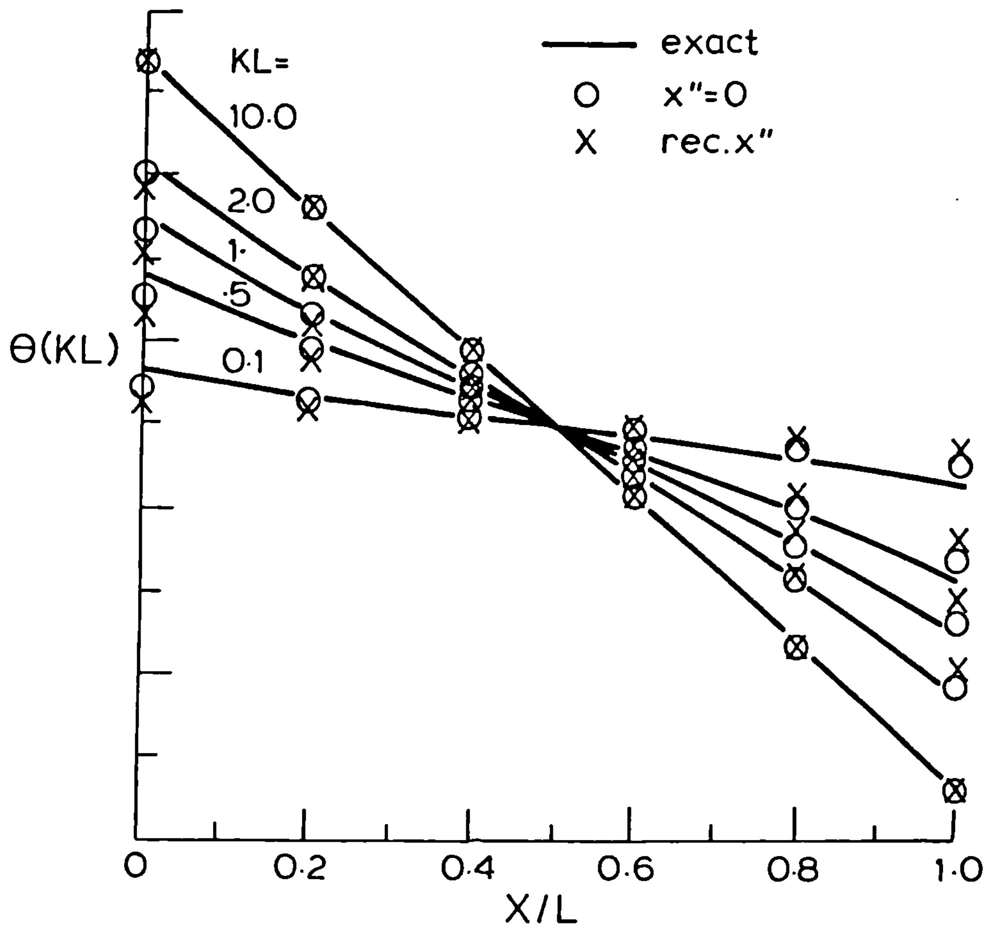

Fig. 3.4 Comparison of exact (Heaslet and Warming, 1964) and flux model solution for θ

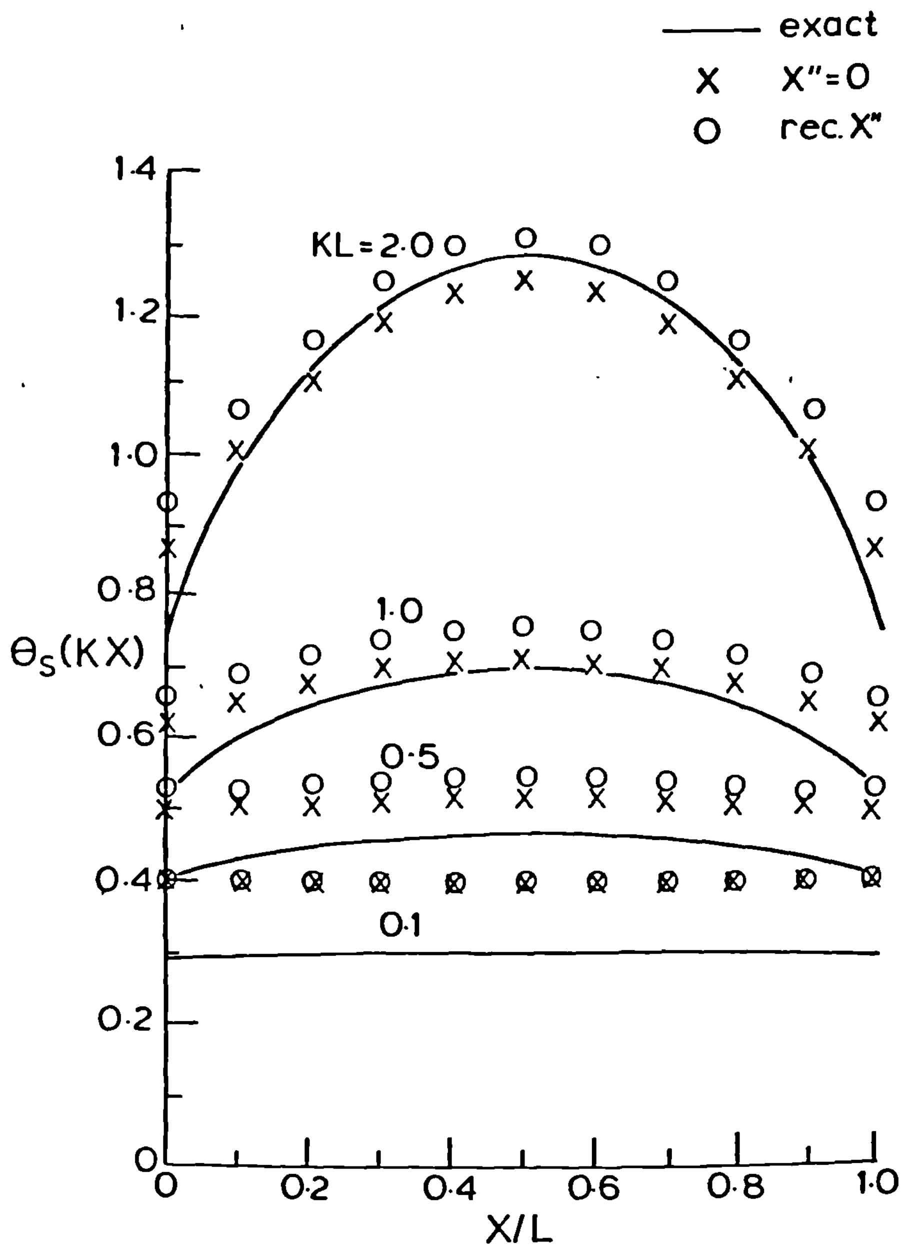

Fig. 3.5 Comparison of exact (Heaslet and Warming, 1964) and flux model solution for θ_s

Two sets of solutions for θ^* and θ^*_S using eqs. (A3.4.10) and (A3.4.11) respectively are plotted against the analytical solutions Fig. 3.4 and Fig. 3.5 respectively. One set of results is for the case $X_Q = 1(X'' = 0.0)$ and the other set is obtained using the recommended values of X_Q obtained from table 3.1. The solutions for both θ^* and θ^*_S for this particular set of recommended values of X_Q, are worse than for the simple recommendation of $X_Q = 1.0$, while the flux agreement is better for the values of Table 3.1 rather than for $X_Q = 1.0$. It would be possible to find a set of X_Q where the reverse is true. Therefore we can conclude from this that X" is a function of more variables than just the optical thickness. Wall temperatures, emissivities, interior source strengthes are just some of them.

For $X_Q = 1$, the expression for θ^* and θ^*_S (eqs. (A3.4.10) and (A3.4.11)) reduce to:

$$\theta^* = \frac{\frac{1}{2} + \frac{3}{4}(KL-KX)}{(1+\frac{3}{4}KL)} \tag{3.2.25}$$

and $$\theta^*_S = -\frac{3}{8}K^2x(X-L) + \frac{KL}{4} + \frac{3}{8} \tag{3.2.26}$$

The expressions for Q^*, Q^*, θ^* and θ^*_S (eqs. (3.2.23)) are all identical to similar approximations obtained by Heaslet and Warming (1964).

3.2.4 One-Dimensional Cartesian Test Case with Constant Interior Temperature

The analytical solutions for this test case has been presented in section 2.2.2. As in the previous section, the parameter X" is assumed to vary with the optical thickness only. Hence for this test case eqs. (3.2.1) to (3.2.6) and the boundary conditions (3.2.7) and (3.2.8) are used.

Consider two infinitely long parallel cold black walls 1 and 2. The walls are distance L apart, and the gas inside has a uniform absorption coefficient K and is at a uniform temperature T_g. The wall fluxes are calculated using expression (3.1.22). The net flux at wall 1 is calculated numerically (fig. 3.6). Values of X" and X_Q were then adjusted by trial and error to give numerically exact solutions. Table 3.3 and fig. 3.7 show these recommendations.

τ	X_Q	X"
0.0	1.0	0.0
0.1	1.042	0.228
0.2	1.070	0.301
0.3	1.091	0.350
0.4	1.107	0.385
0.5	1.120	0.412
0.6	1.130	0.431
0.7	1.137	0.444
0.8	1.141	0.452
0.9	1.143	0.456
1.0	1.143	0.456
1.5	1.123	0.417
2.0	1.101	0.373
2.5	1.091	0.350
3.0	1.088	0.3

Table 3.3 The recommended values for X_Q and X" for various optical thicknesses for one-dimensional Cartesian geometry with temperatures prescribed.

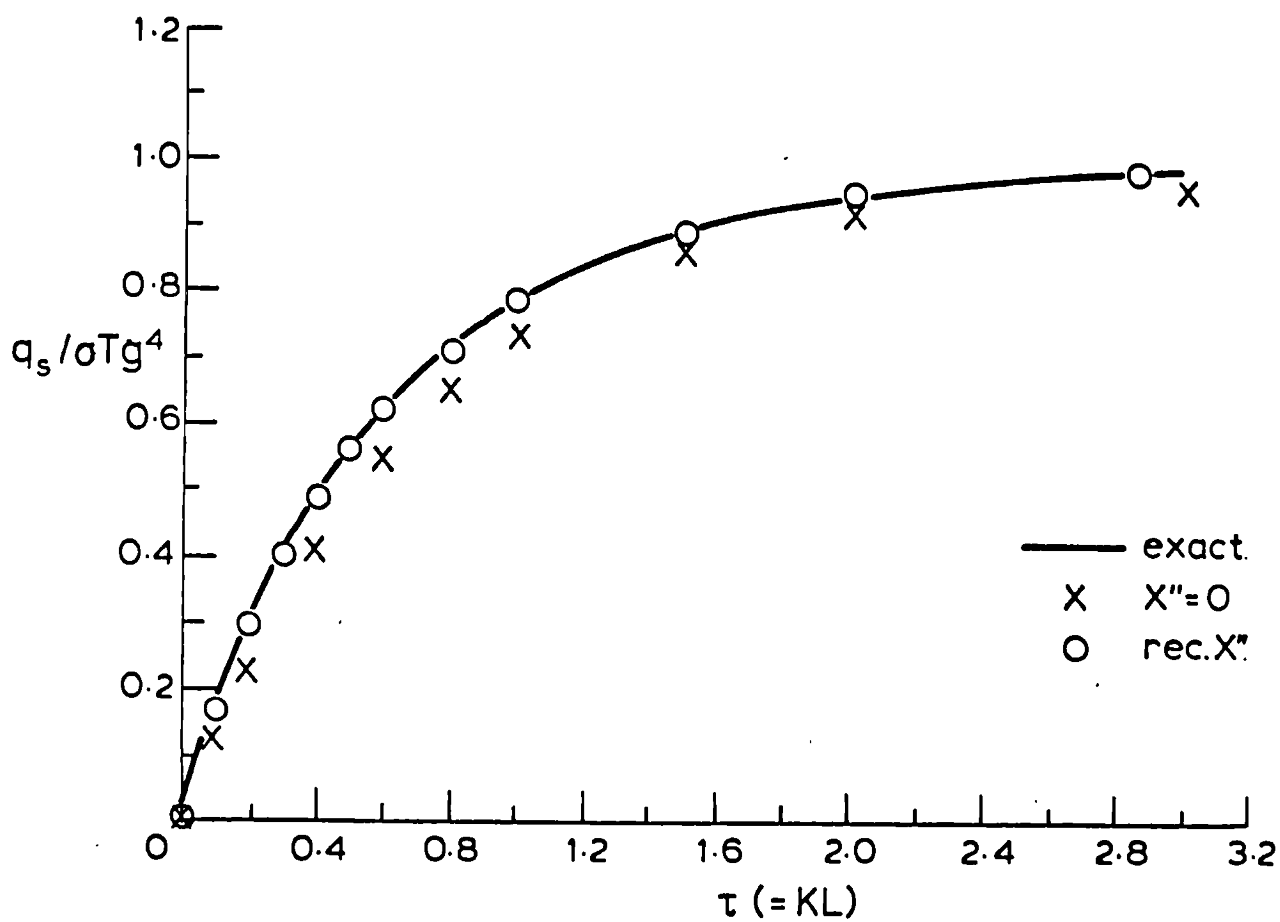

Fig. 3.6 Comparison of exact solution of flux against the flux model solution using the recommended values of X" for one-dimensional constant temperature case

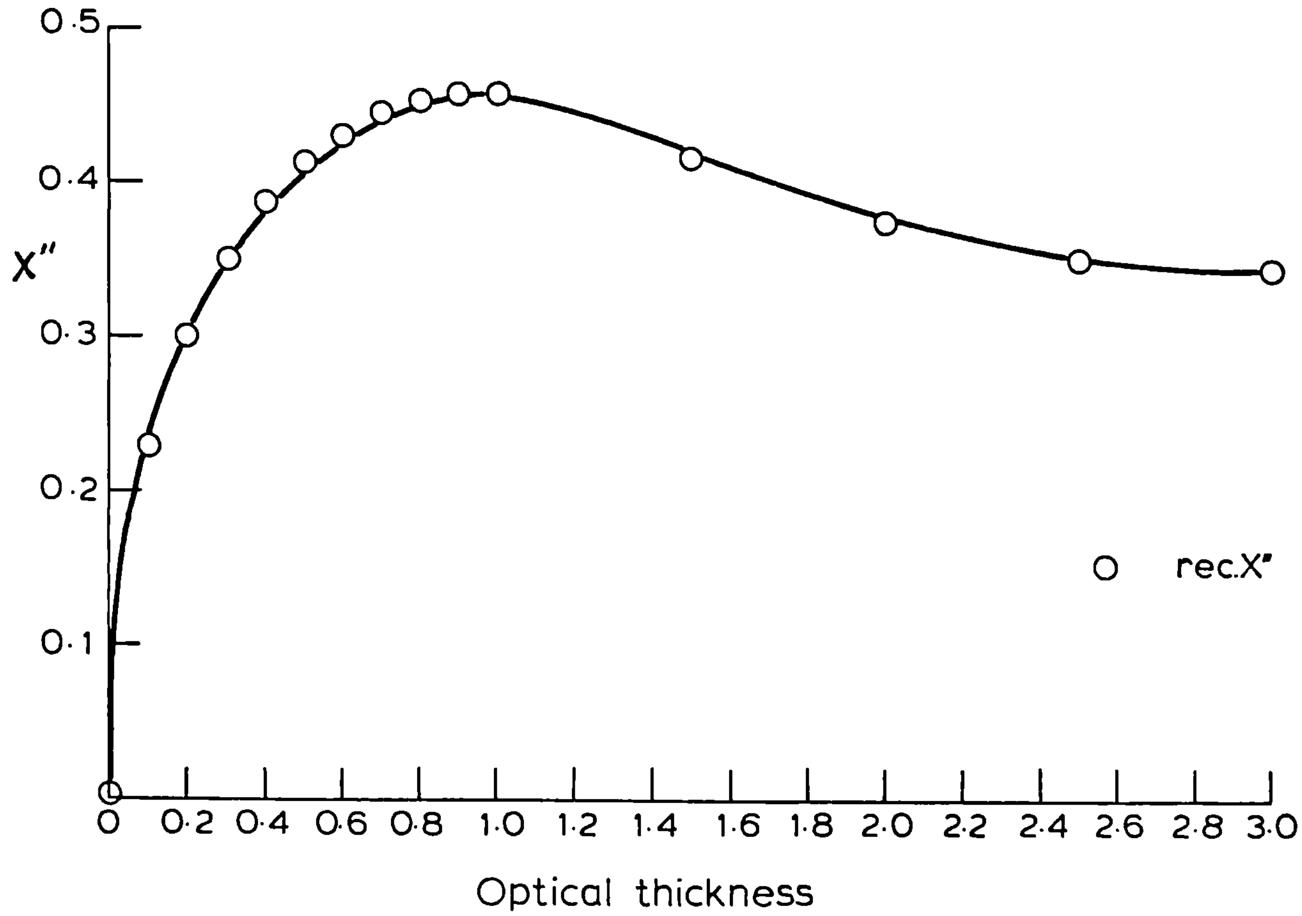

Fig. 3.7 Recommended values of X" for various optical thicknesses

We now have two sets of tables, one for temperature specified problems and one for source specified problems. It is to be hoped that the recommendations obtained in these two sections will carry through for the corresponding problems in two and three dimensional geometries. We shall now turn to this question.

3.2.5 Two-Dimensional Cartesian Test Case With Constant Interior Temperature

The one-dimensional recommendations for X''^2 and X_Q (table 3.3) have given better heat flux solutions through the walls. We would like to test these recommendations to see whether they can be extended into two and indeed three dimensions. The main difficulty is to produce and compare the enormous number of solutions for all the permutations of these cases. An analytical solution for a simple two dimensional test case has been presented in section 2.2.3.

Consider an infinitely long square cavity with cold black walls The gas inside is at a uniform temperature ($\sigma T_g^4 = 1.0$) and the optical thickness of the cavity is 1 x 1 in both co-ordinate directions. The wall fluxes are calculated using expression (3.1.22). The analytical solution of heat flux along one of the walls is in Fig. 3.8, plotted for two values of X'': (i) $X'' = 0.0$, (ii) $X'' = 0.456$. The flux model solution has been obtained by numerical techniques. For the first case the flux agreement is reasonable in the centre regions but becomes worse as we approach the corners. While the flux for the recommended value is better at the centre it worsens near the corners. Hence the

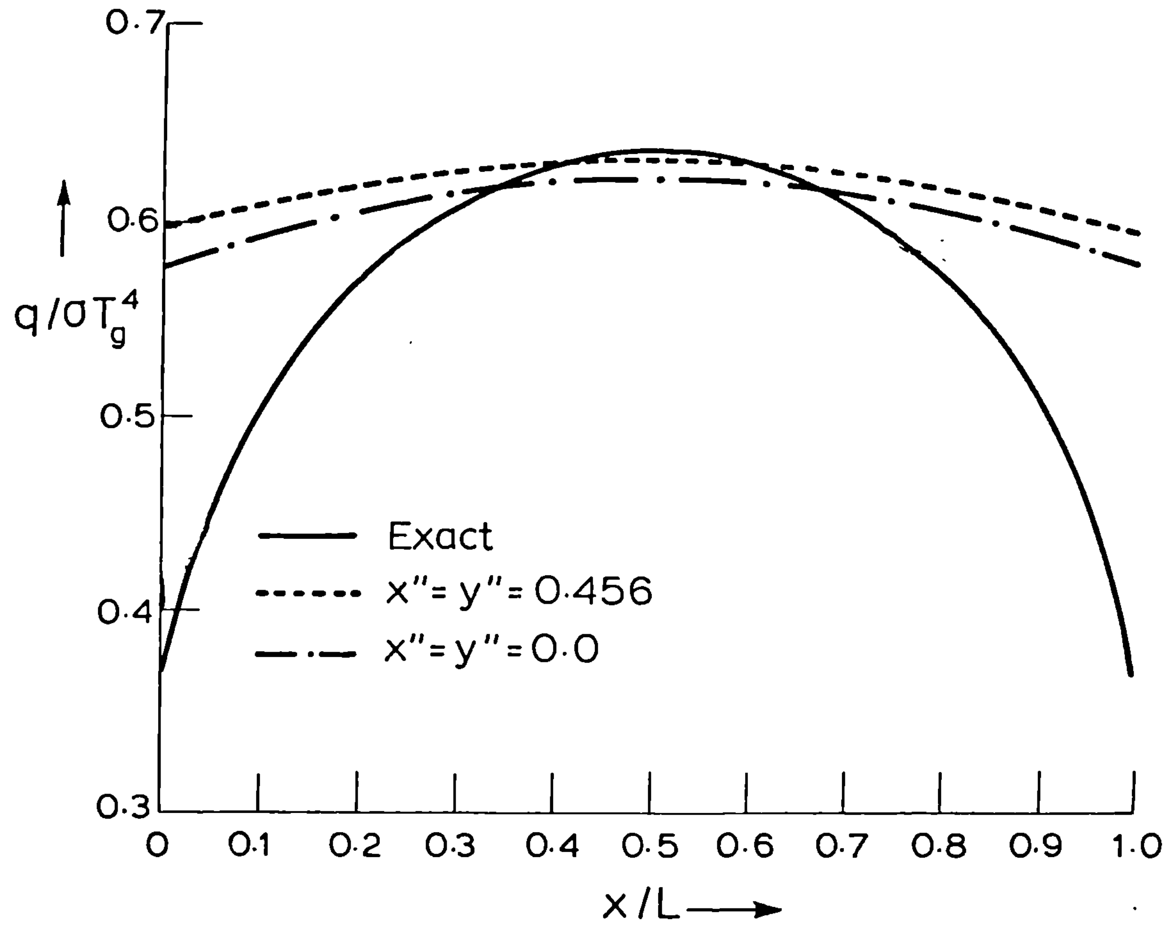

Fig. 3.8 Comparison of exact and two flux solutions of flux out of a wall for a two-dimensional constant temperature case

deductions made from one dimensional cases must be employed with caution to two and three-dimensional cases.

CHAPTER 4

THE PRESENT FLUX MODEL IN CYLINDRICAL COORDINATES

4.1 Formulation

4.1.1 Transformation of Radiative Transport Equation to Cylindrical Coordinates

As mentioned earlier in Chapter one, one of the difficulties of dealing with the radiative transfer is the problem of associating the intensity with a known group of mathematical entities and hence of being able to apply the transformations associated with the group. Intensity is not a scalar quantity because it has directional properties. But more importantly intensity is not a vector in the traditional sense of the term because a vector at any point has resultant which has a magnitude in only one direction. Once the direction of the ray is fixed, intensity can be treated as a scalar quantity. The transport equation relates neighbouring intensities for a particular ray, not two intensities in neighbouring directions.

In a good deal of the earlier literature (see Truelove, 1975) the left hand side of the transport equation has the del notation $(\underline{\nabla}.\underline{\Omega})I$ (eq. 4.1.1) which appears in a special sense. The del notation is expanded as a dot product of a divergence vector operator with the direction cosine vector yielding a scalar operator on intensity. This yields the same expression as $\frac{dI}{ds}$ for a cartesian coordinate system. But this interpretation of del notation does not yield the same expression as $\frac{dI}{ds}$ if the standard transformations of divergence to other coordinate systems are employed. This will now be proved for the cylindrical system.

$$(\underline{\nabla}.\underline{\Omega})I = -kI + \frac{k\sigma T^4}{\pi} \qquad (4.1.1)$$

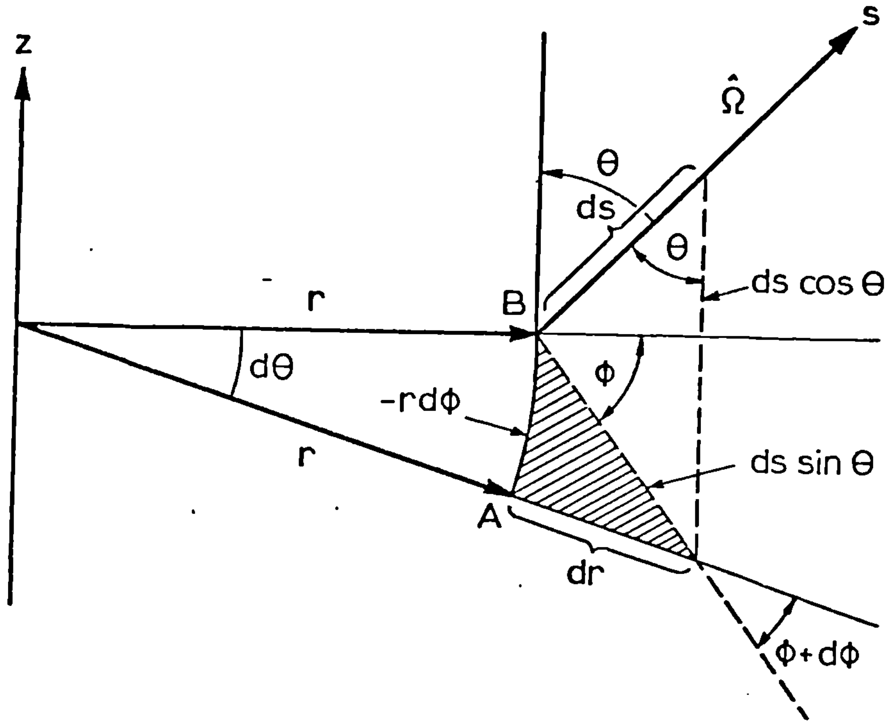

Fig. 4.1 Coordinates for cylindrical system

Fig. 4.1 describes the co-ordinate system used. Eq. (4.1.2) relates as with r, θ and z.

$$ds^2 = dr^2 + r^2 d\theta^2 + dz^2 \; . \tag{4.1.2}$$

The chain rule is applied to yield:

$$\frac{d}{ds} = \frac{\partial}{\partial r}\frac{dr}{ds} + \frac{\partial}{\partial \Theta}\frac{d\Theta}{ds} + \frac{\partial}{\partial z}\frac{dz}{ds} \tag{4.1.3}$$

Further the following relationships can easily be derived:

$$\frac{dr}{ds} = \sin\theta \, \cos\phi \;\; = r' \tag{4.1.4}$$

$$\frac{d\Theta}{ds} = - \frac{d}{ds} = \frac{\sin\theta \, \sin\phi}{r} \;\; = \frac{\Theta'}{r} \tag{4.1.5}$$

and $$\frac{dz}{ds} = \cos\theta = z' \tag{4.1.6}$$

where r', Θ' and z' are direction cosines in r, Θ and z directions. Substituting (4.1.4), (4.1.5) and (4.1.6) into (4.1.3) yields:

$$\frac{dI}{dS} = \frac{\partial}{\partial r}(I.r') + \frac{\partial}{r\partial\Theta}\{I.\Theta'\} + \frac{\partial}{\partial z}\{I.Z'\} \qquad (4.1.7)$$

This transformation agrees with that of (McCann and Whitacre, (1975) Ozisik (1975) for example). However this transformation can also be successfully achieved by using the del notation in eq. 4.1.1 as a grad operator, but one needs to be very careful to obey the rules of vector notations.

4.1.2 Derivation of the Flux Equations

To obtain the final equations, a method similar to that of section 3.1 for the Cartesian case is used with similar assumptions, except that now x, y and z axis are replaced by r, Θ and z axis. Hence the series now becomes

$$I = A_1 r' + A_2\Theta' + A_3 z' + B_1 r'^2 + B_2\Theta'^2 + B_3 z'^2 \qquad (4.1.8)$$

where r', Θ' and z' are direction cosines as before and A_1, A_2, A_3, B_1, B_2 and B_3 are only dependent on special coordinates. The surface of integration is now the intersection of a sphere of unit radius with a plane normal to the radius axis and passing through the point (r", o,o) from the point P. The surfaces of integration about the Θ and z directions are similarly defined. Here Θ'' is denoted to mean distance Θ'' from the point P on axis perpendicular to r and z axis, that is the Θ axis. The transport equation (eq. 1.2.1) with the transformation (eq. 4.1.7) becomes

$$\frac{\partial}{\partial r}\{Ir'\} + \frac{1}{r}\frac{\partial}{\partial \Theta}\{I.\Theta'\} + \frac{\partial}{\partial z}(Iz') = - KI + \frac{K\sigma T^4}{\pi} \qquad (4.1.9)$$

The series (4.1.8) is next substituted in eq. (4.1.9) and integrated as before to yield the following set of equations:

$$- \frac{1}{K(1-r''^2)} \frac{\partial}{\partial r}\{(1-r''^2)C_1\} = A_1 \qquad (4.1.10)$$

$$- \frac{1}{K(1-\Theta''^2)} \frac{1}{r}\frac{\partial}{\partial \Theta}\{(1-\Theta''^2)C_2\} = A_2 \qquad (4.1.11)$$

$$- \frac{1}{K(1-z''^2)} \frac{\partial}{\partial z}\{(1-z''^2)C_3\} = A_3 \qquad (4.1.12)$$

$$- \frac{1}{(1-r''^3)} \frac{\partial}{\partial r}\{(1-r''^3)A_1\} = KB_1 - \frac{K\sigma T^4}{\pi} \qquad (4.1.13)$$

$$- \frac{1}{(1-\Theta''^3)} \frac{\partial}{r\partial \Theta}\{(1-\Theta''^3)A_2\} = KB_2 - \frac{K\sigma T^4}{\pi} \qquad (4.1.14)$$

$$- \frac{1}{(1-z''^3)} \frac{\partial}{\partial z}\{(1-z''^3)A_3\} = KB_3 - \frac{K\sigma T^4}{\pi} \qquad (4.1.15)$$

where C_1, C_2 and C_3 are defined as follows

$$C_1 = \frac{1+ r''^2}{2} B_1 + \frac{1-r''^2}{4} B_2 + \frac{1-r''^2}{4} B_3 \qquad (4.1.16)$$

$$C_2 = \frac{1-\Theta''^2}{4} B_1 + \frac{1+\Theta''^2}{2} B_2 + \frac{1-\Theta''^2}{4} B_3 \qquad (4.1.17)$$

$$C_3 = \frac{1-z''^2}{4} B_1 + \frac{1-z''^2}{4} B_2 + \frac{1+z''^2}{2} B_3 \tag{4.1.18}$$

Again simple recommendations for the parameters are sought. For this system with the parameters related to the optical thickness only simplifies to:

$$-\frac{1}{K}\frac{\partial C_1}{\partial r} = A_1 \tag{4.1.19}$$

$$-\frac{1}{Kr}\frac{\partial C_2}{\partial \Theta} = A_2 \tag{4.1.20}$$

$$-\frac{1}{K}\frac{\partial C_3}{\partial z} = A_3 \tag{4.1.21}$$

$$-\frac{\partial A_1}{\partial r} = KB_1 - \frac{K\sigma T^4}{\pi} \tag{4.1.22}$$

$$-\frac{\partial A_2}{r\partial \Theta} = KB_2 - \frac{K\sigma T^4}{\pi} \tag{4.1.23}$$

$$-\frac{\partial A_3}{\partial z} = KB_3 - \frac{K\sigma T^4}{\pi} \tag{4.1.24}$$

Notice the similarity between the eq. (4.1.10) to eq. (4.1.24) and eq. (3.1.4) to eq. (3.1.18). There are three parameters for each direction, and dx is replaced by dr and dy is replaced by $rd\Theta$. Without providing rigorous proof we may state that for any orthogonal system x_1, x_2, x_3, care being taken to define the series and surfaces of integration, one would expect to obtain a similar set of equations with appropriate dx_1, dx_2, dx_3 being the elemental length increments.

Now eqs (4.1.19) to (4.1.24) can be reduced to the following three second order equations

$$\frac{\partial}{\partial r}\left(\frac{1}{K}\frac{\partial C_1}{\partial r}\right) = KB_1 - \frac{K\sigma T^4}{\pi} \tag{4.1.25}$$

$$\frac{\partial}{r\partial\Theta}\left(\frac{1}{Kr}\frac{\partial C_2}{\partial\Theta}\right) = KB_2 - \frac{K\sigma T^4}{\pi} \tag{4.1.26}$$

$$\frac{\partial}{\partial z}\left(\frac{1}{K}\frac{\partial C_3}{\partial z}\right) = KB_3 - \frac{K\sigma T^4}{\pi} \tag{4.1.27}$$

Hence only C_1, C_2 and C_3 need be solved for. A similar manipulation of eqs (4.1.10) to eq. (4.1.15) can be performed. The simplicity and perhaps the familiar nature of the final equations is a major advantage of the present method over some of the other available flux methods. The present method can be readily incorporated into existing finite difference schemes for the flow.

4.1.3 <u>Boundary Conditions</u>

The treatment of the boundary conditions is similar to that of the cartesian case (section 3.1.3) after an appropriate replacement of the variables. It is useful to write out all six boundary equations in full, using relations (4.1.19) to (4.1.21).

Let the inner radius wall be at r_1 and the outer radius wall be at r_2 with emissivity ε_1 and ε_2 and at temperatures T_1 and T_2 respectively. Then the boundary conditions become

$$\frac{2}{3K}\left(\frac{1+r_Q}{\varepsilon_1} - 1\right)\frac{\partial C_1}{\partial r} + \left(\frac{1}{\varepsilon_1} - 1\right)\left(\frac{B_1}{2} + \frac{B_2}{4} + \frac{B_3}{4}\right) + \frac{\sigma T_1^4}{\pi} = \frac{C_1}{\varepsilon_1} \tag{4.1.28}$$

for the 1st wall and

$$-\frac{2}{3K}\left(\frac{1+r_Q}{\varepsilon_2}-1\right)\frac{\partial C_1}{\partial r}+\left(\frac{1}{\varepsilon_2}-1\right)\left(\frac{B_1}{2}+\frac{B_2}{4}+\frac{B_3}{4}\right)+\frac{\sigma T_2^4}{\pi}=\frac{C_1}{\varepsilon_2} \tag{4.1.29}$$

for the 2nd wall with

$$r_Q=\frac{1-r''^3}{1-r''^2} \tag{4.1.30}$$

If the smaller angle is Θ_1 then let wall three be at Θ_1 and wall four at Θ_2 with emissivity ε_3 and ε_4 and at temperatures T_3 and T_4 respectively. Hence the boundary conditions for the theta direction become

$$\frac{2}{3Kr}\left(\frac{1+\Theta_Q}{\varepsilon_3}-1\right)\frac{\partial C_2}{\partial \Theta}+\left(\frac{1}{\varepsilon_3}-1\right)\left(\frac{B_1}{4}+\frac{B_2}{2}+\frac{B_3}{4}\right)+\frac{\sigma T_3^4}{\pi}=\frac{C_2}{\varepsilon_3} \tag{4.1.31}$$

for wall three and

$$-\frac{2}{3Kr}\left(\frac{1+\Theta_Q}{\varepsilon_4}-1\right)\frac{\partial C_2}{\partial \Theta}+\left(\frac{1}{\varepsilon_4}-1\right)\left(\frac{B_1}{4}+\frac{B_2}{2}+\frac{B_3}{4}\right)+\frac{\sigma T_4^4}{\pi}=\frac{C_2}{\varepsilon_4} \tag{4.1.32}$$

for wall four with

$$\Theta_Q=\frac{1-\Theta''^3}{1-\Theta''^2} \tag{4.1.33}$$

Similarly if Z_1 is smaller than Z_2 then let wall five be at Z_1 and wall six be at Z_2 with emissivity ε_5 and ε_6 and at temperatures T_5 and T_6 respectively. Hence the boundary condition for the Z direction becomes:

$$\frac{2}{3K}\left(\frac{1+Z_Q}{\varepsilon_5}-1\right)\frac{\partial C_3}{\partial z}+\left(\frac{1}{\varepsilon_5}-1\right)\left(\frac{B_1}{4}+\frac{B_2}{4}+\frac{B_3}{2}\right)+\frac{\sigma T_5^4}{\pi}=\frac{C_3}{\varepsilon_5} \tag{4.1.34}$$

for wall five and

$$-\frac{2}{3K}\left(\frac{1+Z_Q}{\varepsilon_6}-1\right)\frac{\partial C_3}{\partial z}+\left(\frac{1}{\varepsilon_6}-1\right)\left(\frac{B_1}{4}+\frac{B_2}{4}+\frac{B_3}{2}\right)+\frac{\sigma T_6^4}{\pi}=\frac{C_3}{\varepsilon_6} \tag{4.1.35}$$

for wall 6, and Z_Q defined as before in section 3.1.3.

The boundary conditions for a general orthogonal system would be similar if the walls followed the axis. For skew walls however, the boundary conditions are more complicated and they are not dealt with in this work.

4.1.4 Relation Between Sources and Temperatures

So far the basic structure of the equations has remained the same. This is primarily because the Taylor's series has been related to the axis. But the flux-source relation is related to the full enclosure so care must be taken in transforming this to other coordinate systems.

Manipulations similar to those described in section (3.1.4) yield the relation

$$q = \frac{4\pi}{3}(A_1, A_2, A_3) \tag{4.1.36}$$

The temperature and the source are connected via $\nabla q = S$ (eq. 1.2.7). Using eq. (4.1.36) and div in cylindrical coordinates, the following relation can easily be derived,

$$\frac{4\pi}{3}\left(\frac{1}{r}\frac{\partial(A_1 r)}{\partial r} + \frac{\partial A_2}{r\partial\theta} + \frac{\partial A_3}{\partial Z}\right) = S \tag{4.1.37}$$

Substituting eqs. (4.1.19), (4.1.20) and (4.1.21) into eq. (4.1.37) and rearranging the terms, gives the following relation

$$-\frac{1}{3rK}\frac{\partial C_1}{\partial r} + \frac{K\sigma T^4}{\pi} - \frac{K}{3}(B_1 + B_2 + B_3) = \frac{S}{4\pi} \tag{4.1.38}$$

Note the extra partial derivative term. In changing to other orthogonal systems, the terms that emerge from the del operator have to be carefully handled. Further similar manipulations can be effected for more general parameters using eqs. (4.1.13), (4.1.14) and (4.1.15).

4.2 Validation Studies in Cylindrical Coordinates

4.2.1 One-Dimensional Solution for an Infinite Cylinder with Black Walls and Constant Source Inside

One dimensional axisymmetric problems can be divided into two types: cylinders and annulii, since the boundary condition of the inner wall for cylinders is different from that of annulii. The case of cylinders is considered first. The governing equation is

$$\frac{1}{K}\frac{d^2C_1}{dr^2} = KB_1 - \frac{K\sigma T^4}{\pi} \tag{4.2.1}$$

from eq. (4.1.25). On the axis there is no net flux so eq. (4.1.36) and eq. (4.1.19),

$$\underline{q} = \frac{4\pi}{3}A_1 = -\frac{4\pi}{3}\frac{\partial C_1}{\partial r} = 0 \tag{4.2.2}$$

The second boundary condition remains the same as eq. (4.1.29). This system can now be solved with temperature replaced by using eq. (4.1.38). Appendix A4.1 solves for only black walls, but results for non unity values of wall emissivities can be derived using a similar approach.

The flux out of the circular wall is

$$q = \frac{Sr_2}{2} \tag{4.2.3}$$

as in equation (A4.1.12). This result is what one would expect from the energy balance equation as given by relation (A4.1.13).

The solution can be tested by examining the ratio of the flux into the wall to the fourth power of the temperature difference between the wall and the centre. The ratio (A4.1.16) is restated:

$$\phi = \frac{-q_W}{(\sigma T_W^4 - \sigma T_C^4)} = \frac{1}{\frac{3}{4\tau_0}(1+r''^2)+\frac{r_Q}{2} + \frac{3}{16}\tau_0} \tag{4.2.4}$$

Here $\tau_0 = 2Kr_2$ is the optical diameter.

Comparisons of the ratio ϕ evaluated by Monte-Carlo and that evaluated by a differential approximation are presented by various authors (see Cess, (1966) for example). Fig. 4.2 compares the present model with $r''^2 = 0$ and $r''2 = 0.5$ with the Monte Carlo solutions. The value of $r''^2 = 0.5$ has been chosen with the aid of Fig. 4.3 whose derivation is explained in section 4.2.2. It can be seen that the results are improved when the value of the parameter r" is 0.707 ($r''^2 = 0.5$). For any particular problem with specified optical thickness, finer adjustment of the parameters can yield better accuracy. Because so many situations are possible and only very few solutions are available, one can only conclude that the model works well for the particular situation considered.

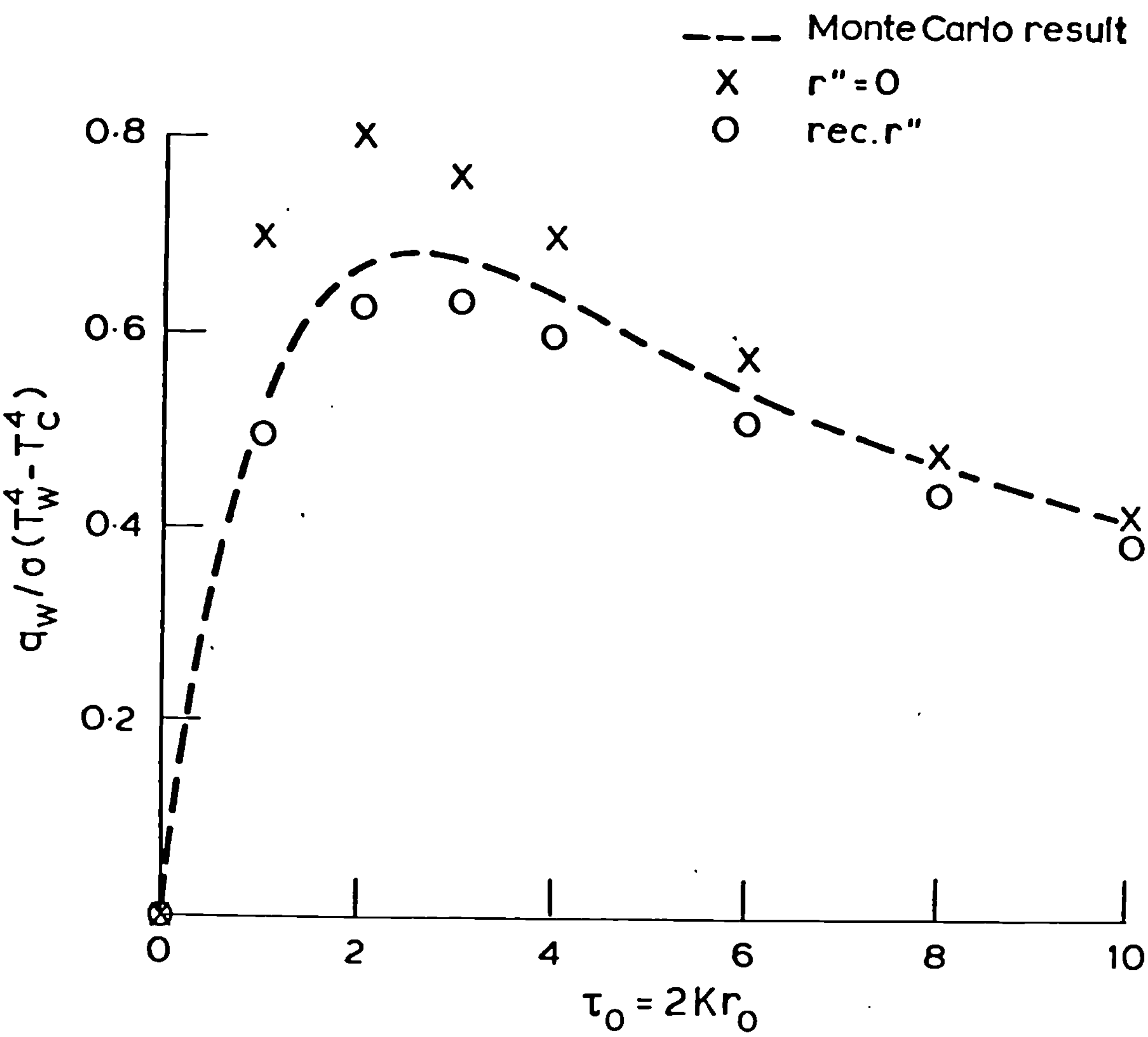

Fig. 4.2 Comparison of results for a circular cylinder with uniform internal heat generation

4.2.2 One-dimensional Solution for an Infinitely Long Set of Co-axial Cylinders with Constant Source Inside

The situation of the inner radius wall diminishing to zero is not necessarily the same as that of a cylinder since in the first case, there may be a net flux out of the inner wall, while in the second case there is no net radial flux on the axis.

Now consider two concentric walls with both temperatures and emissivities prescribed. Let there be a constant heat source S per unit volume inside. The governing equation remains the same, eq. (4.2.1) but the boundary conditions are now described by eqs. (4.1.28) and (4.1.29). Since in this problem, the sources are prescribed, Eq. (4.1.38) is used to elminate the temperature term in the system. The solution of these equations is presented in Appendix A4.2. The results will now be compared with some special restrictions.

As pointed out by many authors, Diessler (1964) and Cess (1966), for instance, the differential type approximations fail for small optical thicknesses especially if the inner radius is small as well. This is also the case for the present model. From the eqs. (A4.2.9) and (A4.2.11) and for no heat source and black walls, the following relationship can be derived, for the ratio ϕ, defined as

$$\phi = \frac{\sigma T_1^4 - \sigma T_2^4}{-q_{W_1}} = \frac{3}{4} K r_1 \ln \frac{r_2}{r_1} + \frac{r_Q}{2} \left(1 + \frac{r_1}{r_2}\right) \qquad (4.2.5)$$

This is equivalent to the Deissler (1964) eq. (31), first order boundary jump solution. The parameter r" hence r_Q can be used to improve the solution in the optically thin regions, especially for r_1 tending to zero. Defining the optical thickness as $\tau_0 = K(r_2 - r_1)$,

ϕ can then be rewritten as

$$\phi = \frac{r_Q}{2}(1 + \frac{r_1}{r_2}) + \frac{3}{4} \frac{\tau_0}{(\frac{r_2}{r_1} - 1)} \ln \frac{r_2}{r_1} \qquad (4.2.6)$$

for every ratio $\frac{r_1}{r_2}$, ϕ should equal 1 for small optical thicknesses. That is

$$\frac{r_Q}{2}(1 + \frac{r_1}{r_2}) = 1 \qquad \text{as} \qquad \tau_0 \rightarrow 0. \qquad (4.2.7)$$

This gives a set of recommendations for r_Q hence r''^2 and r''. If r_Q is linearised to $1/1-r''^2$, a simple straight line recommendation can be derived from the q. (4.2.7) and this is presented in fig. (4.3)

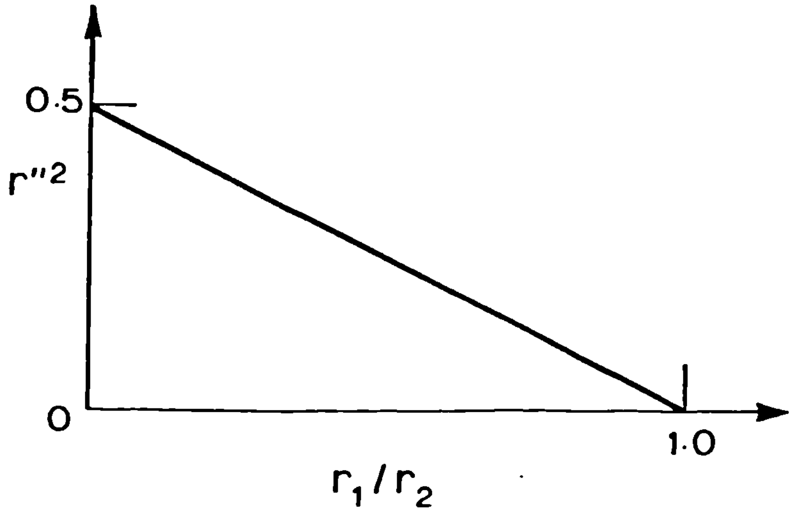

Fig. 4.3 Recommendation of r''^2 for various inner to outer radius ratios

For these recommended values of r_Q, in the case of large optical thicknesses and for the ratio $\frac{r_1}{r_2} = 1$, approximates to

$$\phi = 1 + \frac{3}{4} \tau_0 \qquad (4.2.8)$$

This is also the planar solution (eq. 3.2.22) as one would expect. The optical thickness is plotted in Fig. 4.4 against the reciprocal values of ϕ using r" = 0 and the recommended values of r''^2 from fig. 4.3 and the Monte-Carlo results obtained from (Howell and Prelmutter 1964) for three values of the ratio r_1/r_2. We note that there is marked improvement compared to the specification of r" = 0 everywhere for the simple straight line recommend values of r" from fig. 4.3.

The next case examined is that of co-axial cylinders, with radius ratio $\frac{r_1}{r_2} = 0.1$ and constant source inside. The walls have equal emissivities (ε, say). The value of r_Q is 2 and $r''^2 \approx 0.5$ from figure 4.3. The ratio ϕ is obtained using eqs. (A4.2.9) and (A4.2.11). After substitution of all of the values the following expression for ϕ is obtained:

$$\phi \doteq 0.192 \quad \tau_0 + (\frac{1.55}{\varepsilon_2} - 0.55) + (\frac{1}{\varepsilon_2} - 1)\frac{0.853}{\tau_0} \qquad (4.2.9)$$

For $r_Q = 1$ and r" = 0 the expression for ϕ reduces to

$$\phi = 0.192 \quad \tau_0 + (\frac{2}{\varepsilon_2} - 1)0.55 \qquad (4.2.10)$$

The inverse eqs. (4.2.9) and (4.2.10) are plotted on figs. 4.4 and 4.5 . While the recommendation for r" gave a better solution for the flux for $\frac{r_1}{r_2} = 0.1$ for all optical thicknesses, with black walls in fig. 4.4, the recommendation is in fact worse that than for $r''^2 = 0$ for other values of emissivities as shown in fig. 4.5. This shows that the parameter r" is also dependent on the emissivity of the gases. A table for r''^2 for each $\frac{r_1}{r_2}$ with varying optical thicknesses could be worked out, but this would be too cumbersome to apply in practice.

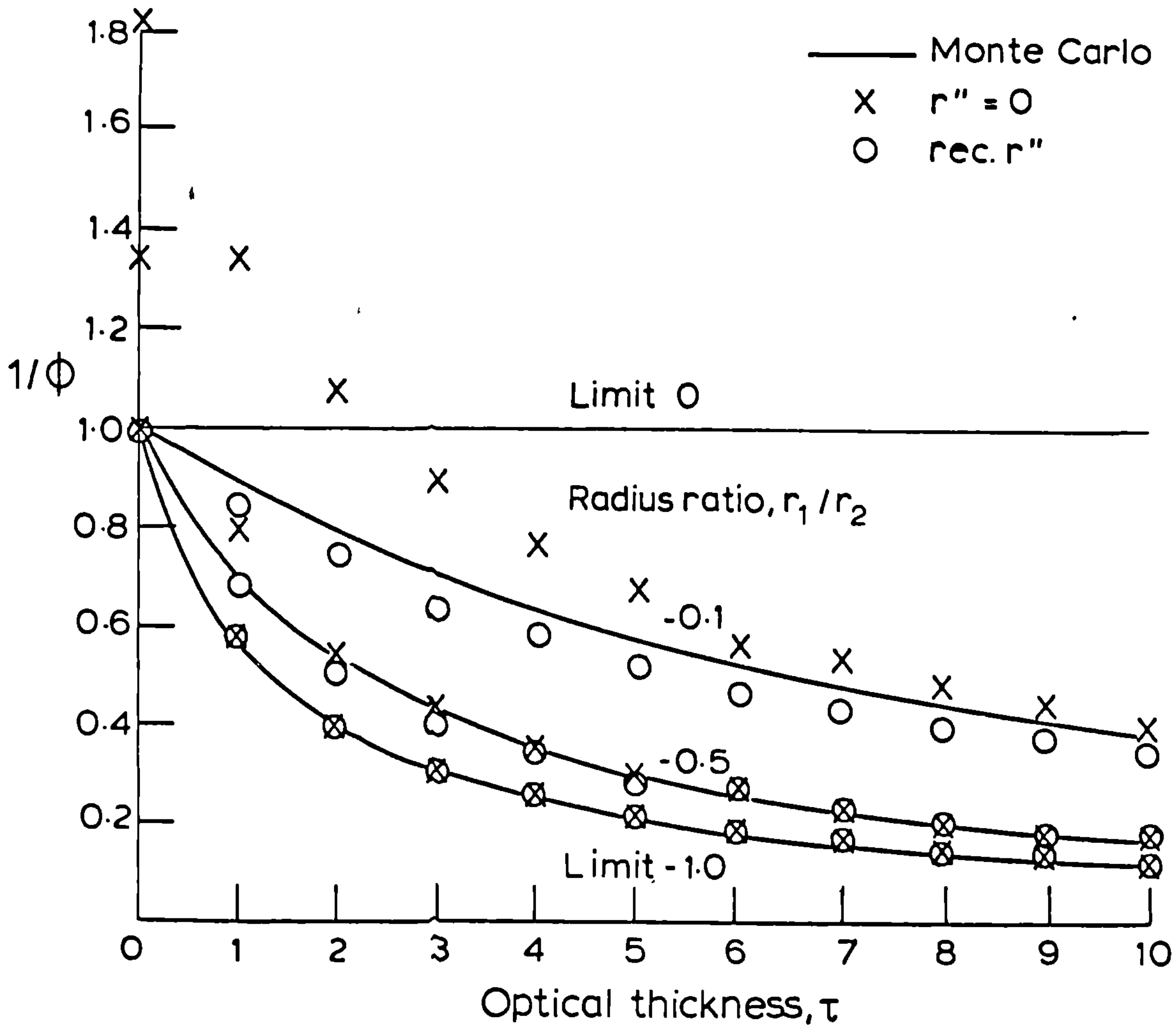

Fig. 4.4 Comparison of eq. (4.2.9) for various optical thicknesses and black walls

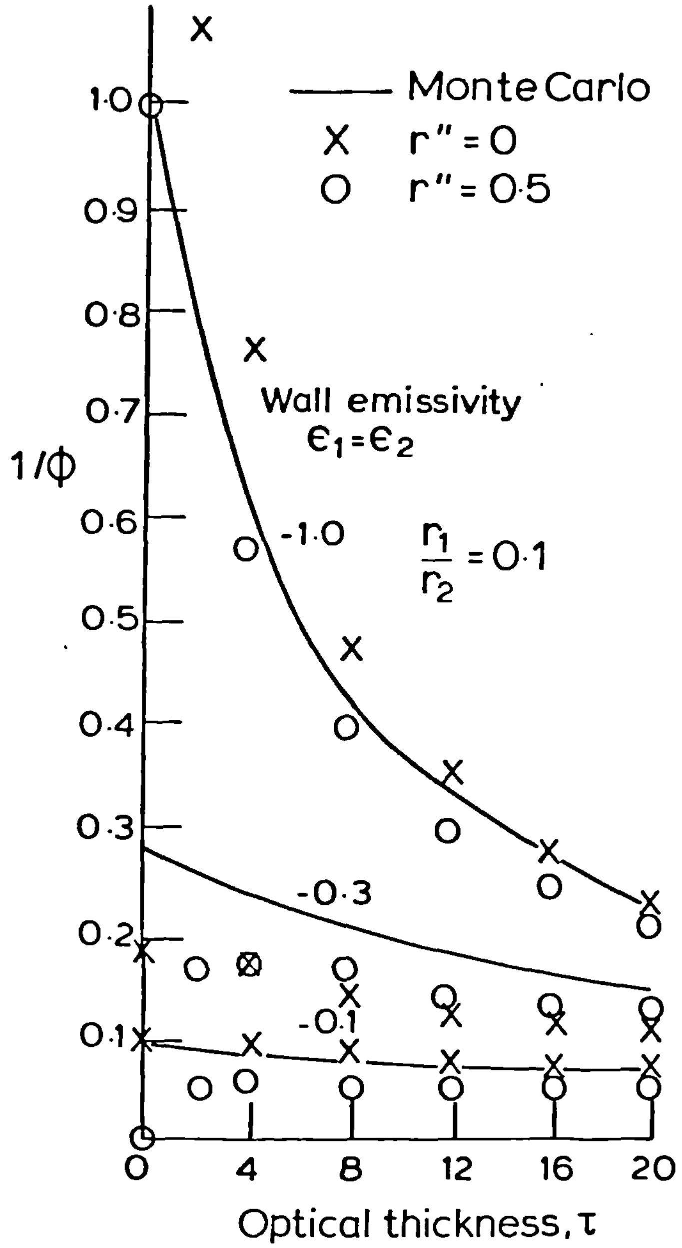

Fig. 4.5 Comparison of eq. (4.2.9) for other values of wall emissivities

CHAPTER 5

A PRINCIPAL FAILING OF THE FLUX MODEL AND SUGGESTED REMEDIES

5.1 The Relation of the Integration Surface Parameters to Other Quantities

5.1.1 The relation between the surface integration parameters and mean free path lengths

So far we have derived a system of three second order flux equations (using eq. 3.1.4 to eq. 3.1.12) and six boundary conditions (eq. 3.1.22) for Cartesian co-ordinates and corresponding equations (eqs. 4.1.10 to 4.1.12 and eqs. 4.1.28 to 4.1.35) for cylindrical co-ordinates. Some one-dimensional cases have been studied, and the flux solutions have been compared with existing analytic and Monte Carlo solutions. It is clear in all the cases studied that the parameters of the flux equations depend on other factors than the optical thicknesses. Two sets of recommendations for the relation between the parameters and the optical thicknesses are presented in section 3.2 (fig. 3.3 and fig. 3.6), for the Cartesian case and (fig. 4.3) for cylindrical case respectively.

We also saw in section 3.2.5 that the extension of the recommended values of the parameters to two and three-dimensional geometries does not yield the expected success, especially in the corner regions. Consider two points on one of the side walls, for the infinitely long square cavity with cold black walls, and hot gas at uniform temperature inside. Let one point be at the centre and another near the corner. For the point in the centre, all walls are distant by the same order of magnitude. While for the second point, two walls are a small distance away and the other two are very far (fig. 5.1). Hence some kind of procedure is needed for characterising the mean free path or mean optical depth. We would then be able to apply one-dimensional recommendations more confidently. In theory many representative directions may be considered, but we choose to find the mean of only two lengths at 45^o to the co-ordinate axis (fig. 5.1). The mean free path length is then

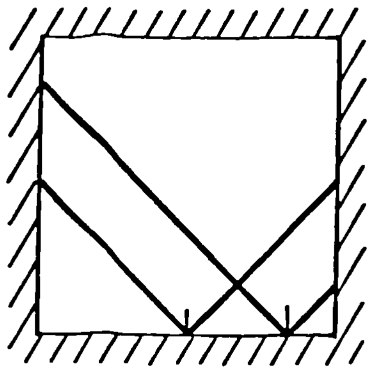

Fig. 5.1 The lengths taken to determine the mean free path length

proportional to the mean of the two lengths. An arbitrary number 0.1 was used for the constant of proportionality. The new recommendation for the values of X" and Y" are then read off from the one-dimensional recommendations. Immediately this is done, we obtain better overall fluxes, especially near the corners as shown in fig. 5.2 .

While this simple method appears to have merit, difficulties can be foreseen. For instance if the absorption coefficient varies continually as an iteration procedure for the flow develops, the mean free path lengths would have to be evaluated at every iteration and this may not be desirable. In any case the procedure cannot be universal and a complete validation coverage is hardly practicable.

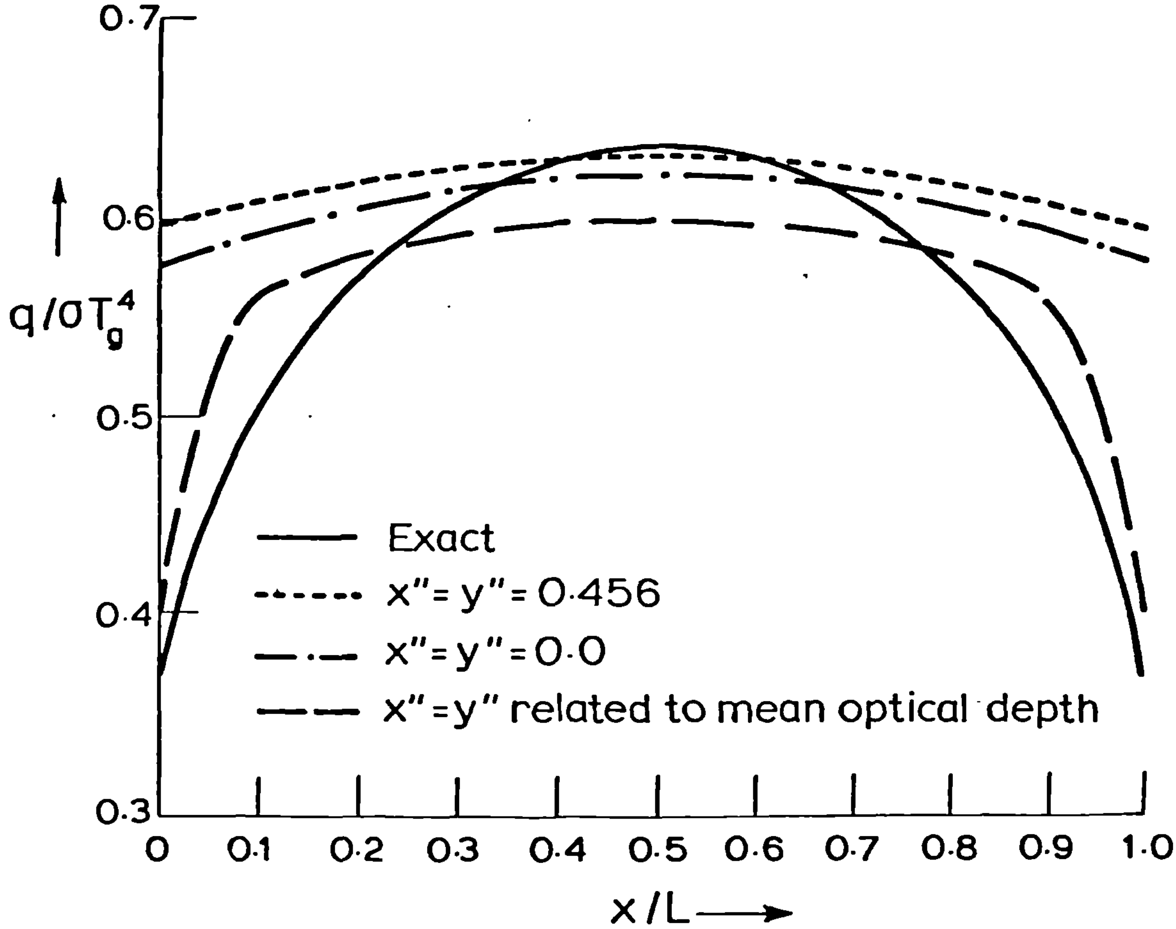

Fig. 5.2 Comparison between the exact wall heat flux and the flux model predictions

5.1.2 The relation of the integration surface parameters and the intensity distribution

While examining the one-dimensional test cases, it was concluded that the optimal integration surface parameters were related to not only the optical thicknesses, but also other quantities such as the wall temperatures, emissivities, source strength, etc.

Intensity is a quantity that depends on all the above variables. To explore further, the nature of the problems, we return to the initial form of the series for intensity eq. (3.1.1)

$$I = A_1X' + A_2Y' + A_3Z' + B_1X'^2 + B_2Y'^2 + B_3Z'^2 \tag{3.1.1}$$

Consider for simplicity a distribution of intensity for zero flux, that is $A_i = A_2 = A_3 = 0.0$. Next let $B_3 = 0$ to facilitate plotting. We now have a two-dimensional problem, but the extension of the following hypothesis can easily be carried to three-dimensional situations.

Now for $B_1 \neq B_2$ the intensity distribution becomes an ellipse (fig. 5.3), and for $B_1 = B_2$, the intensity distribution is isotropic.

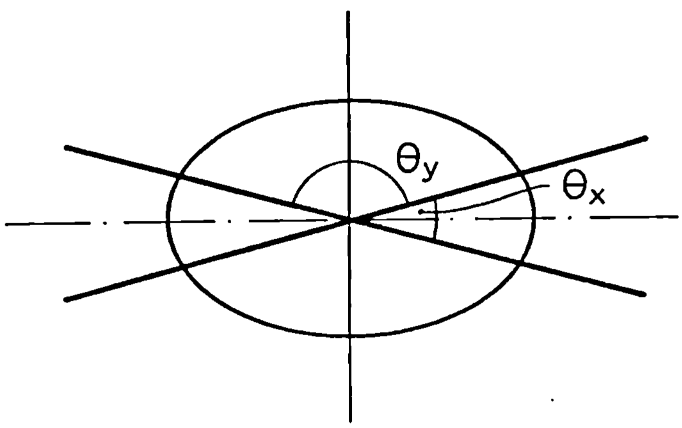

Fig. 5.3 Regions where the difference between the maximum gradient and minimum gradient is less than a certain amount

For isotropic distribution the surfaces of integration are equal (X" = Y"). If we set an upper limit to the amount of change of intensity within an integration surface region, we get two regions, θ_x and θ_y (fig. 5.3). For a case $B_1 > B_2$, the θ_x region will be smaller than θ_y, hence X" >Y" and vice versa. We can relate these ideas by the following mathematical relationships.

$$X'' = \gamma \frac{|B_1|}{\sqrt{(B_1^2+B_2^2+B_3^2)}} \tag{5.1.1}$$

$$Y'' = \gamma \frac{|B_2|}{\sqrt{(B_1^2+B_2^2+B_3^2)}} \tag{5.1.2}$$

$$Z'' = \gamma \frac{|B_3|}{\sqrt{(B_1^2+B_2^2+B_3^2)}} \tag{5.1.3}$$

Again it is impossible to test satisfactorily the above formulation. Vast numbers of intensity distributions would need to be studied before solid conclusions can be arrived at. We have taken the value of γ as 0.1.

This recommendation of X", Y" and Z" is applied to an elongated box with dimensions 4m x 1m x 1m and black walls with temperatures prescribed as:

X = 0.0 ; T = 1200K

X = 4.0, Y = 0.0, Z = 1.0; T = 300K

Y = 1.0, Z = 0.0 ; T = 50K

This case has been studied by DeMarco (1974) and the net flux results were produced by Gibb and Jenner (1974) using the Monte Carlo technique. The grid used was 16 x 4 x 4 (fig. 5.4). The system is in stable equilibrium (i.e. no heat sources) and the absorption coefficient is 2.0. Table (5.1) shows the heat flux at the hot wall ($X = 0.0$) for two cases (a) all parameters $X'' = Y'' = Z'' = 0.0$ and (b) varying parameters according to the relations (5.1.1) to (5.1.3). It can be seen that the results are generally improved especially at the corners. This one test shows no more than that the hypothesis may be useful. It is worth mentioning that it has been used when incorporating the present flux models in flow procedures at Imperial College, Abou Ellail, 1978 .

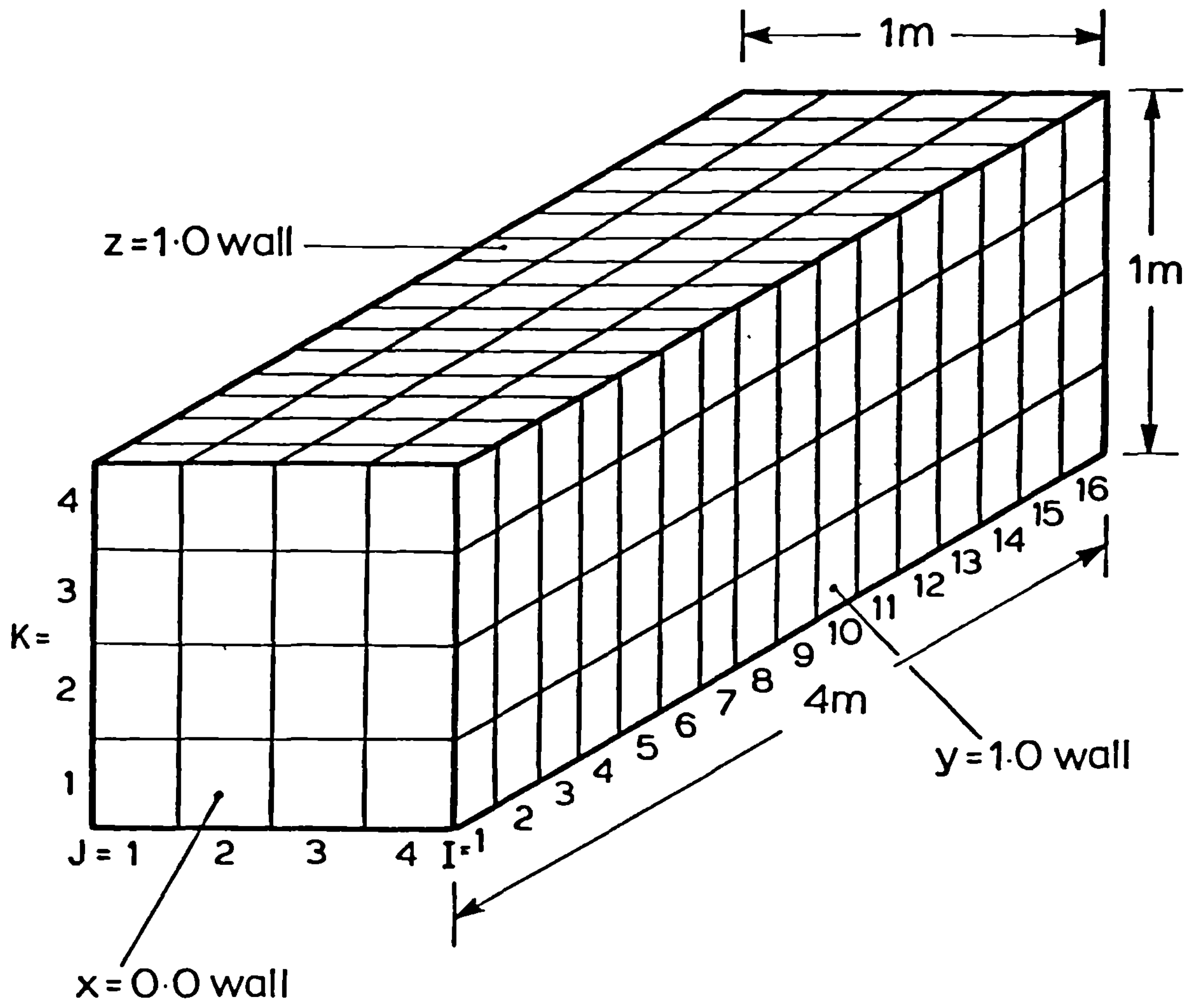

Fig. 5.4 Elongated Box Test Case

		J = 1	J = 2	J = 3	J = 4
	E	$-10.0.10^4$	$-9.39.10^4$	$-9.50.10^4$	$-10.0.10^4$
K = 4	PM1	$-9.49.10^4$	$-9.20.10^4$	$-9.20.10^4$	$-9.50.10^4$
	PM2	$-9.89.10^4$	$-9.53.10^4$	$-9.53.10^4$	$-9.91.10^4$
	E	$-9.47.10^4$	$-8.81.10^4$	$-8.67.10^4$	$-9.57.10^4$
K = 3	PM1	$-9.19.10^4$	$-8.85.10^4$	$-8.85.10^4$	$-9.20.10^4$
	PM2	$-9.44.10^4$	$-8.99.10^4$	$-8.99.10^4$	$-9.45.10^4$
	E	$-9.51.10^4$	$-8.65.10^4$	$-8.72.10^4$	$-9.27.10^4$
K = 2	PM1	$-9.19.10^4$	$-8.84.10^4$	$-8.85.10^4$	$-9.20.10^4$
	PM2	$-9.44.10^4$	$-8.99.10^4$	$-8.99.10^4$	$-9.45.10^4$
	E	$-10.1.10^4$	$-9.52.10^4$	$-9.51.10^4$	$-10.0.10^4$
K = 1	PM1	$-9.45.10^4$	$-9.19.10^4$	$-9.19.10^4$	$-9.49.10^4$
	PM2	$-9.91.10^4$	$-9.54.10^4$	$-9.55.10^4$	$-9.92.10^4$

Wall $x = x_{min}$, K = 2.0: S = 0; E = exact;

PM1: $x'' = y'' = z'' = 0$; PM2 = relations (5.1.1) to (5.1.3)

Table 5.1 Comparison of approximated and exact heat flux predictions for elongated box of fig. 5.4

5.2 A Principle Failing and a Suggested Remedy

5.2.1 A Principal Failing

What has been steadily emerging from sections 5.1.1 and 5.1.2 is that the intensity distribution plays the major role in determining the accuracy of a particular method rather than the flux comparisons which have constituted the chosen criterion throughout almost the whole literature on thermal radiation. Of course there are major practical difficulties involved. The proper utilising of the validation information for flux predictions is a major task, but obtaining and comparing data of the intensity distributions for each individual case represents an even greater undertaking.

Nevertheless some very interesting underlying facts can be brought to light by studying the few intensity distributions that can be calculated analytically. All the flux methods effectively make an assumption about the intensity distribution, (the present model is based on a continuous intensity distribution). So the most stringent case would be a case where intensity distribution is discontinuous.

A number of one-dimensional cases have been studied. The following case brings to light some fundamental ideas. Consider two infinitely long cold black parallel walls containing gas at uniform temperature (σT_g^4 = 1.0). Let the optical distaince (KL) between the plates be 1.0. Now relatively cool walls with high absorptivity bounding hot gas is not an uncommon situation in practice. The solution of flux equations with all parameters yields 0.7294, while the analytic solution gives 0.7806 as shown in section 3.2.4. The recommended value for X"(X" = 0.456) was selected so as to cause the flux model solution for heat transfer to agree with the analytical solution. The supposition that adjusting X" to give correspondence between the flux model and analytic heat transfers would seem reasonable, but this proves not to be the case as we can see by examining comparisons of the flux model and analytic intensity distributions.

Rotating anti-clockwise from the normal at the wall, since the wall is cold and black, there is no emission of energy from 0^{o} to 90^{o}. For small angles with respect to the wall, radiation is received from locations on the opposite wall that are very distant so the intensity here nears unity. As we approach the normal, radiation arrives from points only unit optical depth away (fig. 5.5). The exact solution is evaluated using the analysis in the next Chapter. Also plotted on fig. 5.5 is the solution obtained using the present flux method keeping X" equal to zero.

While the heat flux agreement was reasonable for the flux model, the intensity distribution is not even physically realistic, since for some angles, the intensity is in fact negative. The flux model solution using the recommended values of X" = 0.456 is shown in fig. 5.6. The problem of negative intensities still exists though on a slightly lesser scale. The negative intensities must to some extent be expected since we are approximating a discontinuous distribution by a continuous Taylor's series with only two terms (for a one-dimensional geometry). If the walls were non black, and/or at finite temperature the problem would be less since the true intensity distribution would not be zero in the range 0^{o} to 90^{o}.

A discontinuous intensity distribution flux model would clearly have been preferable in the above example; however, it is not difficult to construct another test case example characterized by a continuous intensity distribution for which a discontinuous intensity distribution flux model would fail. For instance in a central region for a case where the distribution is a thin ellipsoid (fig. 5.3). In the region where the change is sharp, (along the X axis) a discontinuous method would have to assume constant intensity over the whole prespecified angle.

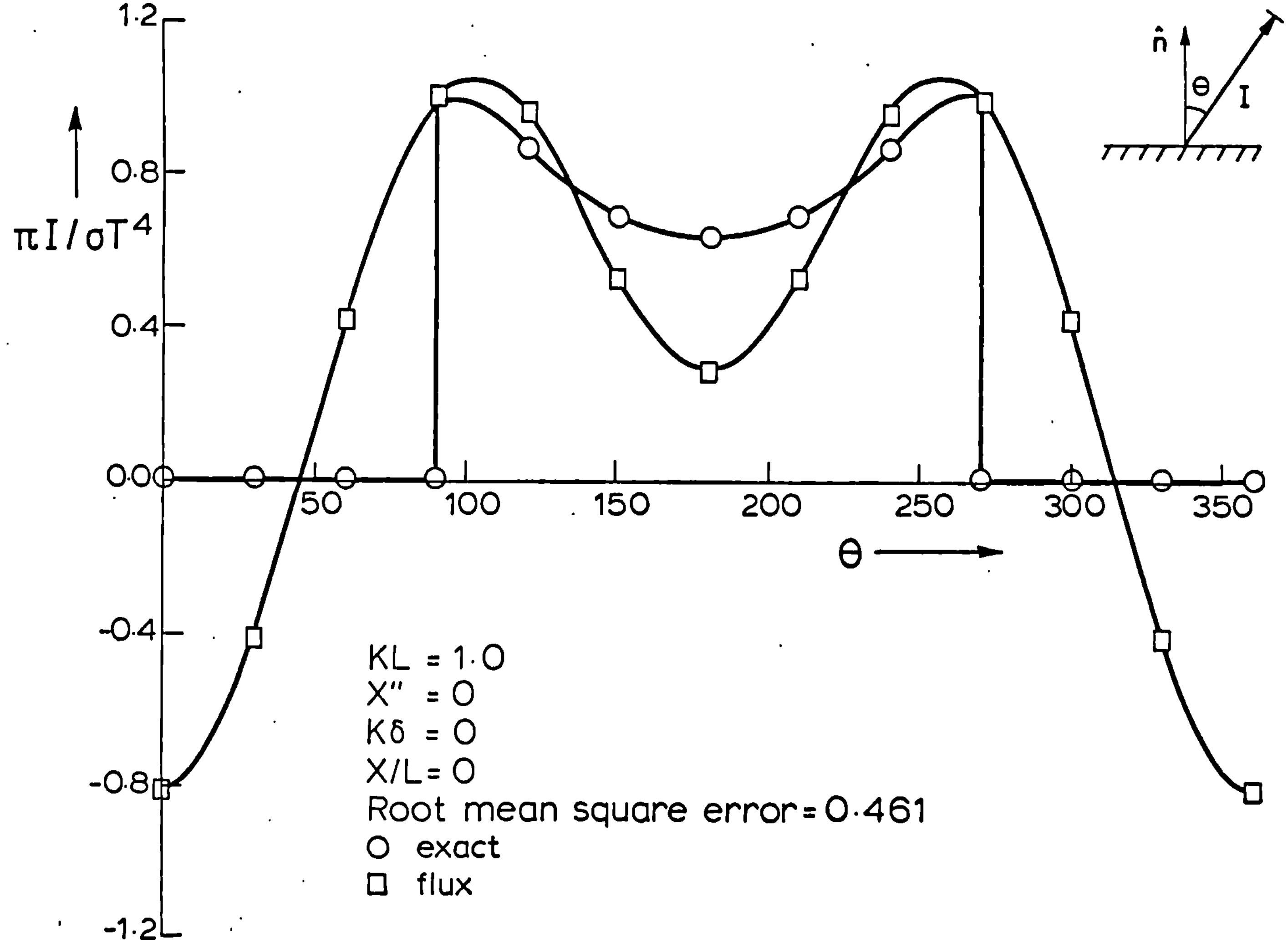

Fig. 5.5 Comparison of analytic and flux intensity distribution at the wall

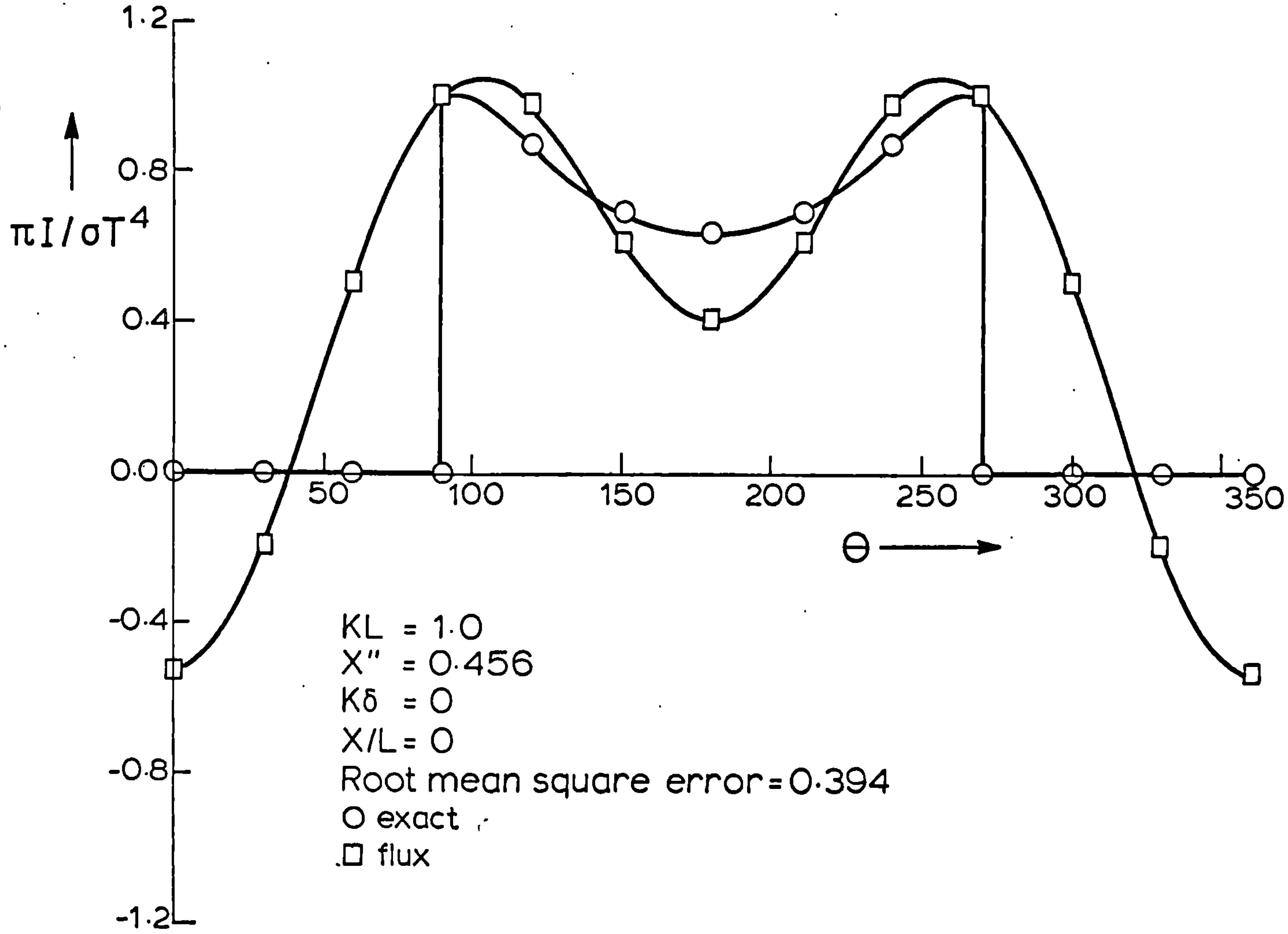

Fig. 5.6 Comparison of analytic and flux (x" = 0.456) intensity distribution at the wall

We see that the reliability of a model must depend on the type of intensity distribution expected in a particular application. In practice, continuous intensity distributions are more common in the inner regions, while the intensity distributions are usually discontinous or nearly so near the walls.

5.2.2 The Boundary Layer Remedy

In principle more terms in the Taylor series could be retained to solve problems similar to the one described in section 5.2.1, but the demands of computer economy of general prediction procedures mentioned in section 1.1.1, are well known. Also higher order methods do not give significant improvement in the centre regions. Hence some special method needs to be devised for boundary regions for the present flux model.

For most problems, the regions of greatest intensity gradient changes with respect to direction are usually near the boundaries. We consider a thin region near a black wall and refer to it, using fluid mechanical terminology, as the 'boundary layer'. The thickness of this layer is such that terms of order $(K\delta)^2$, where K is the absorption coefficient and δ the layer thickness, can be neglected. In this region, the temperature is assumed to be constant, although not necessarily that of the wall. Hence we can solve analytically for the boundary condition at the displaced boundary in the gas; this temperature is given by

$$\frac{2}{3} X_Q A_1 + C_1 = \left(\frac{\sigma T_g^4}{\pi} - \frac{\sigma T_1^4}{\pi}\right) \frac{2K\delta}{1+X''} + \frac{\sigma T_1^4}{\pi} \qquad (5.2.1)$$

at distance δ from the wall and similarly

$$- \frac{2}{3} X_Q A_1 + C_1 = \left(\frac{\sigma T_g^4}{\pi} - \frac{\sigma T_2^4}{\pi}\right) \frac{2K\delta}{1+X''} + \frac{\sigma T_2^4}{\pi} \tag{5.2.2}$$

at $(L-\delta)$, where the second wall is distance L from the first wall. The derivation of equations (5.2.1) and (5.2.2) appears in appendix (A5.1). Hence using eq. (3.1.22) the flux out of wall 1 is now

$$q_{W1} = \left[- \frac{2\pi}{3} A_1 + \frac{\pi}{2} B_1 + \frac{\pi}{2} B_2 + \frac{\pi}{4} B_3\right] + K\delta\left[\pi A_1 - \frac{2\pi}{3}(B_1+B_2+B_3)\right]$$

$$+ 2K\delta(\sigma T_g^4 - \sigma T_1^4) \tag{5.2.3}$$

(equation A5.1.7). Similar boundary conditions can also be derived for source prescribed problems (refer to appendix A5.3).

5.2.3 Application of Boundary Layer Remedy

We re-examine the problem discussed in section 5.2.1, namely two parallel cold black walls, infinitely long and a unit optical distance apart. The gas inside is hot ($\sigma T_g^4 = 1.0$) and at a uniform temperature everywhere. Fig. (5.7) shows the solution of the intensity distribution at distance 0.1 in the absence of the boundary layers treatment. The analytic intensity distribution is smoother here as expected. The parameters in the present model are all zero. The flux model intensity distribution (for X" = 0) is 'less negative'. In fig. (5.8) the intensity distribution is plotted for the present model with the recommended value of X" = 0.456. The

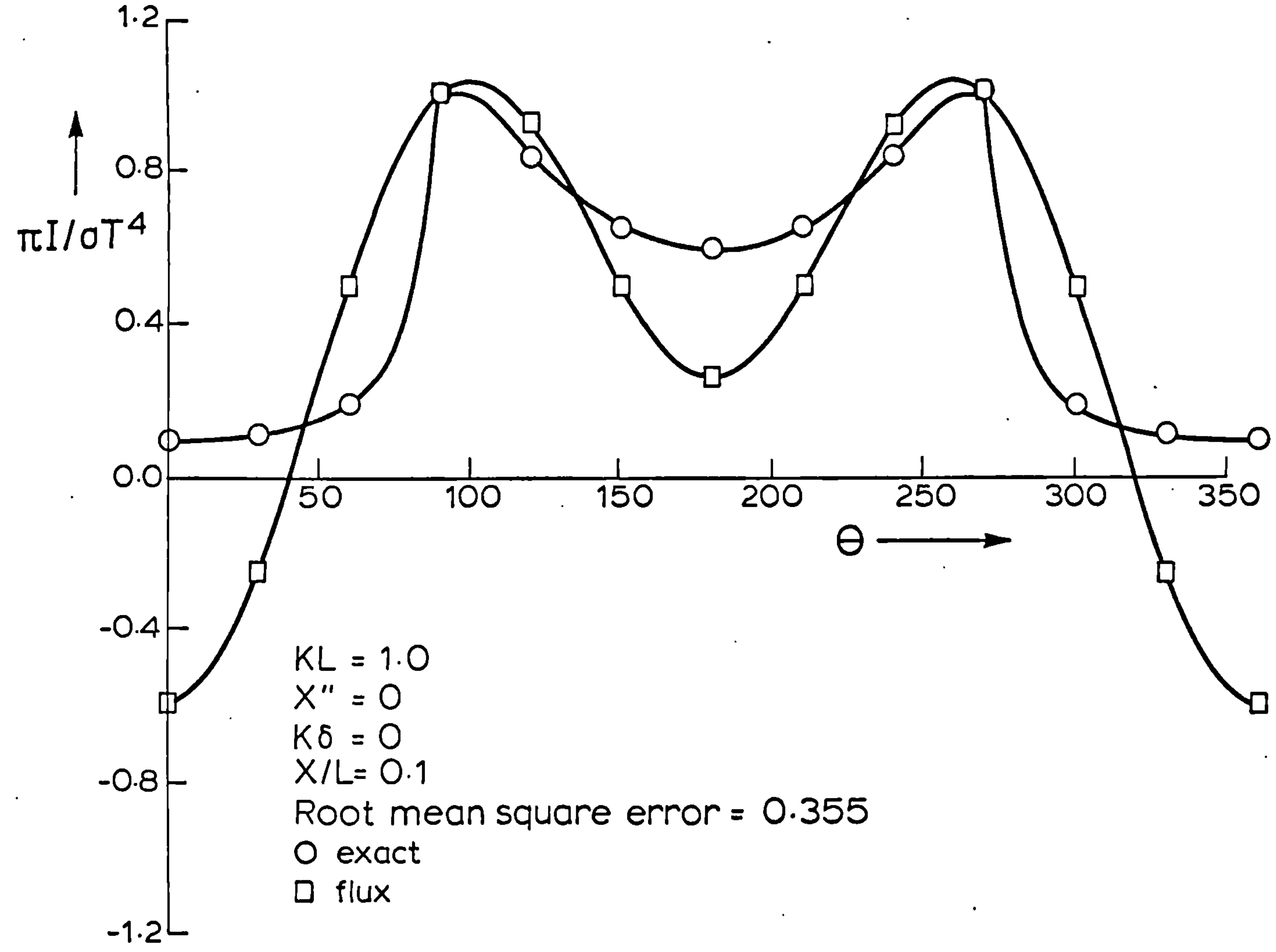

Fig. 5.7 Comparison of analytic and flux intensity distributions a distance δ from the wall, in the absence of boundary layers and integration parameters

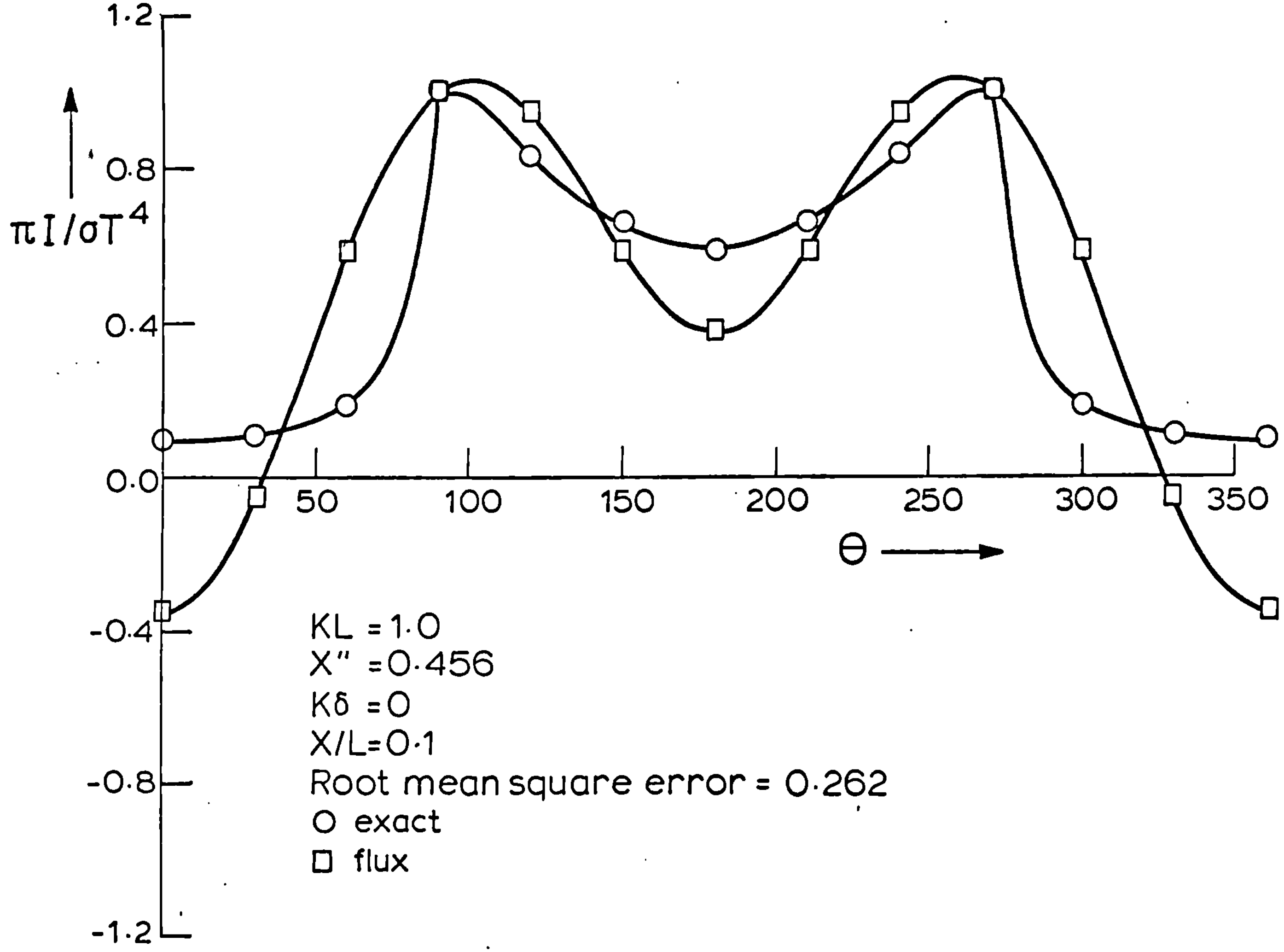

Fig. 5.8 Comparison of analytic and flux ($x'' = 0.456$) intensity distributions a distance δ from the wall, in the absence of boundary layers

root mean square error is improved. Next the boundary layer formulation is applied. The general solution is presented in appendix A5.2 . The root mean square error is further improved. Although the intensity still exhibits negative values (fig. 5.9), they now only occur over a small region.

Using the results shown in appendix A5.2, for each optical thickness, we can choose values for both the boundary layer thickness and parameter X" to give exact fluxes. Table 5.2 shows recommendations for a few optical thicknesses. The intermediate values may be obtained by simpler linear interpolation. A boundary layer thickness of 0.1 is chosen for the corresponding values of X". For regions of less than optical thickness 0.2, the whole region is treated as optically thin. It should be noted that these recommendations give improved flux predictions when the sources are prescribed in one-dimensional analysis.

KL/2	X"	$k\delta$
0.05	-	0.05
0.25	0.360	0.1
0.5	0.455	0.1
1.0	0.398	0.1
750	0.354	0

Table 5.2 Values of X" for some optical thicknesses for a boundary layer thickness of 0.1

The whole concept of boundary layers has helped in the understanding of the real problems associated with the calculation of thermal radiation. It has provided a new means of assessing the various types of models available in the literature. We have learned that continuous intensity distribution problems need different models compared to the discontinuous ones.

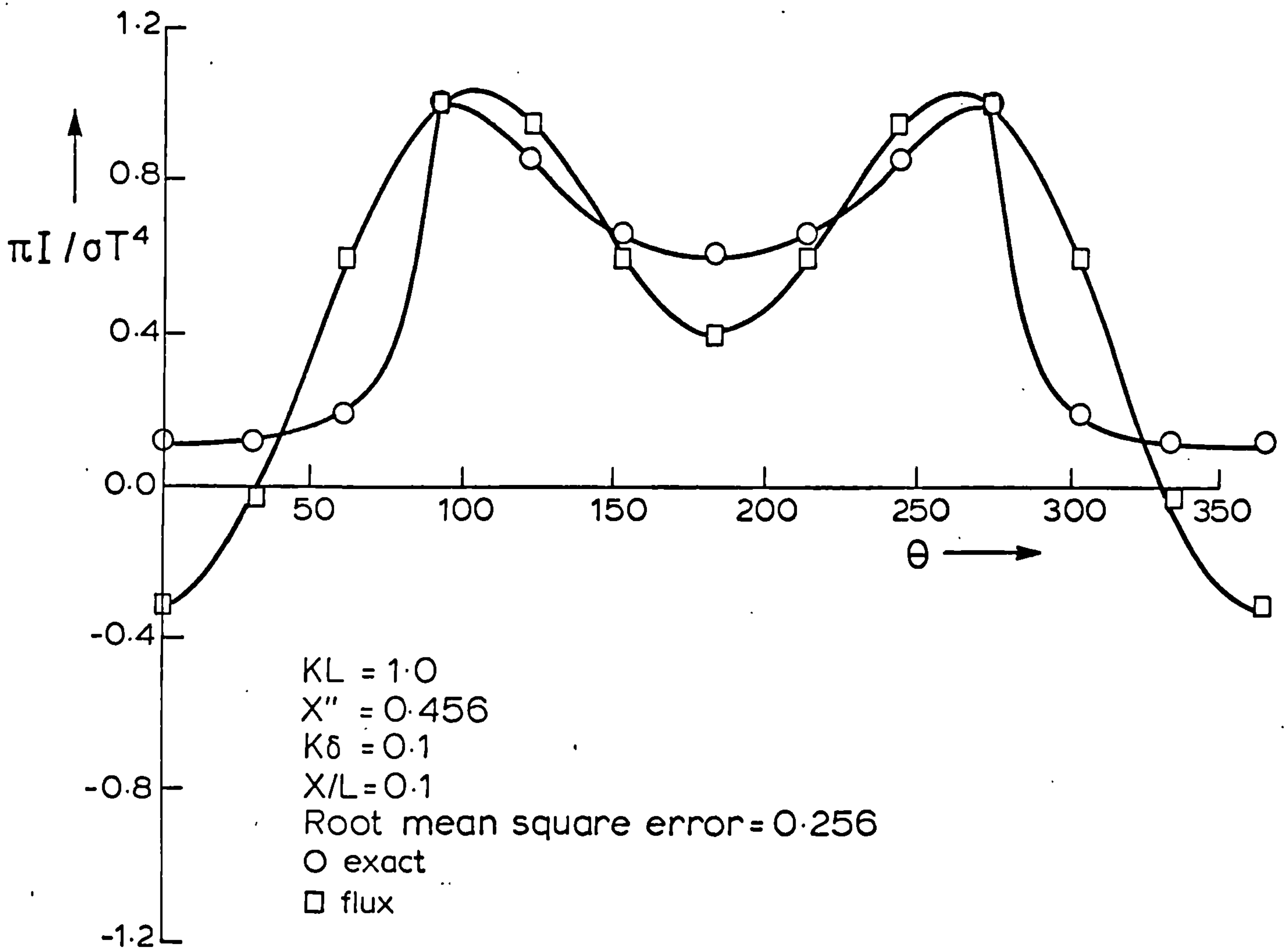

Fig. 5.9 Comparison of analytic and flux (X" = 0.456) intensity distributions a distance δ from the wall, with boundary layers

However the application of the boundary layer treatment in practice would normally demand a different grid system than that of a flow procedure. Also three extra parameters need to be optimised in a system that already comprises three radiation parameters not to mention the many parameters of the other physical models embodied by a complete combustion chamber prediction procedure. The application of boundary layers is further complicated by non-uniform absorption coefficients which implies supplying the whole table of recommended values of X" for various boundary layer thicknesses.

We choose to side-step these problems and adopt a totally new approach based on information and experience gathered in this chapter. We commence its description in the next chapter.

CHAPTER 6

A NEW "DISCRETE TRANSFER" METHOD FOR THE CALCULATION OF RADIATIVE TRANSFER

6.1 Description of the basic method

6.1.1 Limitations of Other Methods

When looking at the limitations of other methods, the kind of applications we have in mind are for very general circumstances. For instance, the shape of the enclosure need not be restricted to a Cartesian or axisymmetric geometries.

The zone method uses a far greater proportion of the calculation time compared to the usual relative importance of radiative transfer but it might be useful near the final emergence of a solution. However, its excessive storage requirement cannot be justified.

For the Monte Carlo type approach, there is always the problem of statistical error and again because of its relative slowness its only use would be near the final emergence of a solution when the radiative transfer is not very predominant, such methods really have no justification at all. The scatter due to the statistical error can be seen in Fig. 8.2, some kind of curve fitting is necessary.

Most flux methods are adequate and economic if the influences from the radiative transfer are not predominant except, of course, if special co-ordinate systems are required, as they often are, in which case all the equations have to be re-derived. The obtaining of greater accuracy by retaining more coefficients means in practice, at least, extra three-dimensional storages are required. Flux methods will not in general yield good results especially near the edges. Special modifications or parameters can be helpful, but one of sufficient universality for engineering purposes do not exist.

A new method will now be described which is essentially a mixture of the flux, Monte Carlo and Zone methods. We choose to call it the "Discrete Transfer" method.

6.1.2 Some Terminology

The points that form a small control volume (grid cell) are termed the grid vertices. The surface that divides each control volume and which passes through these grid vertices is called the grid wall, and the curves that lie on this grid wall, and join grid vertices are called grid lines (fig. 6.1). In two dimensions, grid walls and grid lines are the same. In one dimension, grid walls, grid lines and grid vertices are all the same.

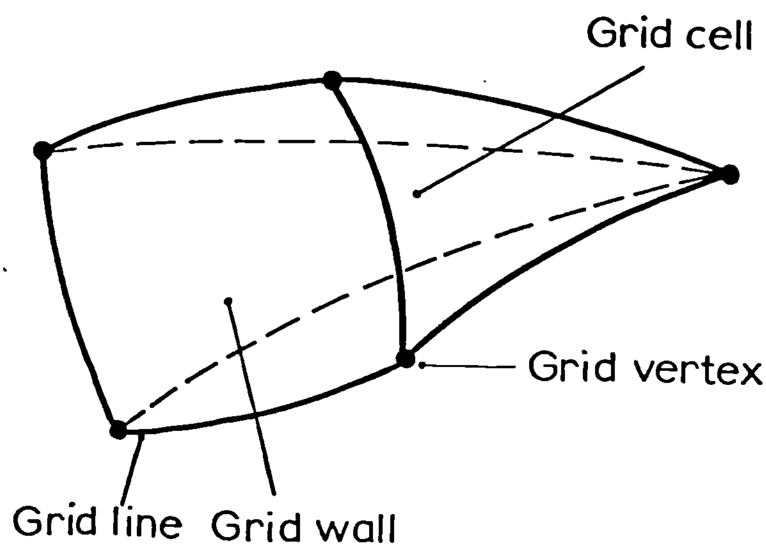

Fig. 6.1 Definition of grid vertex, grid line and grid wall

The chamber wall cell is part of the boundary surface. The wall where a ray begins is termed the origin wall and the wall where the ray ends is termed the impinged wall (fig. 6.2).

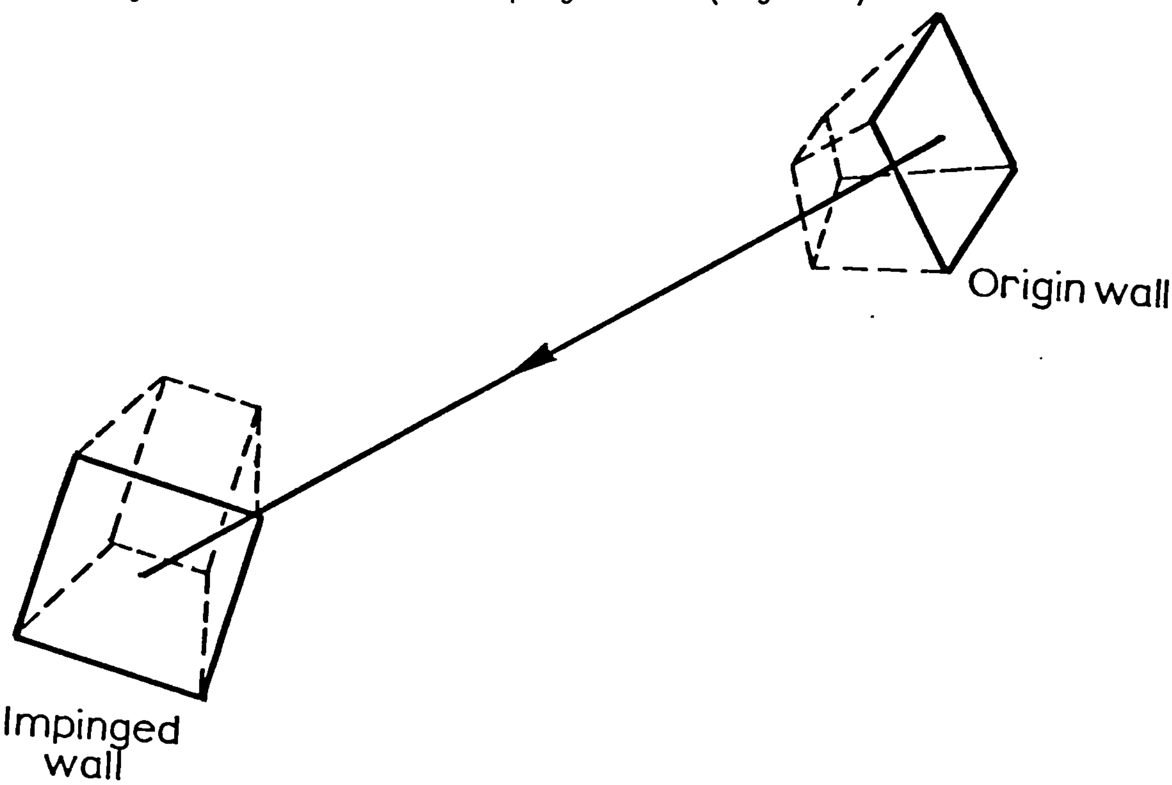

Fig. 6.2 Definition of origin wall and impinged wall

Of course if an identical ray is travelling in the opposite direction, the walls would change names. That is the origin wall would now become the impinged wall, and the impinged wall would become the origin wall.

6.1.3 Basic Features of the Discrete Transfer Method

Consider the transport equation (eq. 1.2.1)

$$\frac{dI}{ds} = - KI + \frac{K\sigma T^4}{\pi} \tag{6.1.1}$$

This equation describes the change in intensity of a ray passing through an absorbing and emitting medium at temperature T. Consider a ray traversing the n'th grid cell (fig. 6.3) of uniform temperature (T_g) and absorption coefficient (K). We can analytically integrate eq. (6.1.1) along the ray to yield a recurrence relation:

$$I_{n+1} = \frac{\sigma T_g^4}{\pi}(1 - e^{-Ks}) + I_n e^{-Ks} \tag{6.1.2}$$

where I_n is theintensity of the ray on entry to the grid cell, I_{n+1} is the intensity of the ray on exiting from the grid cell and s is the distance travelled by the ray in the grid cell (fig. 6.3).

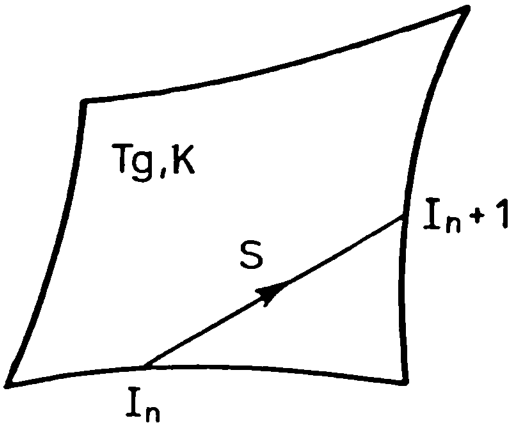

Fig. 6.3 A ray traversing a grid cell

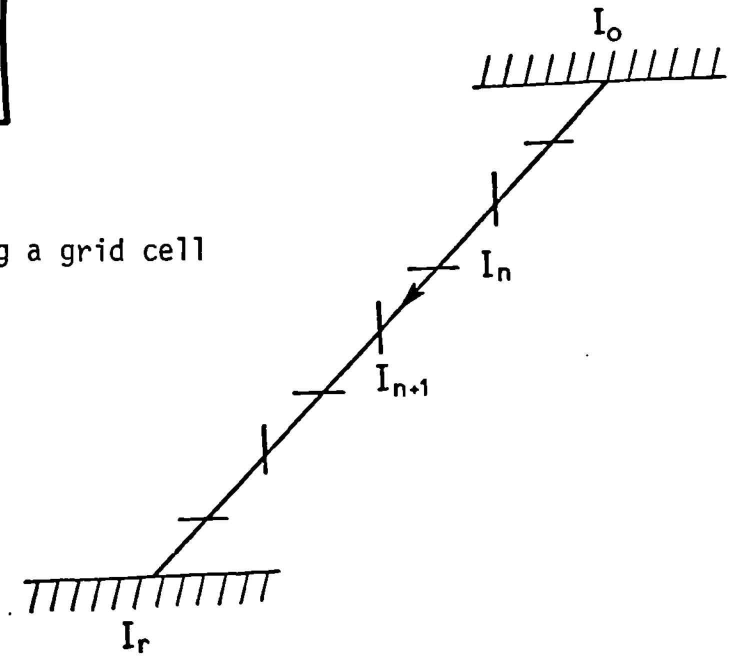

Fig. 6.4 The grid walls traversed as the ray travels from origin wall to impinged wall

If I_o is the intensity leaving a surface (fig. 6.4) the recurrence relation 6.1.2 can be applied repeatedly until the ray impinges on a wall (I_r) and is absorbed/reflected.

6.1.4 Boundary Conditions and Evaluation of the Fluxes

Adhering to the convention of section 1.2.2, the definitions for q_+ and q_- are the fluxes leaving and the fluxes arriving at a wall respectively. The boundary condition stated in eq. (1.2.6) remains the same. If the surface is a Lambert one, it emits isotropically. Hence the intensity (I_o) in every direction is:

$$I_o = \frac{q_+}{\pi} = (1-\varepsilon)\,\frac{q_-}{\pi} + \frac{\varepsilon\sigma T_W^4}{\pi} \qquad (6.1.3)$$

If the net flux is prescribed then eq. (1.2.5) is used and by similar reasoning, we can write

$$I_o = \frac{q_+}{\pi} = \frac{q}{\pi} + \frac{q_-}{\pi} \qquad (6.1.4)$$

where q is the prescribed flux. For adiabatic walls q = 0. If a wall reflects specularly, (like a mirror), then we reflect every ray that impinges on the wall individually and with no change in intensity. Extensions to more complicated boundary conditions can also be incorporated. For example, a part specular and part diffuse reflector.

In order to evaluate q_-, (the incident flux) first we discretise the integral (eq. 1.2.4) into a number of small solid angles. Then we calculate the intensity for each representative ray impinging at this point for every sub-solid angle and sum over the whole hemi-sphere (fig. 6.5). Subsequently q_+ can be calculated from eq. (6.1.3) when T_W is known, or from eq. (6.1.4) when q is known.

If the walls are black, then the I_o's in eq. (6.1.3) do not depend on the value of q_-, therefore the solution is complete when q_- at the point p has been evaluated. On the other hand, if the walls are non-black but Lambert surfaces, the solution must be evolved iteratively.

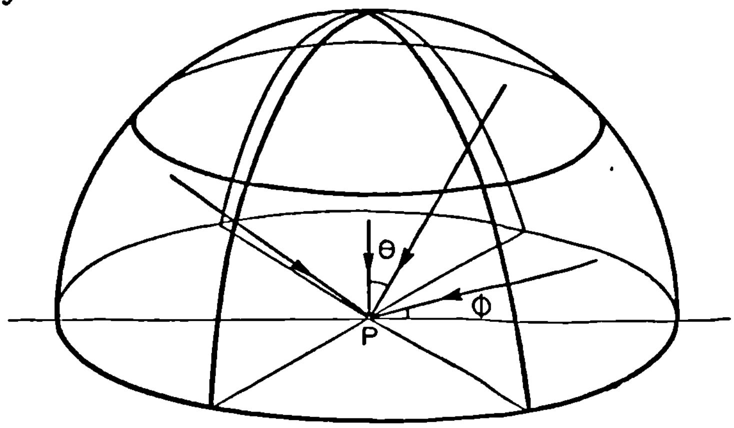

Fig. 6.5 Some typical rays of the hemisphere

6.1.5 Recovering the Sources

Ideally in order to evaluate the cell sources, we need to evaluate q_+ and q_- at a point on every cell wall bydiscretising the integrations (eq. 1.2.3 and 1.2.4) over the solid angles 2π by fixing new rays from these points and applying the existing values of q_-, q_+ and I_0 at the chamber boundaries as boundary conditions for these new rays. This enables us to obtain the fluxes at all cell walls, so sources can be evaluated using eq. (1.2.7). This seems, however, a waste

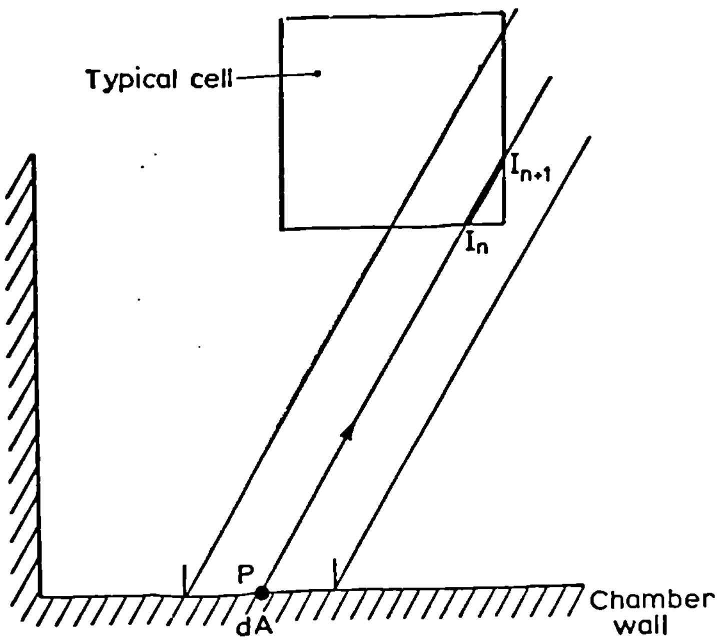

Fig. 6.6 The energy left by a ray as it traverses a typical cell

of effort since these new rays are similar to the ones already considered to evaluate q_- on the chamber boundaries.

An approximate method is adapted. From eq. (1.2.7), it follows that:

$$\int_{\text{volume}} \nabla q . dv = \int_{\text{surface}} q\underline{dA} = \int_{\text{volume}} S dv \qquad (6.1.5)$$

To obtain the source in each cell, we accumulate the amount of energy "left" behind by the rays as they traverse each cell. The energy left behind as a ray crosses a typical grid cell is given by:

$$S_n = (I_{n+1} - I_n)\underline{\Omega} d\Omega \underline{dA} \qquad (6.1.6)$$

Since the area at the origin does not always coincide with the area of the cell wall impinged both in magnitude and orientation we choose to consider a pencil of rays of area equal to the area of the cell wall at the chamber boundary, and containing point P, from which the ray originates (see fig. 6.6).

As can be seen in fig. 6.6, ideally, only a fraction of the pencil of rays should be accumulated in the cell through which a typical ray passes, the rest must be added to the neighbouring cells. There are other typical rays in the same direction which do not pass through neighbouring cells but part of which pass through the cell in question. To account for all these fractions would required considerable computing time, while in many cases they will simply cancel, so we choose to calculate S_n in eq. (6.1.6) assuming all of energy is concentrated along the particular ray. If necessary, some kind of smoothing criterion can be economically employed.

In summary, when viewed from a point P on the chamber wall, while incident fluxes are evaluated using impinging rays, sources are calculated using out going (originating rays). A small energy in balance results which can be reduced by considering more rays and refining the grid. This kind of imbalance is termed statistical noise in the Monte Carlo method of solution. The computational time is not now significantly increased by the source calculations since the distances needed are the same, it is only that they are traversed in the reverse order.

For problems with prescribed sources, and in the absence of convection and diffusion, the temperatures would have to be iterated. For a cartesian system, the integrated transport or energy equation eq. (6.1.1) can be summed over all the rays in the whole solid angle 4π. The left hand side can be equated to the source to yield:

$$S = \nabla q = \int \frac{dI}{dS}\, d\Omega = -K \int I d\Omega + 4K\sigma T^4 \tag{6.1.7}$$

If S_i is the estimate from the previous iteration and $T_{g,i}$ the temperature, and S the prescribed source for any particular mesh cell, then the new temperature $T_{g,i+1}$ is given by:

$$\frac{\sigma T^4_{g,i+1}}{\pi} = \sigma T^4_{g,i} + \frac{(S-S_i)}{4K} \tag{6.1.8}$$

For other coordinate systems, care has to be taken since the second equality in eq. (6.1.7) is not always true (Section 4.1.1). For other orthogonal systems the extra terms emerge from the div. operator, would disappear when similar equations, one with the approximate source and the other with the exact source are subtracted. So eq. (6.1.8) is true for other orthogonal systems as well.

6.2 The computer code and advantages of the method

6.2.1 Storage Organisation

For a three dimensional chamber geometry, the usual storage for the grid vertices, volumes, temperatures, sources and, if necessary, absorption coefficients is required. Further the usual boundary information such as the wall temperatures (or fluxes) emissivities and areas of wall cells is required.

For the flux method described earlier three additional three-dimensional stores were required (C_1,C_2,C_3) with possible further storage for the parameters. Now for the discrete transfer method, we need to store the incident flux (q_-) and sometimes also the emitted flux (q_+) on the chamber wall cells. The emitted flux (q_+) can in principle be calculated using the boundary conditions equations, when needed, but allocating a separate storage for them avoids repeating the calculations. Four other one-dimensional arrays whose length is equal to the maximum number of cells traversed by any one ray are needed. These are used to remember the cells crossed, through the integer co-ordinates ℓ, m, n and distances traversed by one ray at a time. Thus the storage requirement is less than all but the most truncated flux methods, and, of course, it is also less than the Zone and the Monte Carlo methods.

6.2.2 The Computation Procedure

The computation procedure can be divided into four separate stages.

(a) Preliminaries

The rays are fired in selected directions. Together these make up the whole hemisphere on the inside of a wall. We choose to divide the hemisphere into simple constant polar and azimuthal angles (fig. 6.5) (θ and ϕ). We divide θ into N_θ equal angles and ϕ into N_ϕ equal angles. Each subdivision is then $d\theta = \frac{\pi}{2N_\theta}$ and $d\phi = \frac{2\pi}{N_\phi}$ respectively. So the number of rays fired is $N_\theta \times N_\phi$. We also specify the grid vertices and the areas of the chamber wall cells the quantity σT^4 is normally specificed in place of both wall and gas temperatures.

(b) Setting the direction and origin of each ray

The sources are initialised to zero. First of all we select a chamber wall and then the first cell on this wall. From the point P, normally in the middle of this cell, we fire $N_\theta \times N_\phi$ rays in the prescribed directions. For each incoming ray at P we obtain, following the procedure of (c) below, its intensity ($I(\theta,\phi)$). We then calculate the new q_- at P by summing

$$q_- = \sum_{\theta,\phi} I_r(\theta,\phi)(\sin\theta\cos\theta)(\sin d\theta)d\phi \qquad (6.2.1)$$

to replace the old value. Using the boundary condition (6.1.3) or (6.1.4) the value of q_+ can then easily be evaluated . The absolute change in q_+ is also summed, this is called the residual error. All cells are so visited in turn.

(c) Tracing the ray

We enter this subroutine knowing the position of point P and the direction of the ray. By simple geometrical considerations, we calculate the distance the ray travels in all cells in its path. For a three-dimensional problem, this information can be stored in four one-dimensional arrays. Three of them containing the ℓ, m and n integer coordinates of the cell visited and one the distance. Hence the length of these arrays is the maximum number of cells any one ray can visit. If the ray impinges a chamber wall cell which is a specular reflector, we reflect the ray and carry on until the ray hits a chamber wall cell that is not a specular reflector. The value of the rays intensity at the far wall, I_0, is evaluated from the value of q_+ at the chamber wall cell by dividing by π. Using this value of I_0 and the recurrence relation (6.1.2), we calculate the value of $I_r(\theta,\phi)$ for this ray by using the four one-dimensional arrays in the reverse order back towards P.

If sources are required, we also need to consider an identical ray starting from the point P. We use the area of the chamber wall cell at P and the value of $I_{0,P}$ (the P subscript distinguishes I_0 at P from that at the far wall) obtained from the previous value of q_+ at P and dividing by π. Again we apply the recurrence relation (6.1.2) to get the intensity on exit at each cell by using the four one-dimensional arrays in the same order. The source is accummulated in cell (ℓ,m,n) using eq. (6.1.6).

(d) Final Calculations

If it is a source prescribed problem, then we evaluate the new temperatures using eq. (6.1.8) and measure the residual change from the last iteration. If the residual error or change does not fall within our requirements, we go back to stage (b), or if the number of rays also need to be changed, to stage (a). Otherwise we calculate the quantities we are interested in. For example the net flux which is simply $q_+ - q_-$; the source required may be per unit volume in which case we divide by each cell volume. Smoothing the sources if necessary can be done at this stage, although this was not done for the calculations in the next chapter.

6.2.3 Principal Advantages of the Discrete Transfer Method

The main advantages which we see for the discrete transfer method will now be cited:

(a) Numerically exact solutions can be achieved simply by using a sufficient number of rays, with no increase in storage.

(b) The storage requirement does not increase with the number of rays so massive improvements in storage problem are obtained.

(c) It is as straightforward to develop a computer code for a general three-dimensional co-ordinate system as for any other.

(d) The user can control the amount of computer time the radiation routine demands and the accuracy obtained.

(e) The convergence is of exponential order. The computation time to convergence is shorter than for the flux method described earlier (although the time per iteration may be higher).

(f) There is no restriction on the maximum length a ray can travel inside a cell. (This contrasts the Zone method which has a restriction on the maximum optical zone size).

(g) Incurable statistical errors are replaced by descritization errors which can always be made sufficiently small by grid refinement.

(h) There are no parameters to optimise.

(i) The method eleminates the problem of the transformation of the transport equation to other coordinate systems (section 4.1.1).

One drawback of the discrete transfer method as described should be mentioned. It is that the sum of the interior sources and the sum of the wall fluxes can, if the grid is not fine enough, differ by as much as 5%. This will not normally be a severe handicap.

CHAPTER 7

VALIDATION OF THE DISCRETE TRANSFER (DT) METHOD

7.1 Cartesian Geometries

7.1.1 One-Dimensional Cartesian with Prescribed Temperatures

Consider two infinitely long parallel black plates at temperatures T_1 and T_2 respectively. Let the gas be at uniform temperature T_g and the absorption coefficient be K everywhere. Then the flux out of walls 1 and 2 are given by eqs. (2.2.17) and (2.2.16) respectively. The numerically exact solutions of both the fluxes are obtained by the DT method. In fig. (7.1) only the solution for cold walls is presented. An accuracy of two decimal places is obtained using 10 rays.

7.1.2 One-Dimensional Cartesian Geometry with Sources Prescribed

Consider two infinitely long parallel black plates at temperature T_1 and T_2 respectively. Let the system be in equilibrium (no heat source). Then the quantity Q (eq. 2.2.3) can be calculated as $\frac{q}{\sigma T_1^4}$. Table 7.1 shows comparison of exact values of Q obtained from Heaslet and Warming (1964) and the values of Q obtained by the DT method for various values of optical thicknesses. Again for 10 rays an accuracy of two decimal places is obtained. The energy balance is exact.

For the same case, we can compare the temperature distribution between the walls (Θ(KL), eq. 2.2.5). This is done in fig. 7.2 where the comparison is against the Heaslet and Warming (1964) exact solution. Again, a similar order of accuracy is obtained for 10 rays.

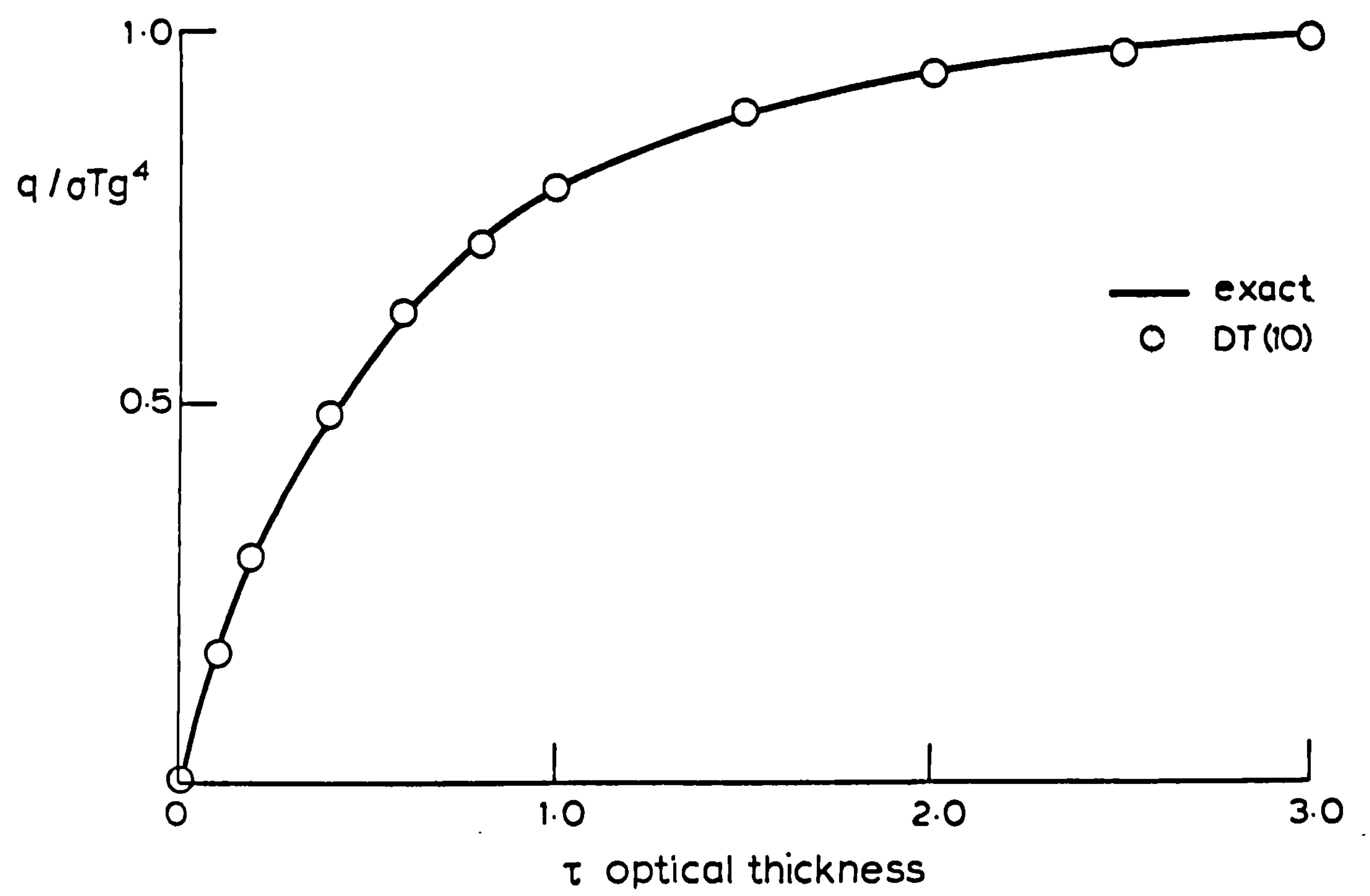

Fig. 7.1 Comparison of the analytical solution of the heat flux for various optical thicknesses with the DT method (10 rays) for one-dimensional cartesian geometry with cold black parallel walls and uniformly hot gas inside

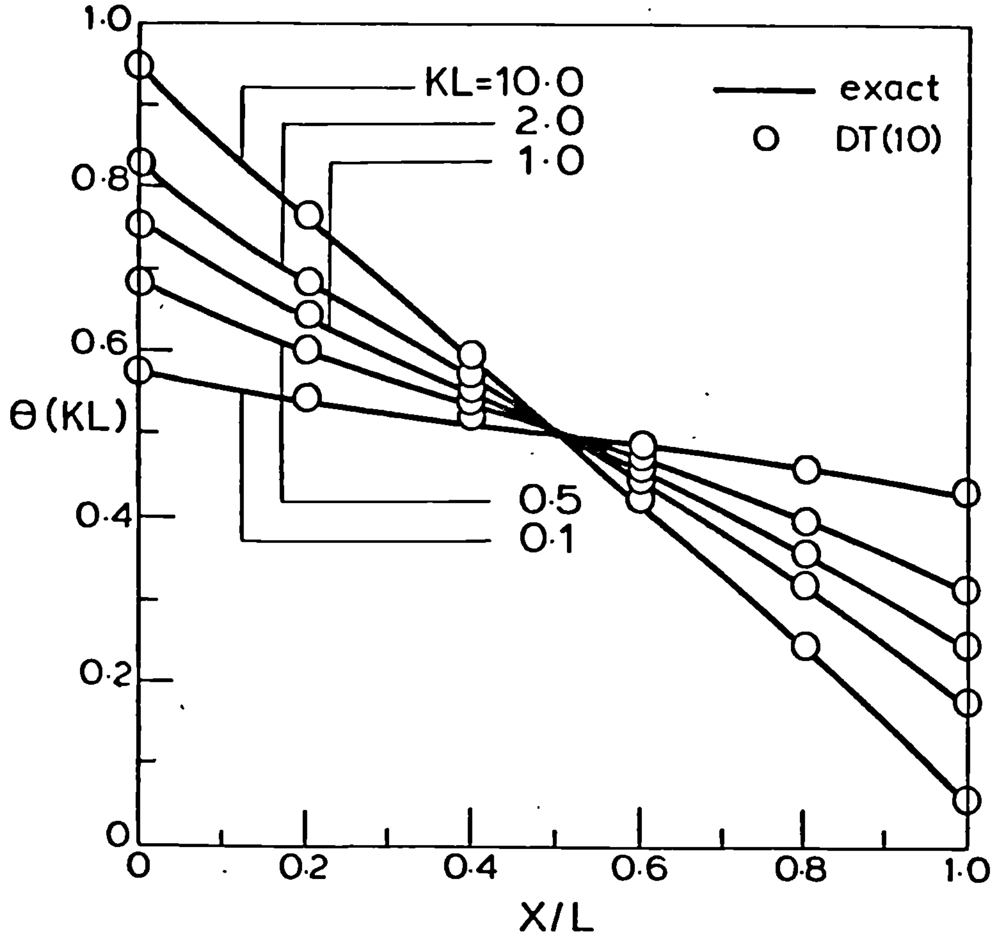

Figure 7.2 Comparison of exact value of θ(KL) (Heaslet and Warming, 1964) with DT method (10 rays)

Optical thickness	Exact solution	DT solution
0.1	0.9157	0.9147
0.5	0.7040	0.7036
1.0	0.5532	0.5537
1.5	0.4572	0.4588
2.0	0.3900	0.3929
2.5	0.3401	0.3444
3.0	0.3016	0.3073

Table 7.1 Comparison of exact values of Q (Heaslet and Warming, 1964) with the DT method (10 rays)

Now consider a situation where both the walls are black, but for uniform heat generation ($\frac{S}{K}$ = 1.0) inside. Then the temperature distribution between the walls is given by $\theta_S(KL)$ (eq. 2.2.6). The exact solution (Heaslet and Warming, 1964) is compared with the DT method for 10 rays and the accuracy is again of the same order in fig. 7.3 . The energy balance is exact.

Next, we examine the fluxes at wall and for both (zero source and hot walls and finite source and cold walls), for the cases where the emissivity at wall 1 is 0.8, and where the emissivity of wall 2 is varied for different optical thicknesses. Figs. 7.4 and 7.5 compares the Heaslet and Warming, (1964) results with the DT solution (10 rays). Again the accuracy is good and the energy balance is exact.

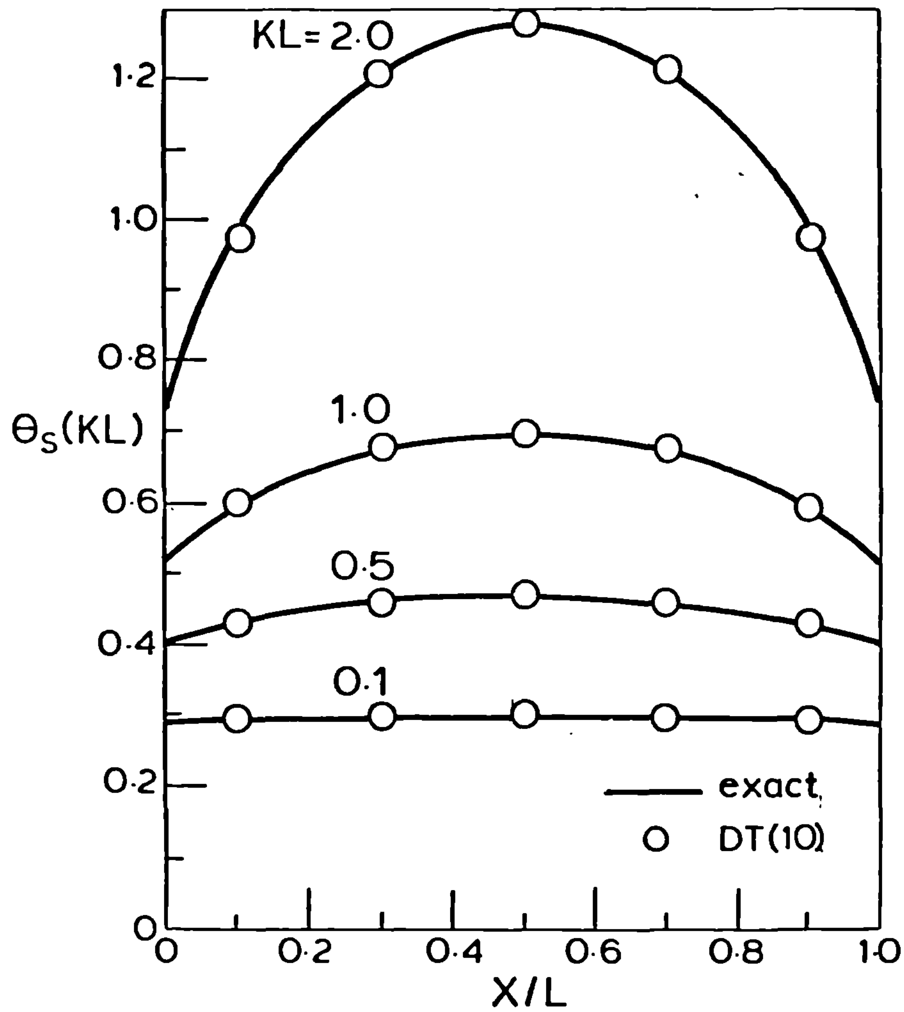

Figure 7.3 Comparison of exact value of θ_S(KL) (Heaslet and Warming, 1964) with DT method (10 rays)

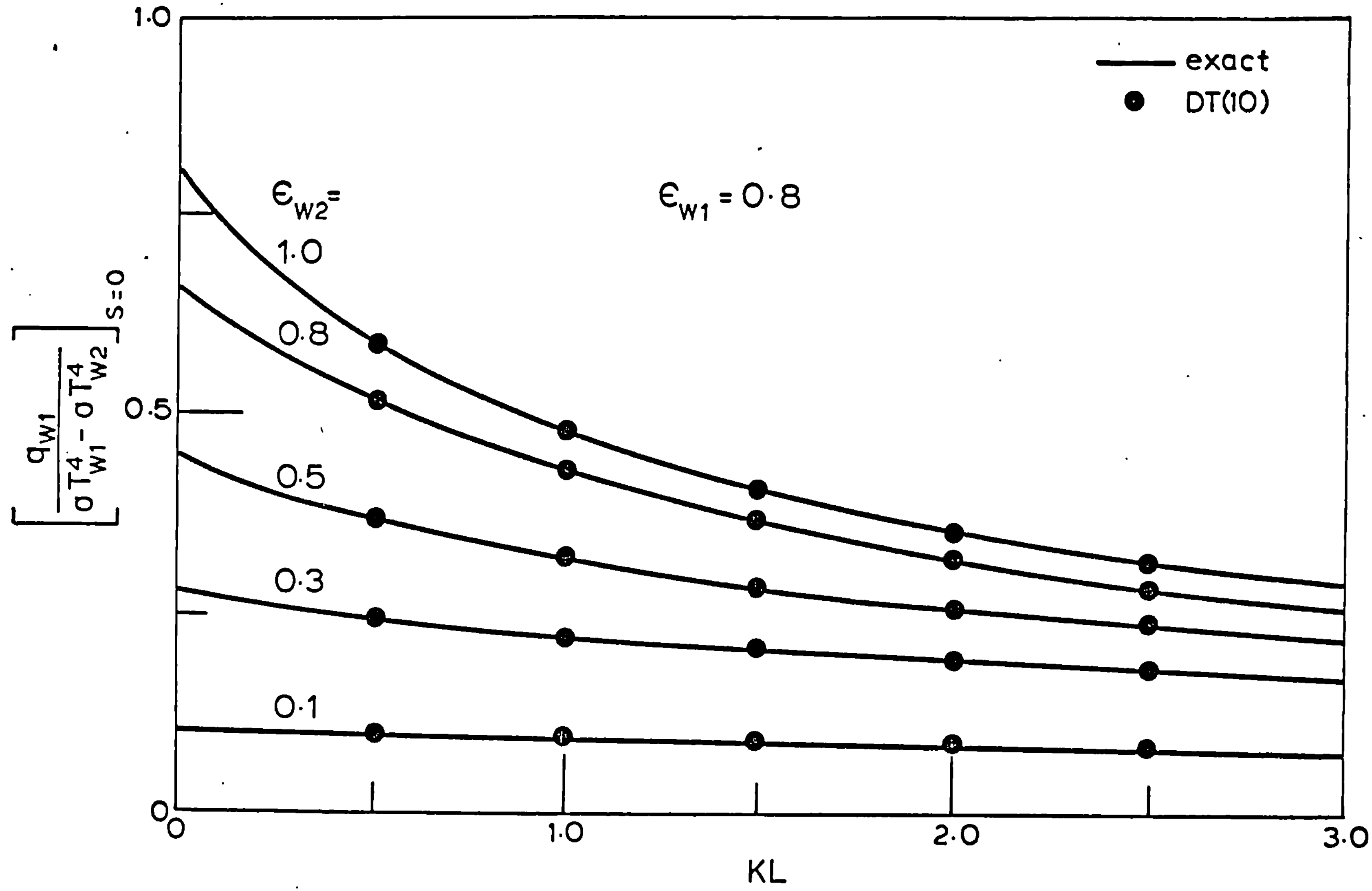

Fig. 7.4 Comparison of the dependence of dimensionless flux; for zero source strength, on optical thicknesses and wall emissivities (Heaslet and Warming, 1964) with the DT method (10 rays).

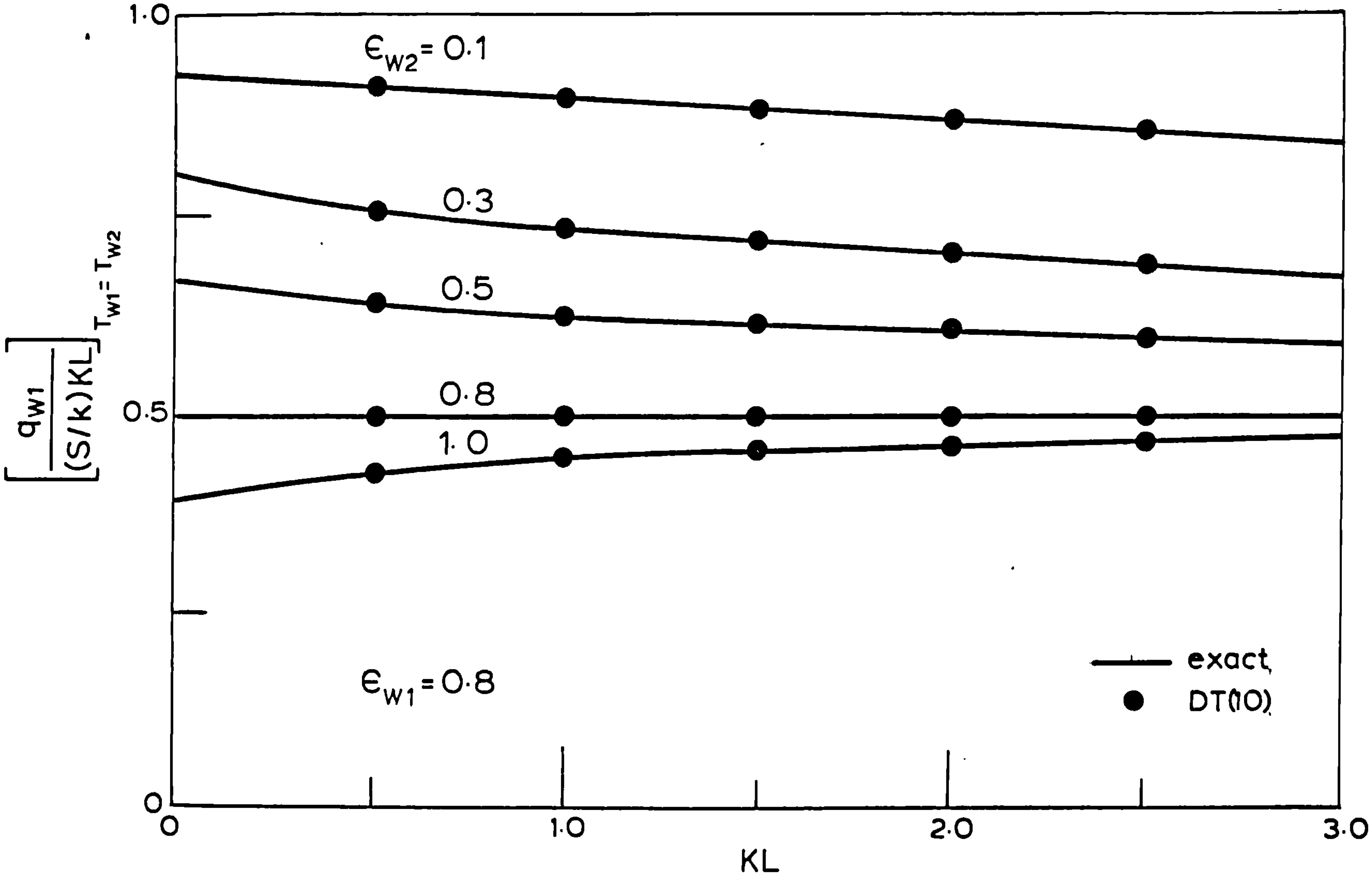

Figure 7.5 Comparison of dimensionless flux for equal wall temperatures showing dependence on optical thickness and wall emissivities (Heaslet and Warming, 1964) with the DT method (10 rays).

For the same two sets of cases, we now examine the temperature slip near the walls for situations when the emissivity of wall 1 is 0.8 and the emissivity of wall 2 is varied as before. Figs. 7.6 and 7.7 compares the Heaslet and Warming (1964) results with the DT solution (10 rays). The accuracy is good and the energy balance is exact.

7.1.3 Two-Dimensional Cartesian Geometry with Temperatures Prescribed

The treatment of the analytical solution for this test case is shown in section 2.2.3. Consider an infinitely long square cavity with all the walls being cold and black. The gas inside is at a uniform temperature ($\sigma T_g^4 = 1.0$) and the absorption coefficient is constant (K) throughout. The geometry is now more complicated than the one-dimensional case used so far. Hence in order to pick out more detail, more rays are required. Figs. 7.8, 7.9 and 7.10 show the fluxes along a wall for optical thicknesses 0.1, 1.0 and 10.0 respectively. The number of rays considered is 64 from each surface cell. For all three cases, the solution coincides with the analytic solution. For optical thickness 1.0, a solution is also presented for 16 rays on fig. 7.9. The agreement is generally reasonable and good near the centre; it is better than that for the flux solution (fig. 5.2). The energy balance is to the order of 3 digits.

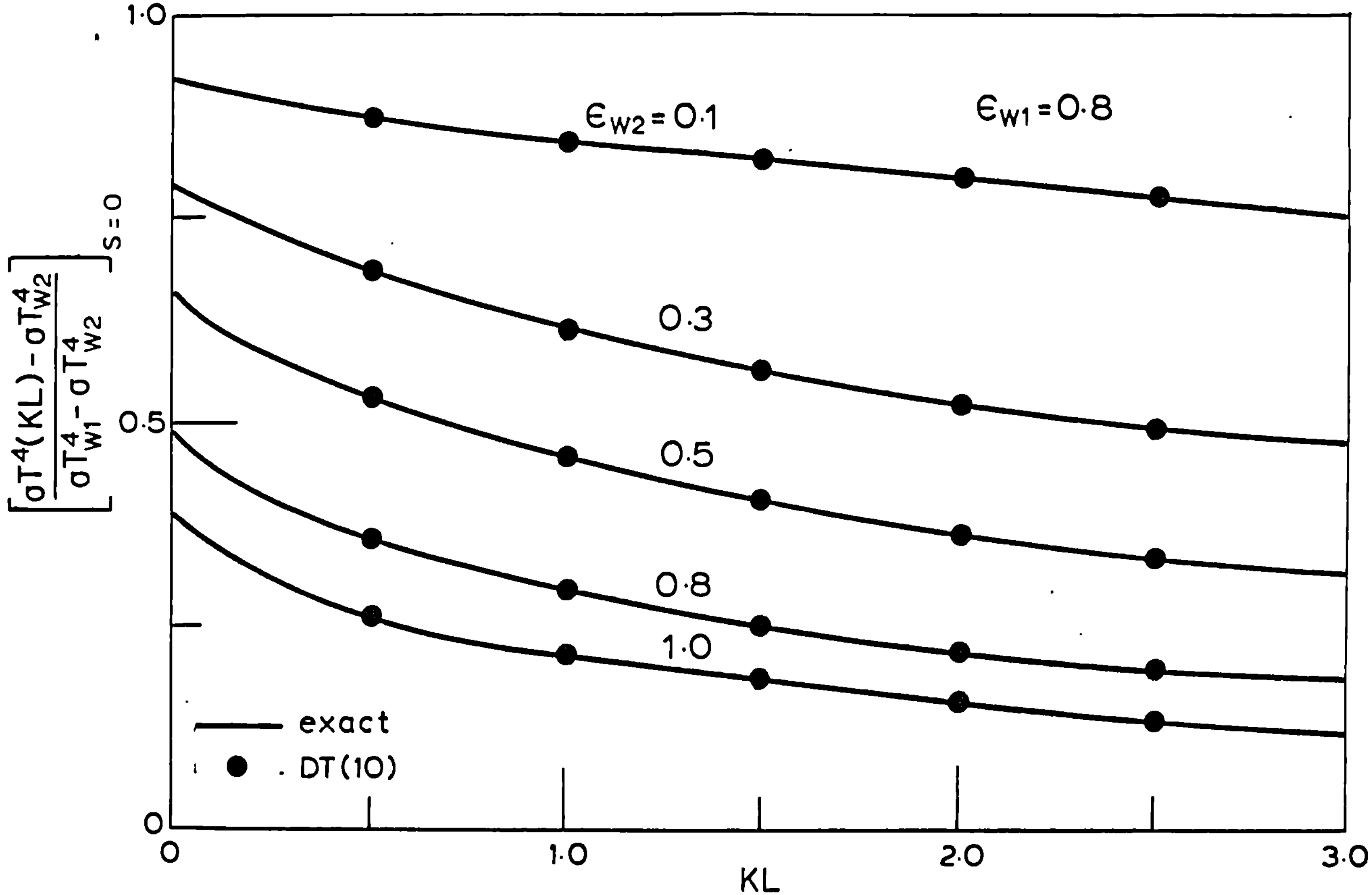

Figure 7.6 Comparison of dimensionless temperature slip for zero source strength showing dependence on optical thickness and wall emissivities (Heaslet and Warming, 1964) with the DT method (10 rays).

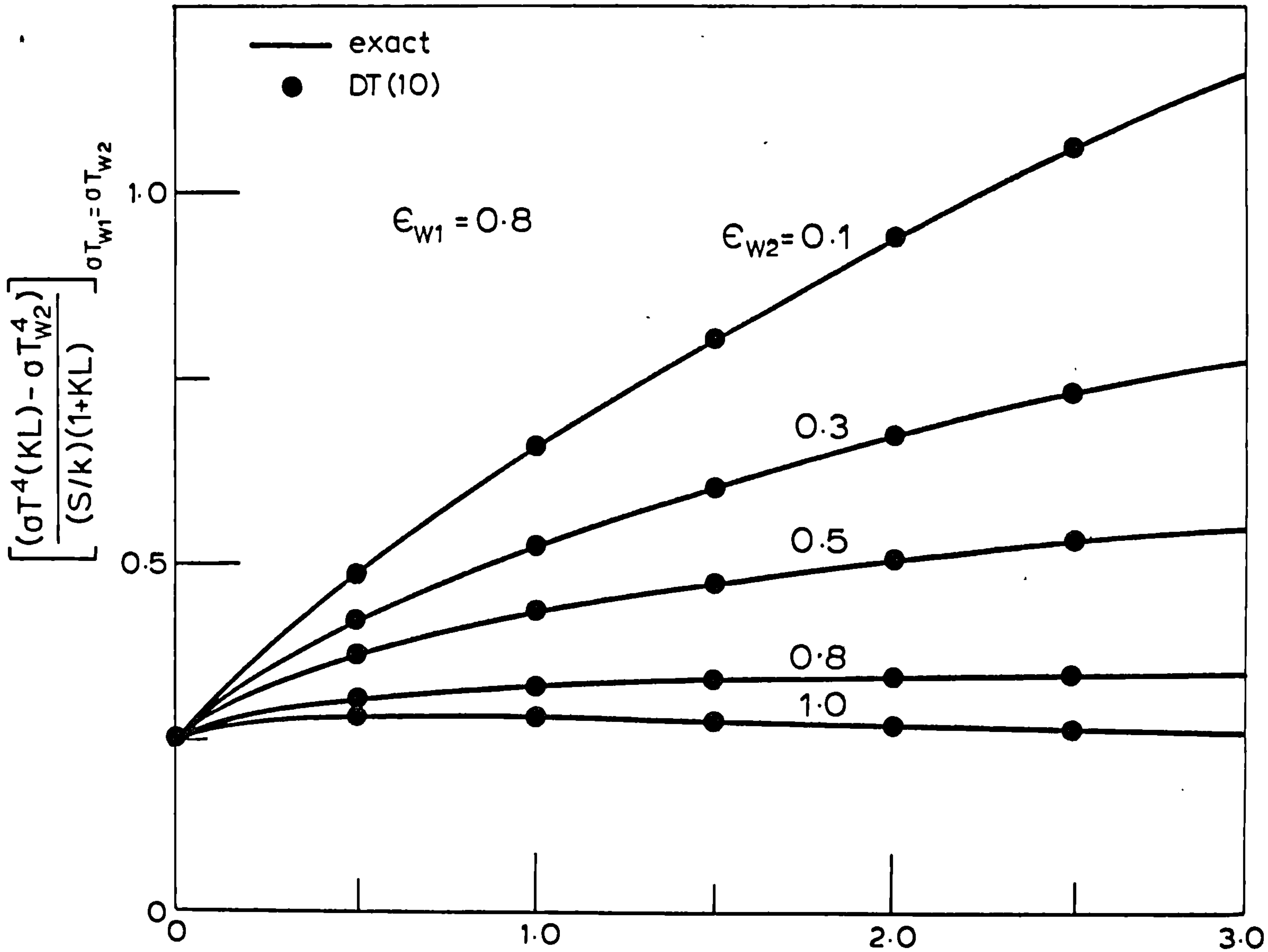

Figure 7.7 Comparison of dimensionless temperature slip for equal wall temperatures showing dependence on optical thickness and wall emissivities (Heaslet and Warming, 1964) with the DT method (10 rays).

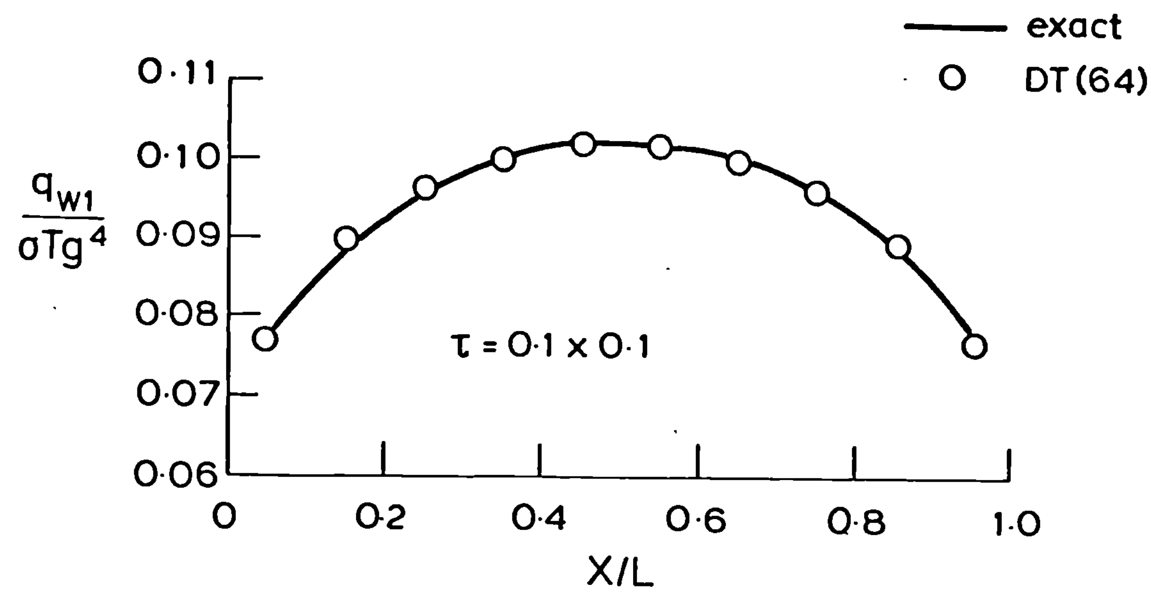

Figure 7.8 Comparison of the analytic solution for flux along the cold black walls of an infinitely long square cavity with that of the DT method (64 rays) for optical thickness 0.1

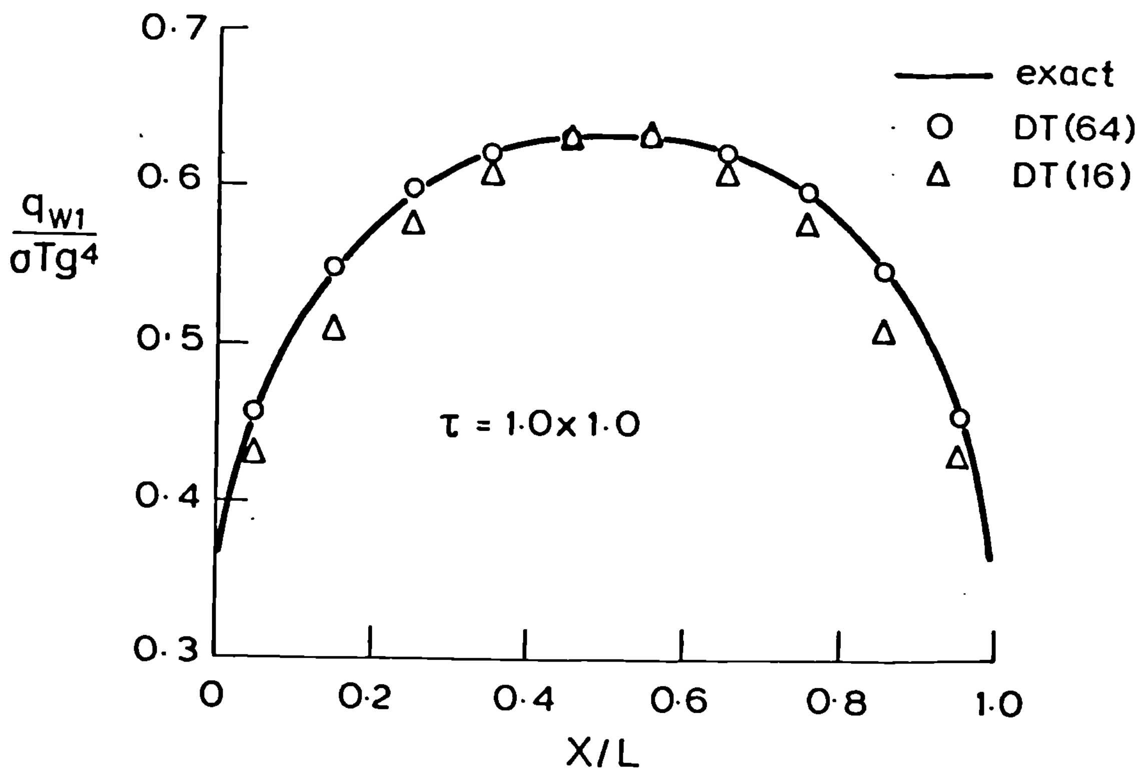

Figure 7.9 Comparison of the anlytic solution for flux along a cold black walls of an infinitely long square cavity with DT method (64 rays and 16 rays) for optical thickness 1.0

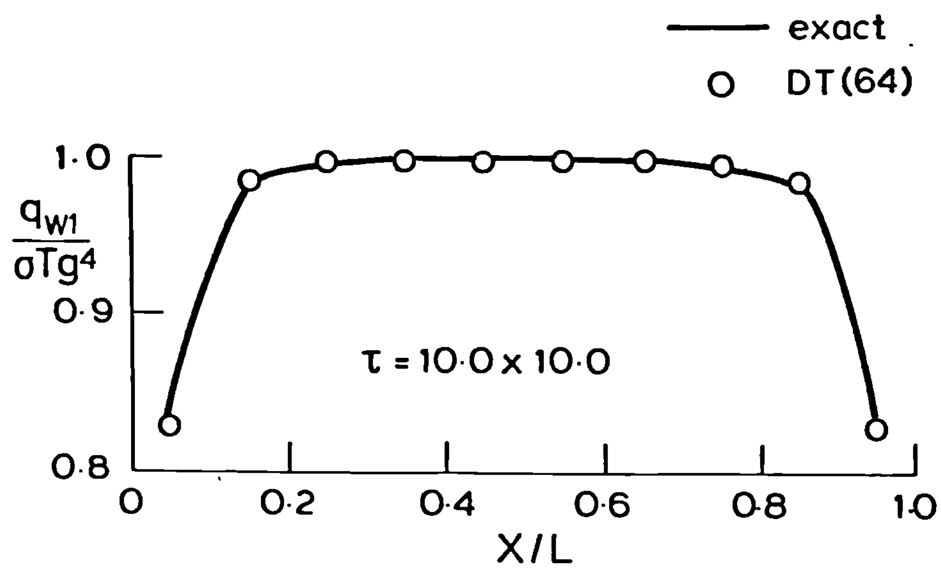

Figure 7.10 Comparison of the analytic solution for flux along a cold black walls of an infinitely long square cavity with the DT method (64 rays) for optical thickness 10.0

7.1.4 Three-Dimensional Cartesian Geometry with Temperatures Prescribed

In this section we consider two cases. The first one is a rectangular enclosure with dimensions 1.6m x 3.2m x 1.6m with all walls at 400^0C and the emissivity of the walls is 0.9. The gas inside is at a uniform temperature of 1000^0C and the absorption coefficient is $0.2m^{-1}$. Fig. 7.11 shows the flux at each cell just before impinging on the wall. The fluxes are evaluated using the flux method described in Chapter 3 together with the recommendation described in section 5.1.2. For the solution to converge to a certain level, it took 10 iterations and needed 10 secs. of C.D.C. 6600 of computer time.

For the same geometry and conditions a DT solution was computed using 4 rays from each cell (8 flux). This is presented in Fig. 7.12. For the solution to converge to a similar level of accuracy, about 4 iterations were required and 7.96 secs. of CDC 6600 time were consumed.

Another solution is generated using 36 rays (72 flux) leaving each cell. This is presented in Fig. 7.13. It required 2 iterations and 30 secs of CDC 6600 computer time. If Fig. 7.13 is regarded as a numerically "exact" solution, then the solution on Fig. 7.12 (DT method) has an overall advantage over the flux model on Fig. 7.11.

Consider another rectangular enclosure whose dimensions are 6m x 2m x 2m. (Truelove, 1977). The inside temperatures are prescribed by the figures shown on Fig. 7.14. The gas absorption coefficient is $0.2m^{-1}$. The surface boundary conditions are prescribed as:

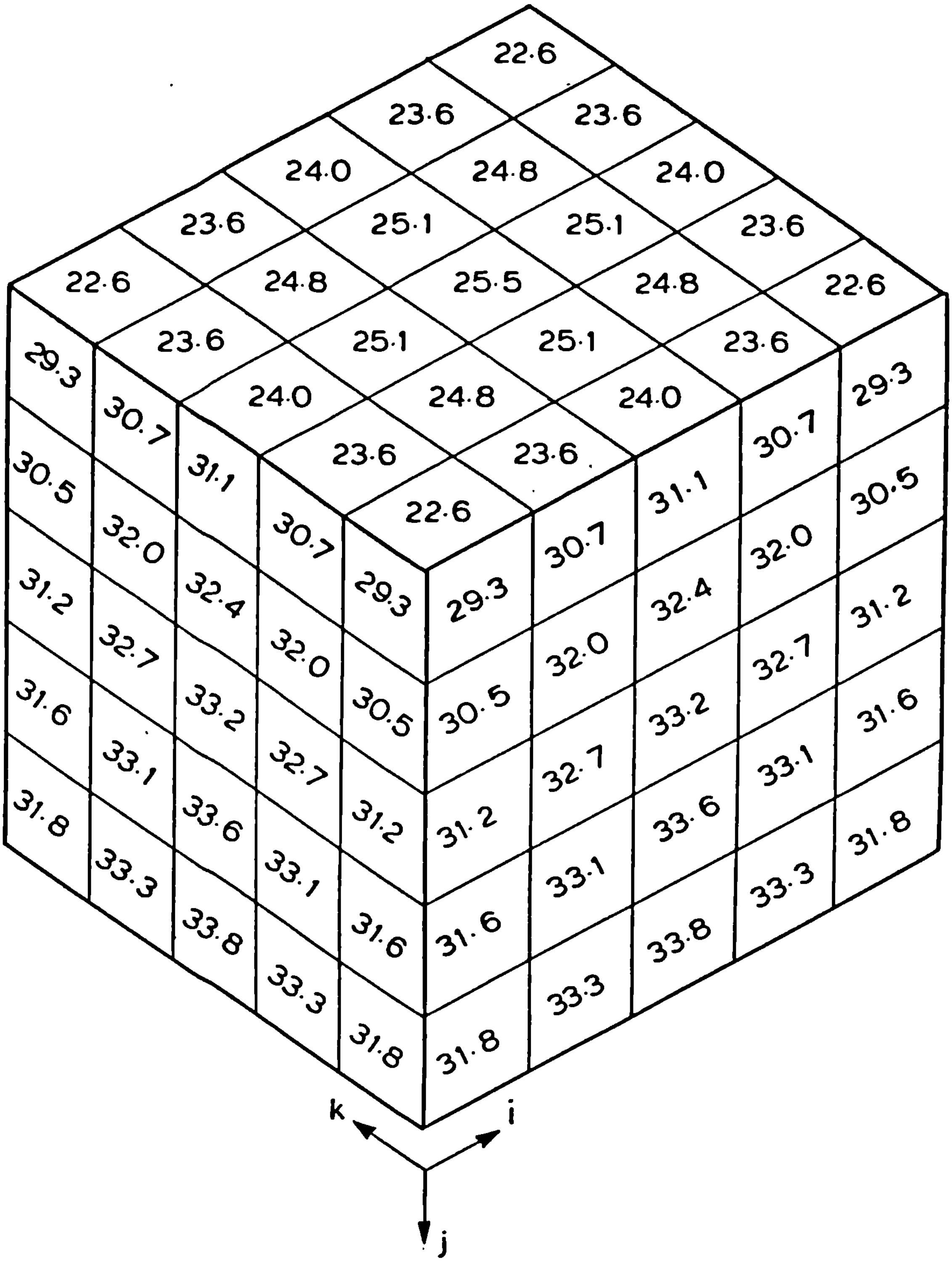

Figure 7.11 The fluxes just before impinging on the wall in an enclosure 1.6m x 3.2m x 1.6m (only one half shown here) at uniform temperature 1000^{0}C, absorption coefficient with all the walls at 400^{0}C and of emissivity 0.9, using the flux method (Chapter 3) and recommendation (section 5.1.2)

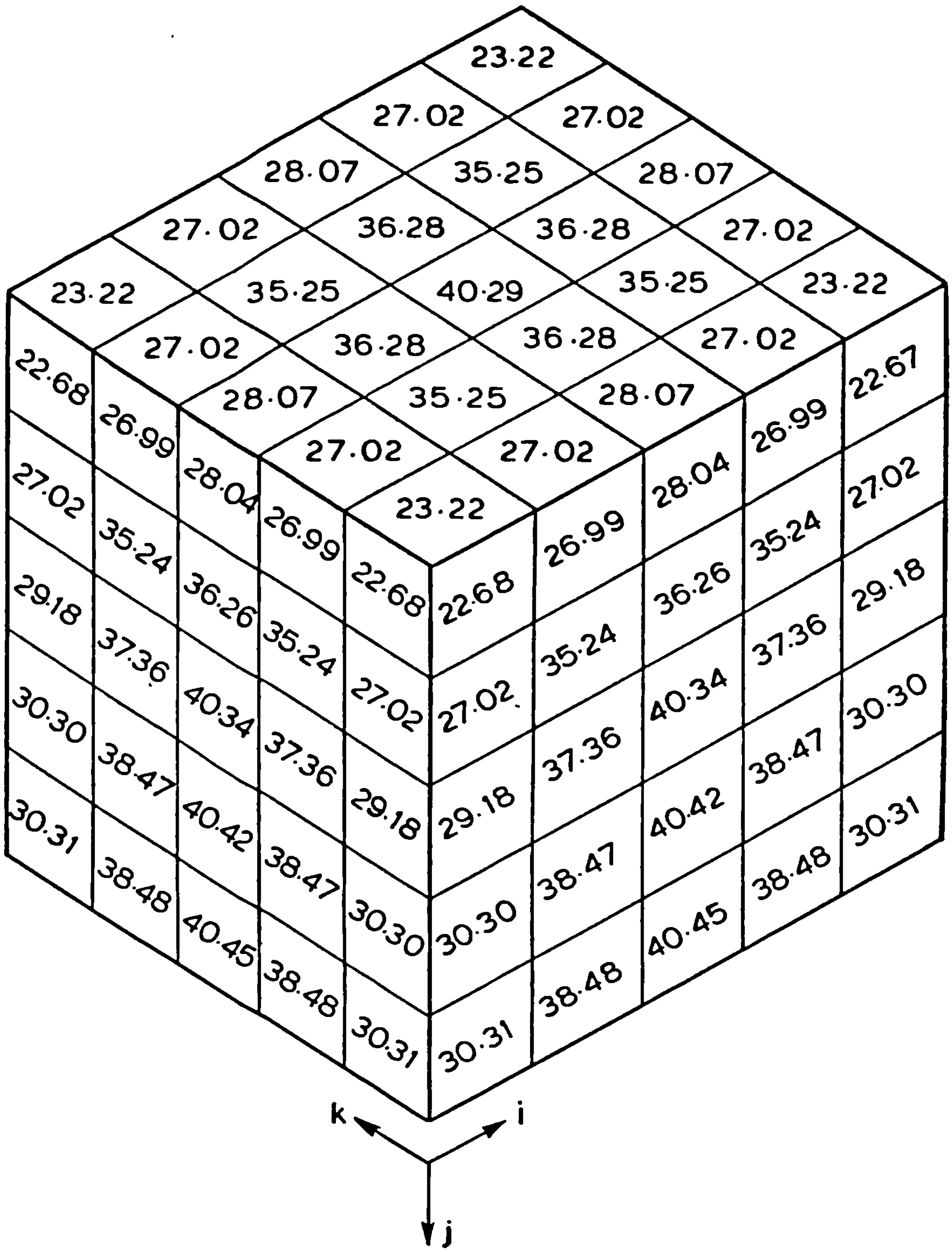

Figure 7.12 The fluxes just before impinging on the wall in an enclosure 1.6m x 3.2m x 1.6m (only one half shown here) at uniform temperature 1000°C, absorption coefficient $0.2m^{-1}$ with all the walls at 400°C and of emissivity 0.9, using the DT method (4 rays).

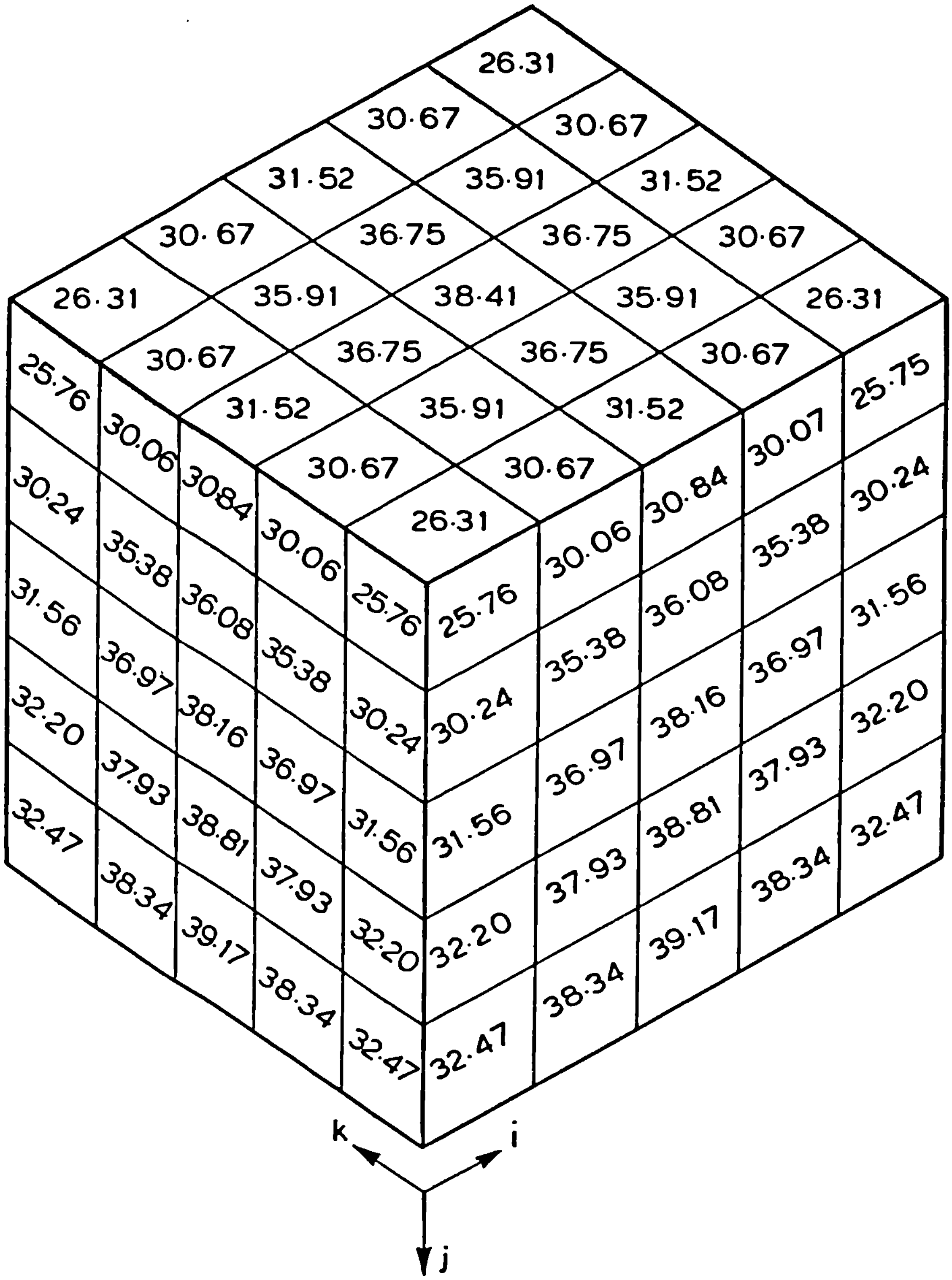

Figure 7.13 The fluxes just before impinging on the wall in an enclosure 1.6m x 3.2m x 1.6m (only half shown here) at uniform temperature 1000^{o}C, absorption-coefficient 0.2m^{-1} and all the walls at 400^{o}C and emissivity 0.9, using the DT method (36 rays).

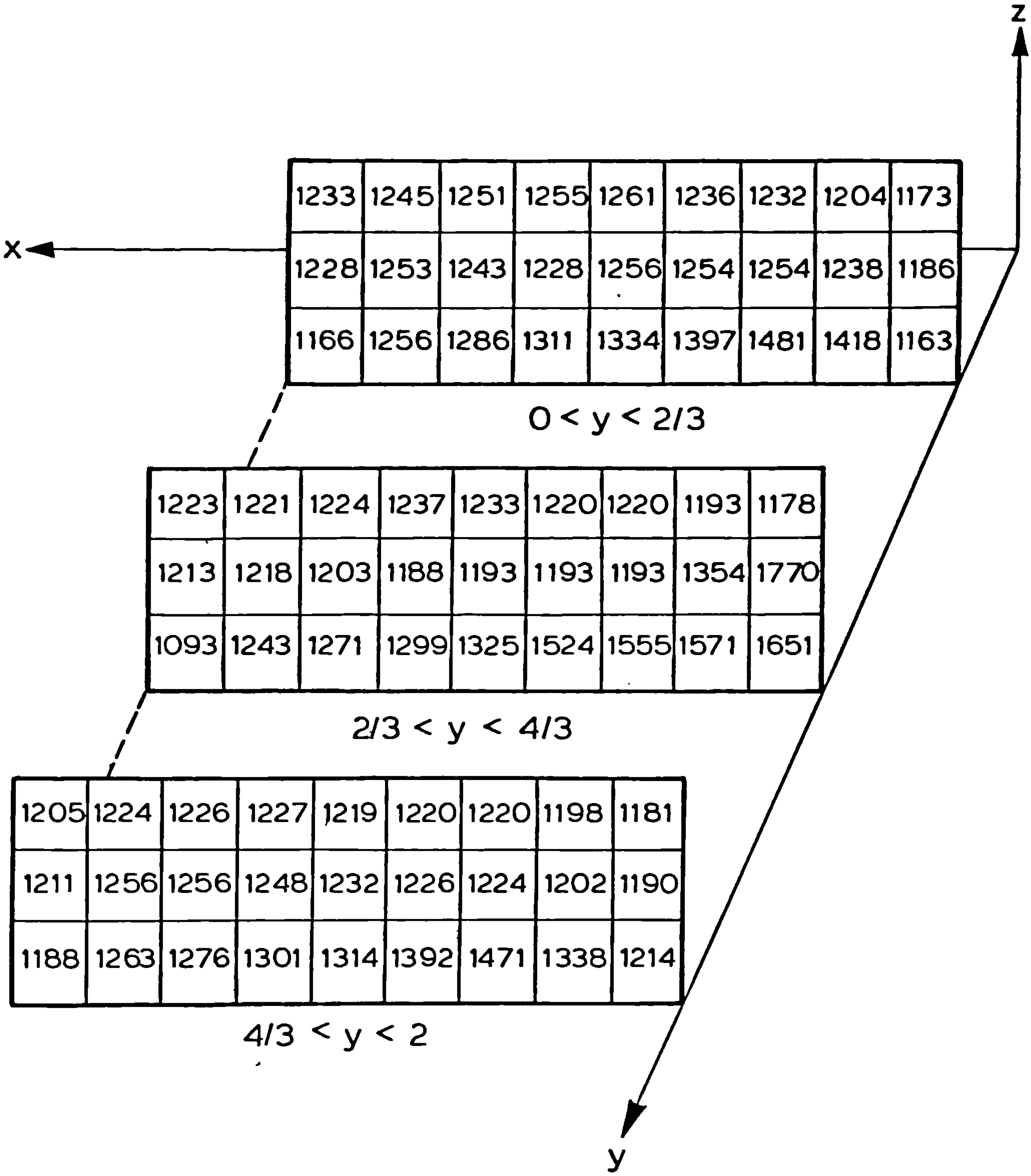

Figure 7.14 Gas temperature (^{o}K) distributions for a rectangular enclosure. Used by Hyde and Truelove (1977).

X = 0, X = 6, Y = 0, Y = 2, Z = 2 T = 1090K ε = 0.7

Z = 0 T = 320K ε = 0.86

Figure 7.15 shows a comparison between the zone model results and the DT results for the incident radiative flux (q_-) on the roof (X, Y = 1, Z = 2) and floor (X, Y = 1, Z = 0) of the enclosure.

7.1.5 Three-Dimensional Cartesian Geometry with Sources Prescribed

Consider a rectangular enclosure whose dimensions are 4m x 1m x 1m. (DeMarco, 1974). The gas inside is in thermal equilibrium (no heat generation) and the absorption coefficient is 2.0. All the walls are black and their temperatures are:

X = 0, T = 1200^oK

X = 4; Y = 0; Z = 1, T = 300^oK

Y = 1; Z = 0 T = 50^oK

The grid is uniform, 16 x 4 x 4. The 'exact' solution has been calculated by Jenner using the Furdec Program which is based on the Monte Carlo technique. The results are presented in DeMarco's M.Sc. thesis (1974). Some typing errors have been uncovered - some obvious ones can be easily detected - (marked x) but there may be more. Nevertheless they can be used as a good guidance. For a complete validation, the temperature distribution has to be compared as well. The discrete transfer solution has been computed using 16 rays off each boundary grid wall. The results are presented in tables 7.2 to 7.11. In general, there is a good agreement between the "exact" solution and the discrete transfer solution.

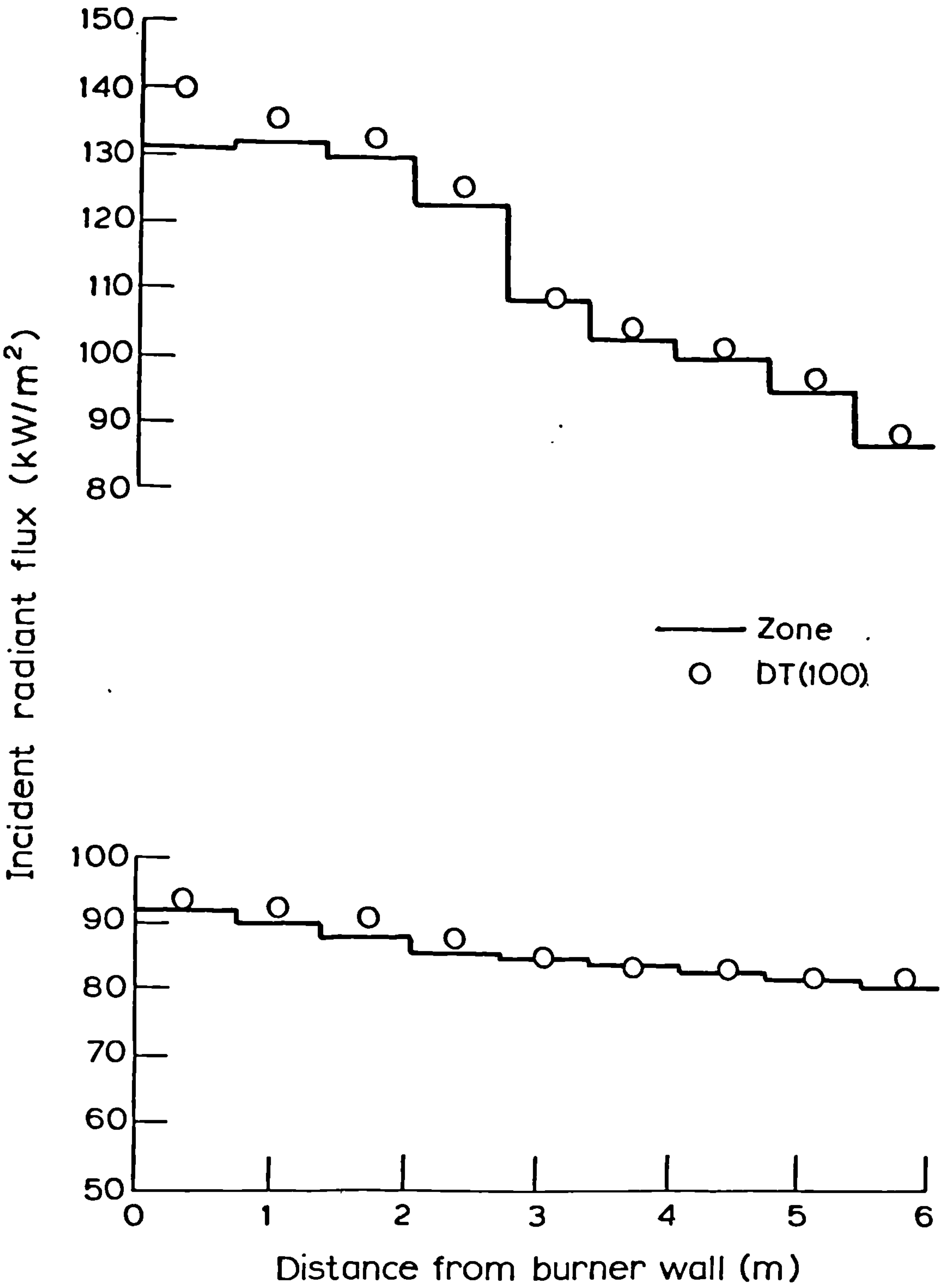

Figure 7.15 Comparison between zone model (Hyde and Truelove, 1977) and the DT method (100 rays) for the incident radiative flux on the roof and floor of the rectangular enclosure with temperatures as in fig. 7.14

Table 7.2 The three-dimensional prescribed source test case; the net flux through the X = 0 wall

	J = 1	J = 2	J = 3	J = 4
K = 1	-10.1E+4 -9.86E+4	-9.52E+4 -9.30E+4	-9.51E+4 -9.30E+4	-10.0E+4 -9.87E+4
K = 2	-9.51E+4 -9.28E+4	-8.65E+4 -8.59E+4	-8.72E+4 -8.60E+4	-9.27E+4 -9.30E+4
K = 3	-9.47E+4 -9.28E+4	-8.81E+4 -8.59E+4	-8.67E+4 -8.59E+4	-9.57E+4 -9.30E+4
K = 4	-10.0E+4 -9.84E+4	-9.39E+4 -9.28E+4	-9.50E+4 -9.28E+4	-10.0E+4 -9.86E+4

Table 7.3 The net flux through the X = 4 wall

	J = 1	J = 2	J = 3	J = 4
K = 1	-0.514E+2 -1.92E+2	-2.92E+2 -2.54E+2	-3.79E+2 -2.92E+2	-3.88E+2 -3.41E+2
K = 2	-0.883E+2 -1.04E+2	-2.51E+2 -1.65E+2	-1.61E+2 -2.10E+2	-3.86E+2 -2.87E+2
K = 3	-1.46E+2 -0.703E+2	-1.46E+2 -1.20E+2	-1.73E+2 -1.65E+2	-2.88E+2 -2.54E+2
K = 4	-1.55E+2 -0.390E+2	-0.804E+2 -0.657E+2	-1.99E+2 -1.03E+2	-0.841E+2 -1.88E+2

Table 7.4 The net flux through the Y = 0 wall and $0 < X < 2$.

	K = 1	K = 2	K = 3	K = 4
I = 1	4.29E+4 4.21E+4	5.00E+4 5.40E+4	5.42E+4 5.41E+4	4.23E+4 4.32E+4
I = 2	2.03E+4 1.67E+4	2.66E+4 2.50E+4	2.53E+4 2.51E+4	1.93E+4 1.80E+4
I = 3	9.93E+3 8.10E+3	x 1.03E+3 1.29E+4	x 1.28E+3 1.29E+4	9.56E+3 8.41E+3
I = 4	4.86E+3 4.39E+3	6.90E+3 7.49E+3	6.48E+3 6.59E+3	5.17E+3 4.68E+3
I = 5	2.66E+3 2.41E+3	3.31E+3 3.62E+3	3.47E+3 3.65E+3	2.69E+3 2.67E+3
I = 6	1.03E+3 1.34E+3	1.88E+3 1.77E+3	1.98E+3 2.11E+3	1.46E+3 1.59E+3
I = 7	6.29E+2 6.98E+2	6.91E+2 9.21E+2	8.05E+2 12.0E+2	7.11E+2 9.37E+2
I = 8	1.27E+2 3.11E+2	2.48E+2 3.90E+2	4.43E+2 4.83E+2	4.46E+2 5.35E+2

Table 7.5 The net flux through the Y = 0 wall and 2 < X < 4.

	K = 1	K = 2	K = 3	K = 4
I = 9	1.32E+2 0.06E+2	1.86E+2 1.11E+2	2.32E+1 1.81E+1	1.66E+2 2.78E+2
I = 10	-2.32E+2 -1.49E+2	-4.26E+1 -6.41E+1	x 1.16E+2 -1.25E+0	9.82E+1 -6.32E+1
I = 11	-3.46E+2 -2.26E+2	-4.23E+1 -1.44E+2	-10.6E+1 -8.07E+1	4.64E+1 2.28E+1
I = 12	-1.74E+2 -2.57E+2	-1.47E+2 -1.78E+2	-1.52E+2 -1.14E+2	-1.23E+2 -0.579E+2
I = 13	-2.16E+2 2.68E+2	-0.77E+2 -1.90E+2	-6.86E+1 -12.6E+1	2.94E+1 7.14E+1
I = 14	-3.61E+2 2.68E+2	-1.82E+2 -1.84E+2	x -1.72E+1 -1.27E+2	-1.92E+2 -0.751E+2
I = 15	-3.28E+2 -2.53E+2	-1.99E+2 -1.64E+2	-2.03E+2 -1.12E+2	-1.79E+2 -0.679E+2
I = 16	-3.05E+2 -1.91E+2	x -1.33E+1 -1.08E+2	-1.31E+2 -0.724E+2	-4.45E+1 -4.27E+1

Table 7.6 The net flux through Y = 1 wall and $0 < X < 2$

	K = 1	K = 2	K = 3	K = 4
I = 1	4.19E+4 4.35E+4	5.26E+4 5.44E+4	5.29E+4 5.45E+4	4.20E+4 4.27E+4
I = 2	1.95E+4 1.83E+4	2.58E+4 2.54E+4	2.60E+4 2.54E+4	1.19E+4 1.73E+4
I = 3	1.0E+4 0.861E+4	1.37E+4 1.33E+4	x 4.39E+4 1.33E+4	x 9.98E+4 8.68E+3
I = 4	5.44E+3 4.87E+3	7.13E+3 6.90E+3	7.29E+3 7.93E+3	5.75E+3 4.98E+3
I = 5	2.80E+3 2.87E+3	3.79E+3 3.95E+3	4.06E+3 4.06E+3	2.77E+3 3.00E+3
I = 6	1.62E+3 1.78E+3	2.08E+3 2.43E+3	1.95E+3 2.21E+3	1.74E+3 1.93E+3
I = 7	9.83E+2 11.3E+2	1.19E+3 1.52E+3	1.40E+3 1.36E+3	1.14E+3 1.28E+3
I = 8	3.92E+2 7.32E+2	6.46E+2 8.00E+2	8.24E+2 8.27E+2	6.38E+2 8.95E+2

Table 7.7 The net flux through Y = 1 wall and 2 < X < 4

	K = 1	K = 2	K = 3	K = 4
I = 9	3.31E+2 4.75E+2	4.98E+2 4.98E+2	4.39E+2 5.48E+2	5.23E+2 5.89E+2
I = 10	x 2.28E+2 2.57E+2	4.12E+2 3.14E+2	3.15E+2 3.72E+2	4.69E+2 4.34E+2
I = 11	x 1.38E+2 1.70E+2	2.17E+2 2.34E+2	3.61E+2 2.94E+2	x 1.74E+2 3.57E+2
I = 12	x 2.58E+2 1.35E+2	1.34E+2 1.99E+2	x 3.36E+2 2.60E+2	x 2.78E+2 3.26E+2
I = 13	x 1.89E+2 1.23E+2	2.18E+2 1.90E+2	2.94E+2 2.48E+2	3.50E+2 3.15E+2
I = 14	1.28E+2 1.24E+2	1.81E+2 1.95E+2	4.05E+2 2.45E+2	2.78E+2 3.15E+2
I = 15	1.99E+2 1.42E+2	2.39E+2 2.18E+2	2.10E+2 2.69E+2	x 5.65E+2 3.31E+2
I = 16	2.40E+2 2.12E+2	2.54E+2 2.88E+2	2.78E+2 3.23E+2	4.82E+2 3.64E+2

Table 7.8 The net flux through Z = 0 wall and 0 <X <2

	J = 1	J = 2	J = 3	J = 4
I = 1	4.28E+4 4.36E+4	5.30E+4 5.45E+4	5.15E+4 5.44E+4	4.28E+4 4.26E+4
I = 2	1.90E+4 1.84E+4	2.59E+4 2.54E+4	2.70E+4 2.54E+4	1.90E+4 1.71E+4
I = 3	9.79E+3 8.80E+3	1.36E+4 1.33E+4	1.32E+4 1.33E+4	1.04E+4 0.849E+4
I = 4	5.49E+3 5.07E+3	6.53E+3 6.96E+3	6.95E+3 7.87E+3	4.92E+3 4.78E+3
I = 5	2.74E+3 3.06E+3	3.44E+3 4.02E+2	3.63E+3 4.00E+3	3.27E+3 2.80E+3
I = 6	2.07E+3 1.98E+3	2,19E+3 2.49E+3	1.76E+3 2.15E+3	1.64E+3 1.73E+3
I = 7	9.82E+2 13.3E+2	1.18E+3 1.58E+3	9.73E+2 13.0E+2	9.43E+2 10.9E+2
I = 8	7.24E+2 9.25E+2	7.32E+2 8.60E+2	7.34E+2 7.67E+2	4.10E+2 7.02E+2

Table 7.9 The net flux through Z = 0 wall and $2 < X < 4$

	J = 1	J = 2	J = 3	J = 4
I = 9	6.14E+2 6.68E+2	5.94E+2 5.58E+2	5.85E+2 4.88E+2	2.80E+2 3.97E+2
I = 10	4.26E+2 4.53E+2	2.61E+2 3.75E+2	4.23E+2 3.12E+2	2.09E+2 2.39E+2
I = 11	4.26E+2 3.66E+2	2.50E+2 2.94E+2	4.67E+2 2.31E+2	2.04E+2 1.62E+2
I = 12	x 2.55E+2 3.31E+2	2.07E+2 2.62E+2	2.26E+2 1.97E+2	2.67E+2 1.32E+2
I = 13	3.24E+2 3.18E+2	1.62E+2 2.50E+2	2.23E+2 1.86E+2	0.94E+2 1.21E+2
I = 14	x 4.05E+2 3.17E+2	3.15E+2 2.51E+2	1.58E+2 1.94E+2	1.84E+2 1.24E+2
I = 15	2.94E+2 3.28E+2	2.24E+2 2.70E+2	2.64E+2 2.18E+2	0.985E+2 1.43E+2
I = 16	3.11E+2 3.64E+2	x 4.36E+2 3.24E+2	2.24E+2 2.89E+2	2.93E+2 2.16E+2

Table 7.10 The net flux through Z = 1 wall and 0 < X < 2

	J = 1	J = 2	J = 3	J = 4
I = 1	4.13E+4 4.23E+4	5.15E+4 5.41E+4	5.05E+4 5.40E+4	4.30E+4 4.31E+4
I = 2	1.87E+4 1.69E+4	2.43E+4 2.51E+4	2.55E+4 2.50E+4	2.03E+4 1.79E+4
I = 3	x 9.67E+4 8.29E+3	1.17E+4 1.29E+4	1.30E+4 1.29E+4	9.12E+3 8.22E+3
I = 4	4.90E+3 4.59E+3	6.80E+3 7.55E+3	6.30E+3 6.53E+3	4.97E+3 4.48E+3
I = 5	2.91E+3 2.61E+3	3.31E+3 3.69E+3	3.62E+3 3.58E+3	2.56E+3 2.48E+3
I = 6	1.26E+3 1.54E+3	1.60E+3 1.83E+3	1.43E+3 2.05E+3	1.08E+3 1.39E+3
I = 7	5.93E+2 8.94E+2	8.59E+2 9.82E+2	8.50E+2 11.42E+2	7.18E+2 7.42E+2
I = 8	2.87E+2 5.05E+2	3.80E+2 4.50E+2	5.11E+2 4.23E+2	1.59E+2 3.42E+2

Table 7.11 The net flux through Z= 1 wall and 2 < X < 4

	J = 1	J = 2	J = 3	J = 4
I = 9	1.62E+2 1.99E+2	- 7.87E+0 1.70E+2	2.40E+0 1.21E+2	-1.34E+2 8.41E+1
I = 10	-4.00E+1 4.52E+1	-6.03E+1 -3.55E+1	1.33E+2 -6.16E+1	-2.61E+2 -1.32E+2
I = 11	-4.79E+1 -3.13E+1	-4.86E+1 -8.27E+1	-1.84E+2 -1.42E+2	-2.23E+2 -2.19E+2
I = 12	-1.29E+1 -6.21E+1	-2.41E+2 -1.16E+2	-1.39E+2 -1.77E+2	-2.49E+2 -2.54E+2
I = 13	-1.23E+2 -7.36E+1	x 2.13E+1 -1.28E+2	-2.03E+2 -1.86E+2	-2.53E+2 -2.67E+2
I = 14	-7.55E+1 -7.61E+1	-7.28E+1 -1.28E+2	-9.47E+1 -1.84E+2	-2.8E+2 -2.68E+2
I = 15	-5.34E+1 -6.46E+1	-2.22E+2 -1.13E+2	-2.76E+2 -1.64E+2	-1.65E+2 -2.53E+2
I = 16	-1.05E+2 -4.34E+1	-1.72E+2 -0.735E+2	-2.49E+2 -1.09E+2	-2.86E+2 -1.95E+2

This completes the analysis for the cartesian geometries, it is by no means exhaustive but it covers a wide range of problems. The energy balance is very good for one and two-dimensional cases. For three dimensions, the imbalance is not so significant in proportion to the magnitude of the fluxes involved.

Further examples using a cartesian enclosure but an orthogonal grid system have been computed and applied successfully in the department.

7.2 Axisymmetric Geometries

7.2.1 An Infinite Cylinder with Prescribed Interior Temperatures

Consider an infinitely long cylinder of radius R with cold balck walls. Let the gas inside be at a uniform temperature ($\sigma T_g^4 = 1.0$) and of absorption coefficient K. Fig. 7.16 shows the analytic solution (Truelove, 1976) of flux through the wall for various optical diameters compared with the discrete transfer solution for the same case using 128 rays. In practice only 32 rays need be solved for, due to the symmetry properties. Both solutions coincide and there is an exact energy balance.

7.2.2 An Infinite Cylinder with Uniform Interior Heat Generation

Consider an infinite cylinder radius R with uniform heat generation inside. The walls are black but at temperature T_w. Fig. 7.17 plots the quantity ϕ defined by:

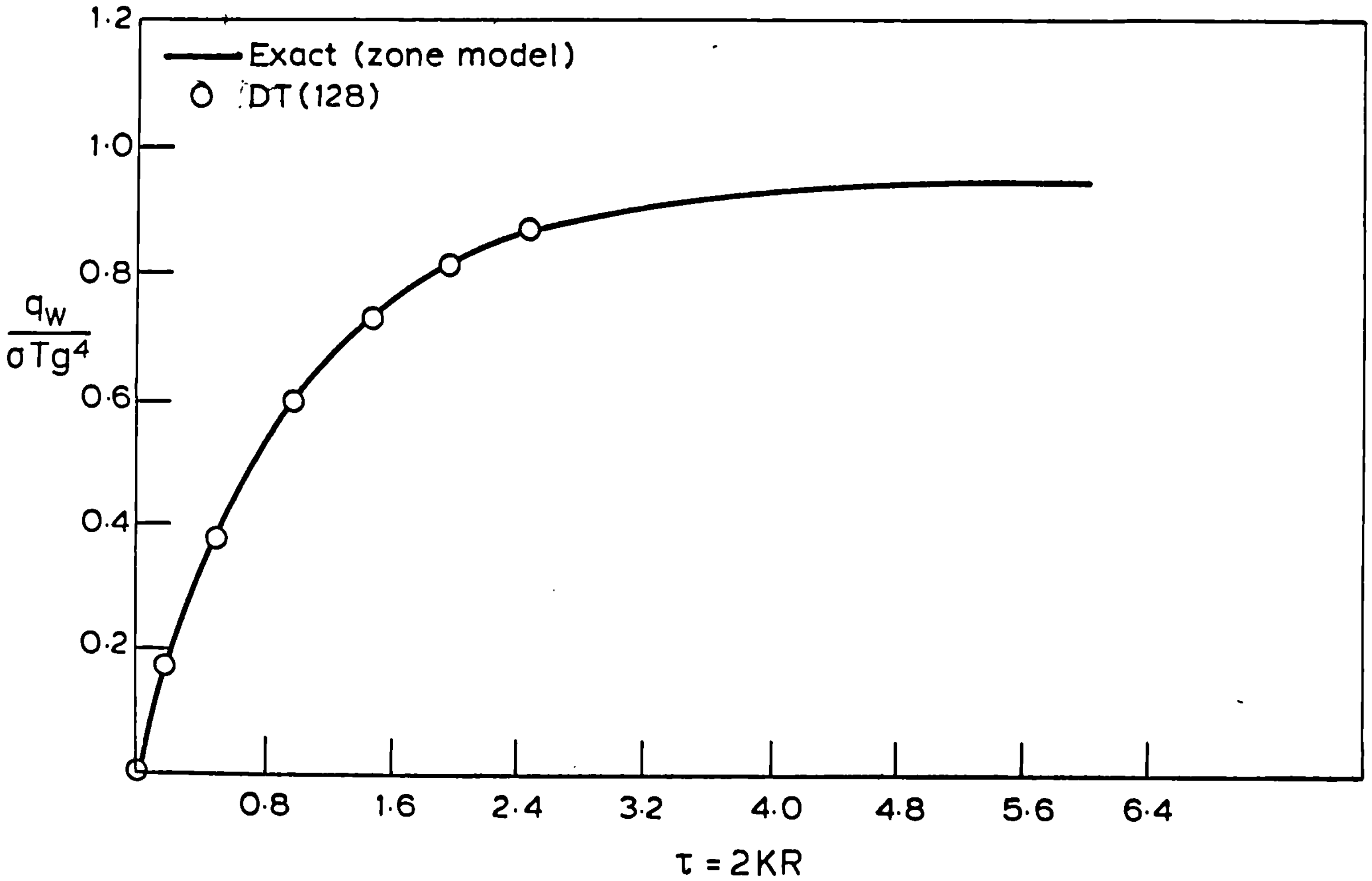

Fig. 7.16 Comparison of the analytic solution with the DT method (128 rays) of the net heat flux through an infinite cylinder having cold black walls at uniform temperature

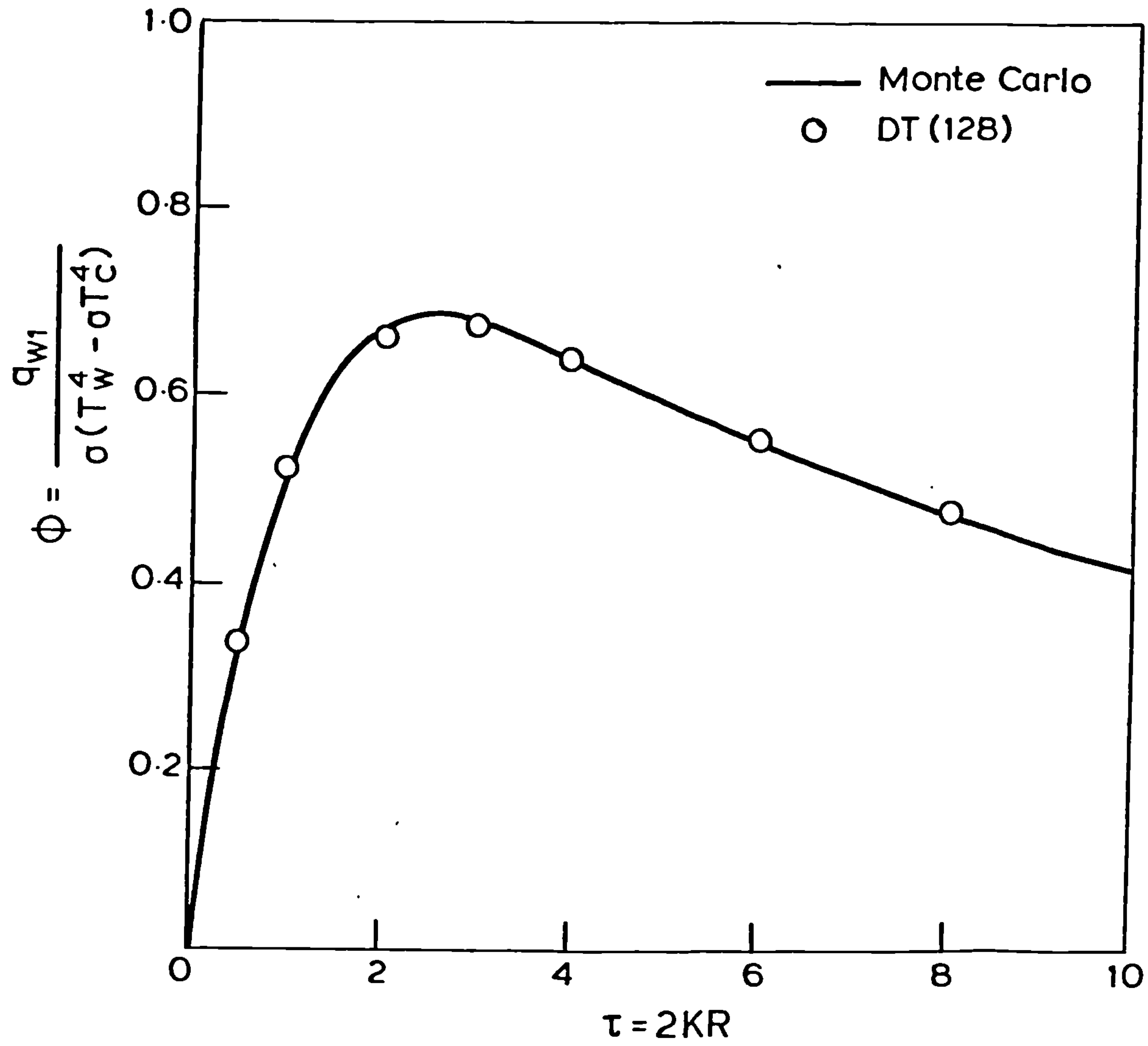

Figure 7.17 Comparison of the Monte Carlo solution of ϕ with the DT method (128 rays) for an infinite cylinder with hot black wall and uniform heat generation inside

$$\phi = \frac{q_w}{\sigma(T_w^4 - T_c^4)} \tag{7.2.1}$$

versus optical thickness where T_c is the temperature at the centre, for various optical diameters. The exact solution has been obtained by the Monte Carlo method (Cess, 1966). The DT solution was derived using 128 rays. There is exact energy balance.

We look at the temperature distribution from the wall to the axis for the above test case, but for a wall temperature of zero (cold wall). Fig. 7.18 compares the Monte Carlo solution (Truelove, 1976) with the DT method using 128 rays leaving each grid wall area. The optical diameter is 4.0. Results for 2.0 and 1.0 are also presented.

7.2.3. Two Infinitely Long Co-Axial Cylinders Sandwiching Gas at Prescribed Temperatures

Consider two infinite co-axial cylinders with cold black walls sandwiching gas inside at a uniform temperature ($\sigma T_g^4 = 1.0$). Table 7.12 shows the net heat fluxes from the inside and outside walls for various outside to inside radii ratios and optical distances between the walls. As the ratio tends to 1, the flux tends to the one-dimensional parallel wall solution (fig. 7.1). For this solution, 16 rays were used. The energy balance is exact.

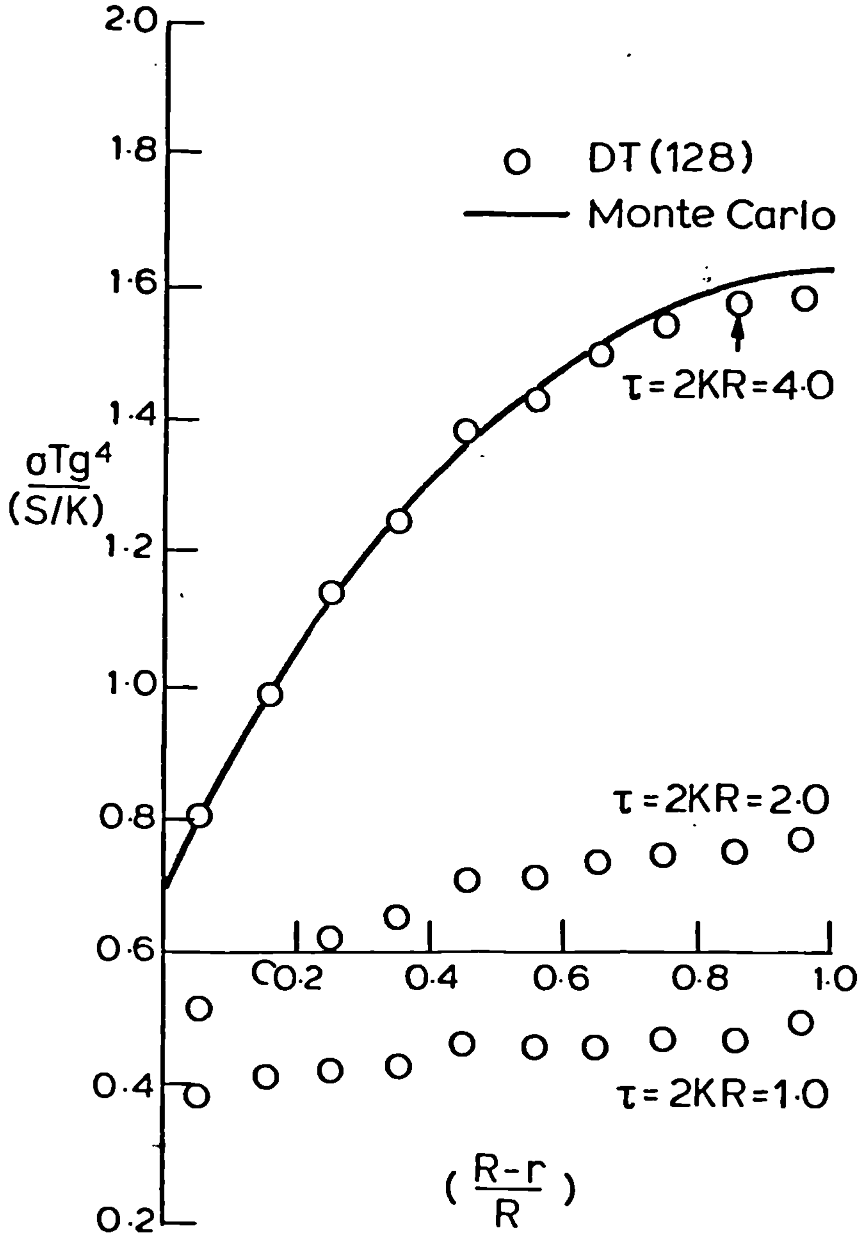

Figure 7.18 Comparison of the Monte Carlo solution of temperature (σT^4) distribution (Hyde and Truelove, 1977) with the DT method (128 rays) for an infinite cylinder for some typical optical diameters, with cold black wall and uniform heat generation inside

Ratio r_2/r_1	Optical thickness $K(r_2-r_1)$	Heat flux to inside wall	Heat flux to outside wall
10	0.1	0.122	0.183
	1.0	0.705	0.814
	2.0	0.907	0.944
	3.0	0.970	0.977
	4.0	0.990	0.989
2.0	0.1	0.133	0.198
	1.0	0.736	0.823
	2.0	0.923	0.950
	3.0	0.976	0.984
	4.0	0.993	0.994
1.0001	0.1	0.171	0.171
	1.0	0.782	0.782
	2.0	0.939	0.939
	3.0	0.982	0.982
	4.0	0.994	0.994

Table 7.12 Solution of heat fluxes through the inside and outside cold black walls for two infinitely long co-axial cylinders sandwiching gas at uniform temperature using the DT method (16 rays)

7.2.4 Two Infinitely Long Co-Axial Cylinders with Prescribed Uniform Heat Generation

Consider two infinitely long co-axial cylinders with black walls and the inner wall at temperature T_{w1} and the outer wall at temperature T_{w_2}. Let there be no heat generation in the annulus. Fig. 7.19 shows the comparison between the Monte Carlo results for ϕ (Cess, 1966) and the discrete transfer method using 128 rays. The optical distance between the wall ranges from 0.0 to 4.0. This is the region where many flux methods fail (Deissler, 1964, for example).

Further the temperature distribution for each case needs to be evaluated. Fig. 7.20 shows the Monte Carlo solution (Hyde and Truelove, 1977) for two optical thicknesses, 2.0 and 1.0 with the ratio $r_2/r_1 = 10.0$.

7.2.5 Finite Cylinders

A number of useful examples have been presented by Bartelds (1976). Most of these have been predicted using the DT method and some of these are presented here. Firstly consider a finite cylinder with black walls at temperature $500^{o}C$ containing gas at uniform temperature of $1000^{o}C$. The absorption coefficient of the gas is $0.25m^{-1}$. The dimensions of the cylinder are given on Fig. 7.21. The incident flux (q_{-}) is compared using the discrete transfer method (128 rays) with the exact solution (Bartelds 1976) on the same figure.

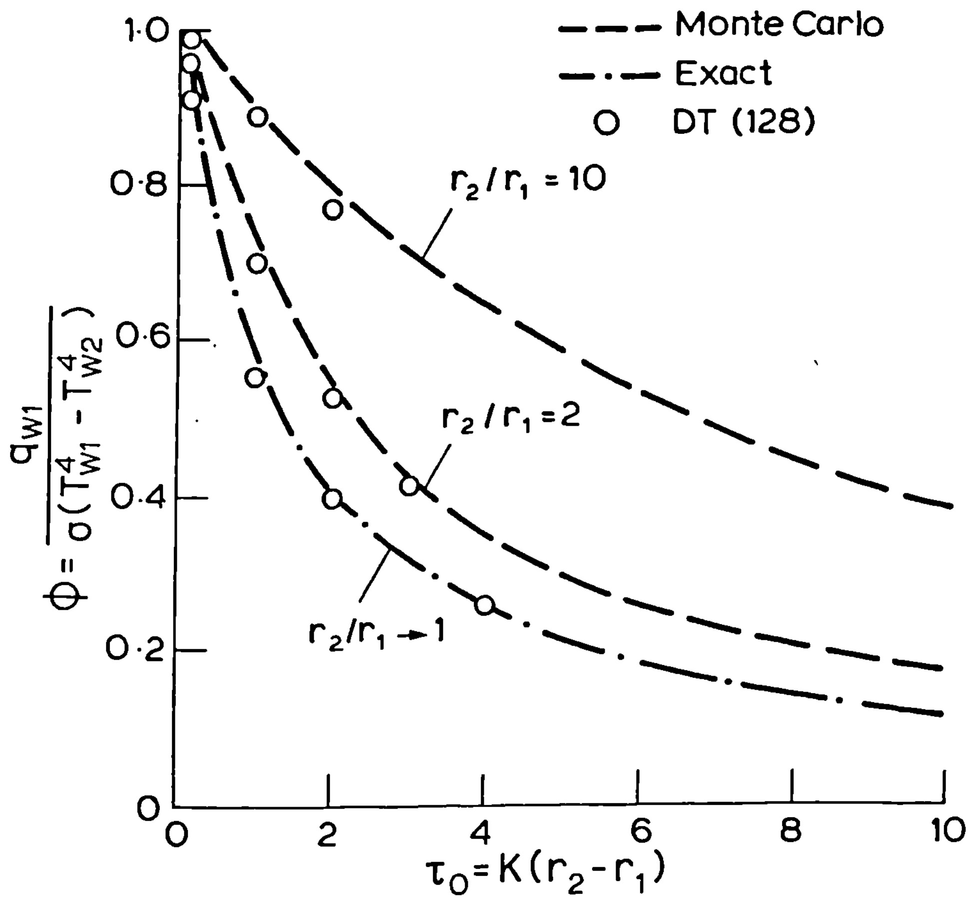

Figure 7.19 Comparison of Monte Carlo solution of ϕ (Cess, 1966) with the DT method (128 rays), for two infinitely long co-axial cylinders with black walls sandwiching uniformly heat releasing gas

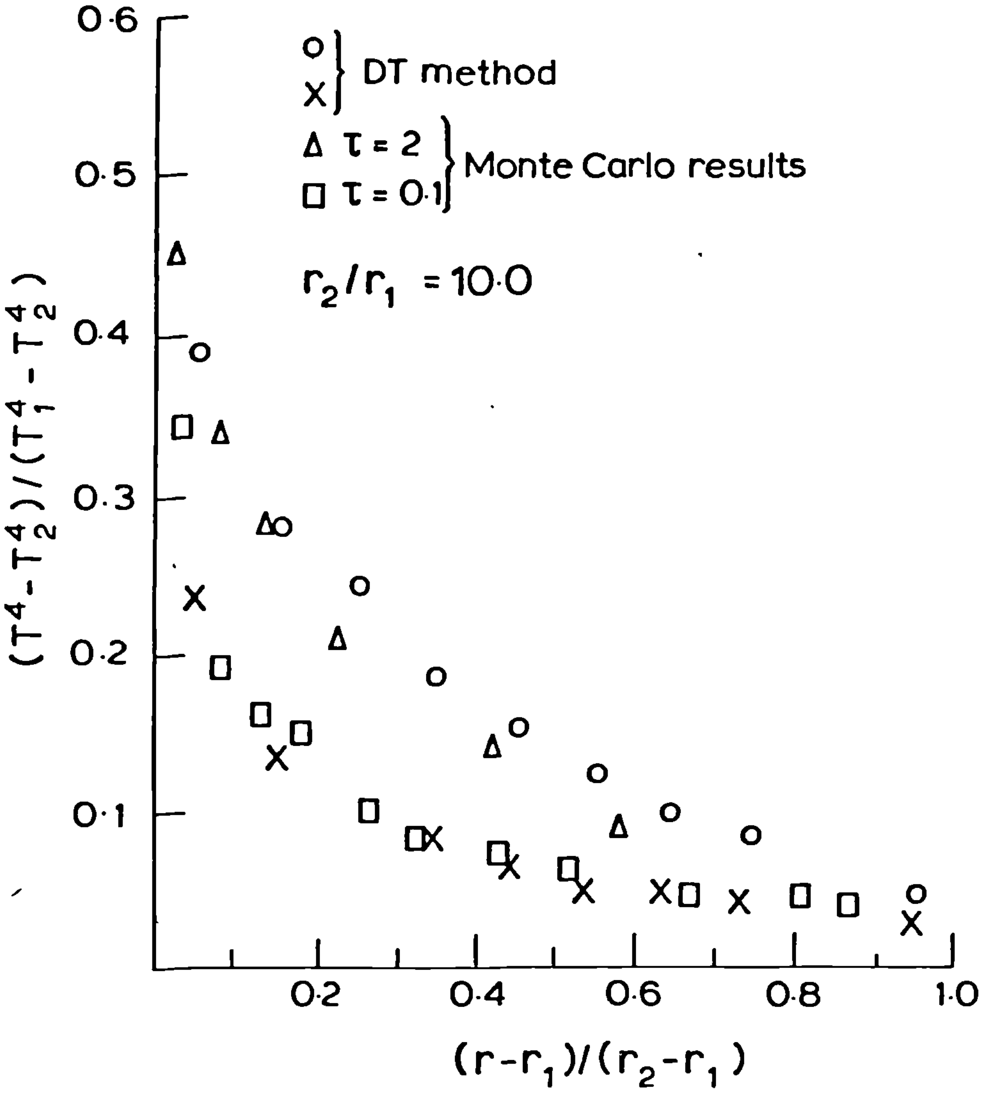

Figure 7.20 Comparison of the temperature distributions for the co-axial cylinders, optical thicknesses 2.0 and 1.0 and ratio r_2/r_1 = 10.0 of the Monte Carlo (Truelove, 1976) and the DT method (218 rays) sandwiching a gas with no internal heat generation

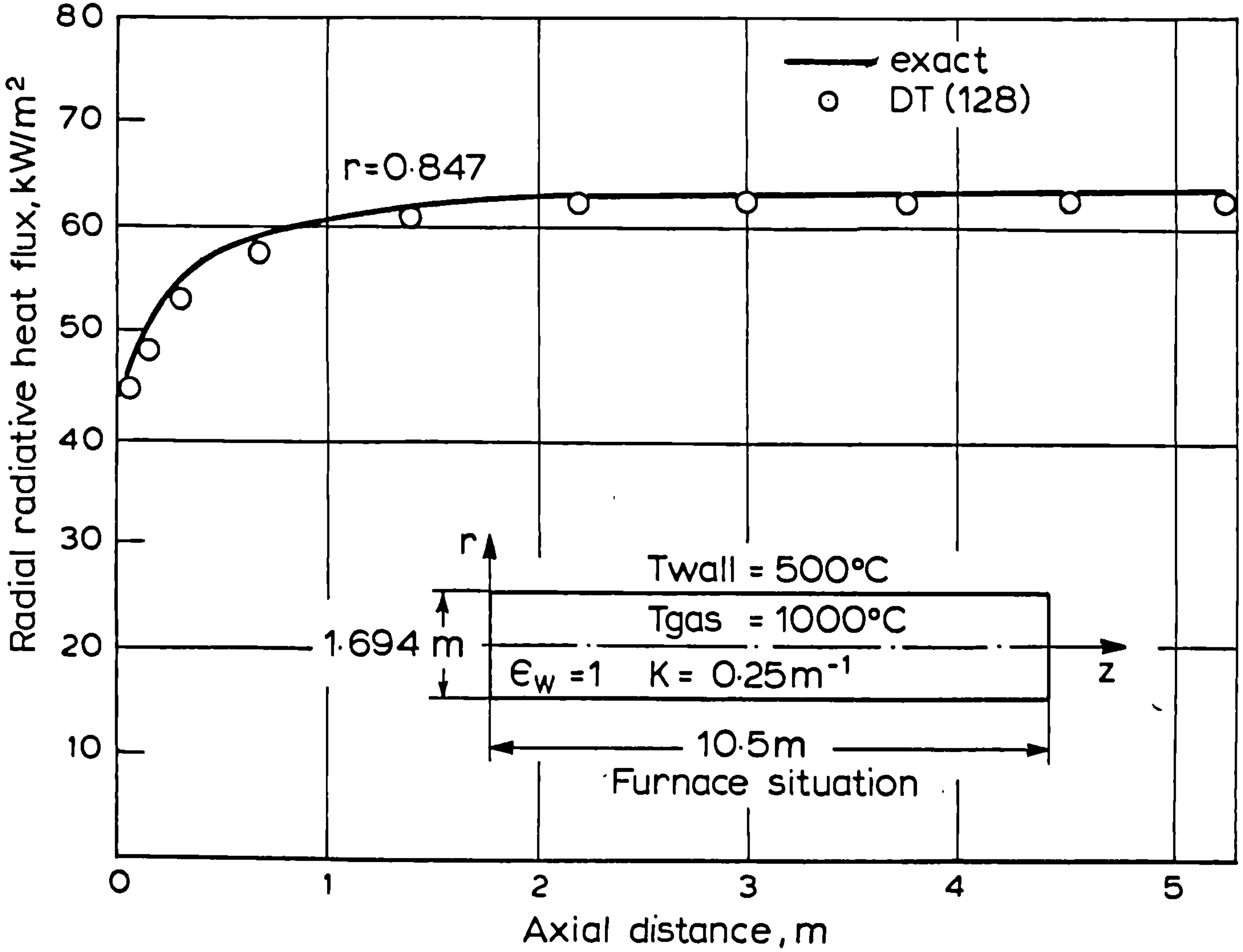

Figure 7.21 Comparison of the incident radiative heat flux of exact solution (Bartelds, 1976) and the DT method (128 rays) for a finite cylinder with black walls containing gas at uniform temperature

The next case to be examined is a finite cylinder with non-black walls. The gas inside is at uniform temperature. The absorption coefficient is varied and the maximum incident flux is recorded. The size and conditions are shown on Fig. 7.22. For this validation a computer code for any orthogonal grid was used simply to illustrate the flexibility of the discrete transfer method, as opposed to the code for the other validations in this section which takes the axi-symmetric property of cylinders into account. It should be noted that the second code would normally be used because it would consume less computer time. The orthogonal grid code can easily be adapted to other shaped objects, while the second one is specifically for axi-symmetric enclosures only. The grid used is shown in Fig. 7.22. Table 7.13 shows the results for the maximum incident flux obtained by the discrete transfer method (4 rays) and the zone method for two different wall temperatures and various absorption coefficients.

	Zone		DT method (4 rays)	
	I - 1	I - 2	I - 1	I - 2
K = 0.1	200.8	89.5	201.	90.1
K = 0.2	224.4	143.5	225.	144.9
K = 0.5	258.5	221.1	259.8	224.7
K = 0.8	271.5	251.3	273.7	256.5
K = 1.2	278.8	268.6	281.5	

Table 7.13 Comparison of the maximum incident radiative heat flux densities at side wall, K_w/m^2 using the zone method (Bartelds 1976) and the DT method (orthogonal version, 4 rays) for the enclosure described on Fig. 7.22

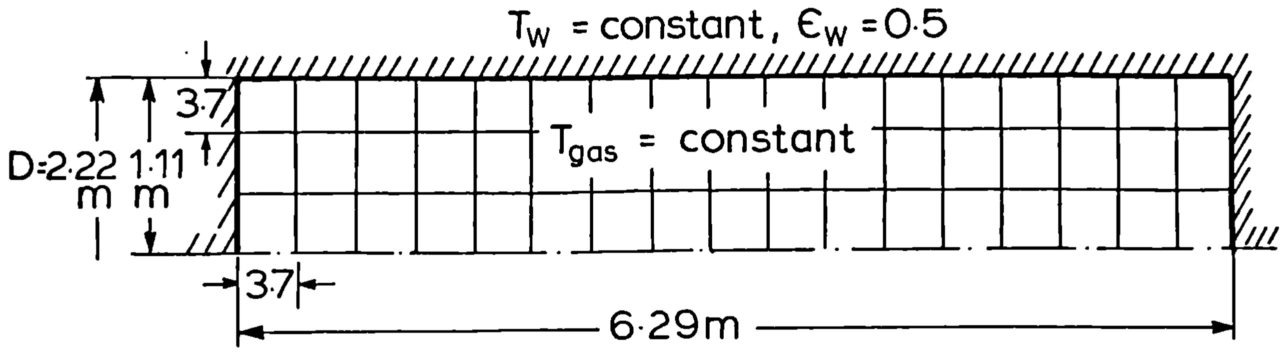

Case I - 1 T_g = 1500 K

T_w = 1300 K

Case I - 2 T_g = 1500 K

T_w = 300 K

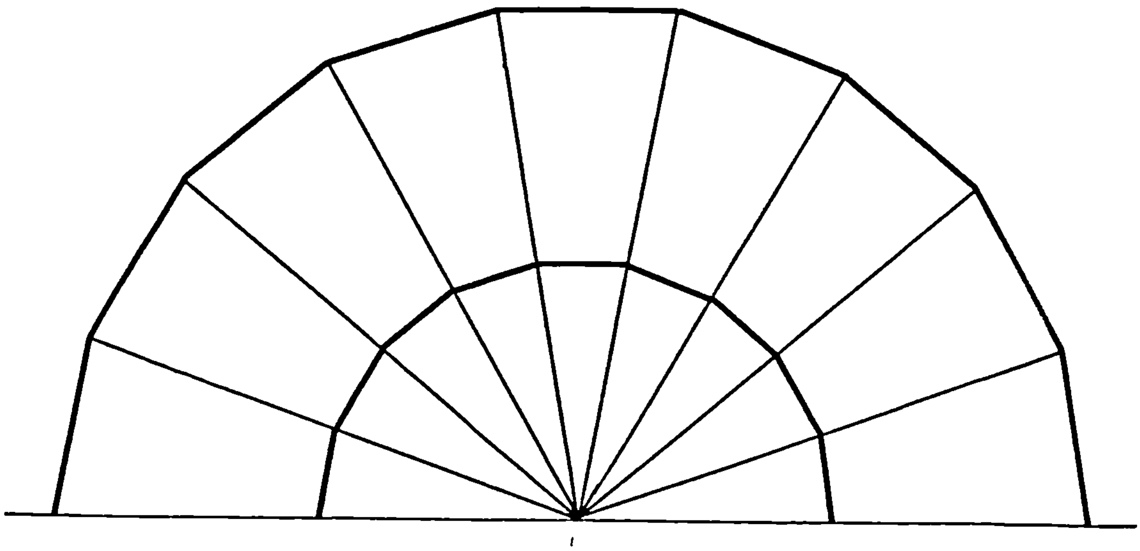

Fig. 7.22 The dimensions of the finite cylindrical enclosure with the conditions both inside and on the boundary, and the end view of the orthogonal grid used for this validation

Consider a finite cylinder with walls at temperature 300K and emissivity 0.5. The dimensions of the enclosure and the grid used are shown on Fig. 7.23. Now let the temperature drop smoothly as shown on Fig. 7.23. Using the more usual axi-symmetric computer code version of the discrete transfer model with 128 rays, the incident flux (q_-) is plotted with the zone solution (Bartelds 1976) in Fig. 7.24.

Now the temperature distribution is altered to the one shown on Fig. 7.25. The boundary conditions and the dimensions remain the same. The absorption coefficient is altered to 0.1. Using the discrete transfer method (128 rays), the incident flux (q_-) is plotted with a similar solution derived using the zone method (Bartelds, 1976) in Fig. 7.26.

7.2.6 Finite Cylinder with Varying Temperatures and Absorption Coefficients

As a final example, we consider what is perhaps a more realistic situation. Consider a finite cylinder raidus 1m and 5m long. The walls are at 500^oK and the emissivity is 0.8. There is a hot region (Fig. 7.27) where the temperature is 1700^oK and absorption coefficient $0.6m^{-1}$. The rest of the chamber is at 1100^oK and the absorption coefficient there is $0.05m^{-1}$. Two solutions of the discrete transfer method (128 rays, 8 rays) are presented in Fig. 7.28. The comparisons are made with a Monte Carlo solution (Gibb, 1974).

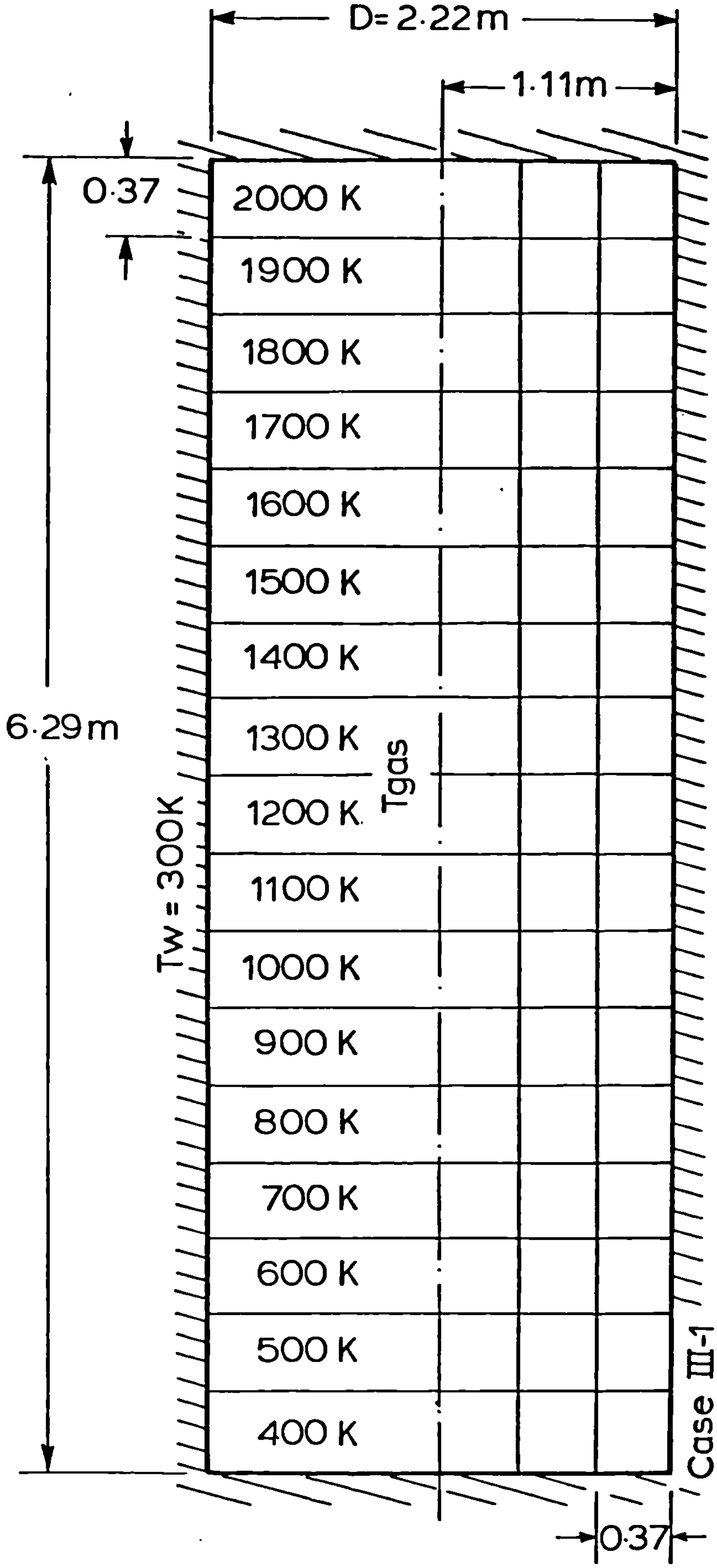

Figure 7.23 The dimensions and specification of conditions in a finite cylindrical enclosure with smoothly dropping temperature and non-black walls

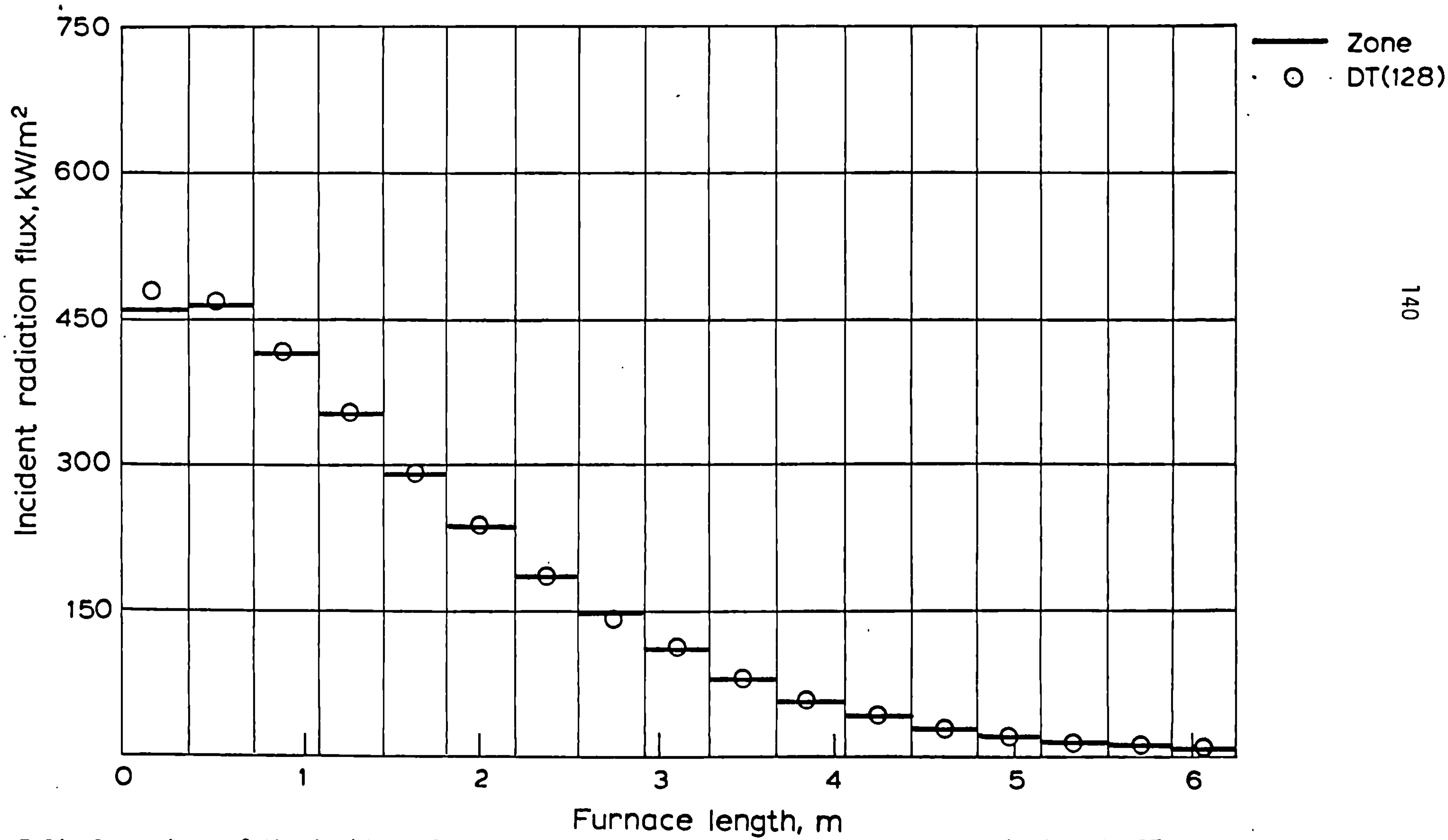

Figure 7.24 Comparison of the incident flux obtained by the zone method (Bartelds, 1976) with the DT method (128 rays) for the case described on Fig. 7.23

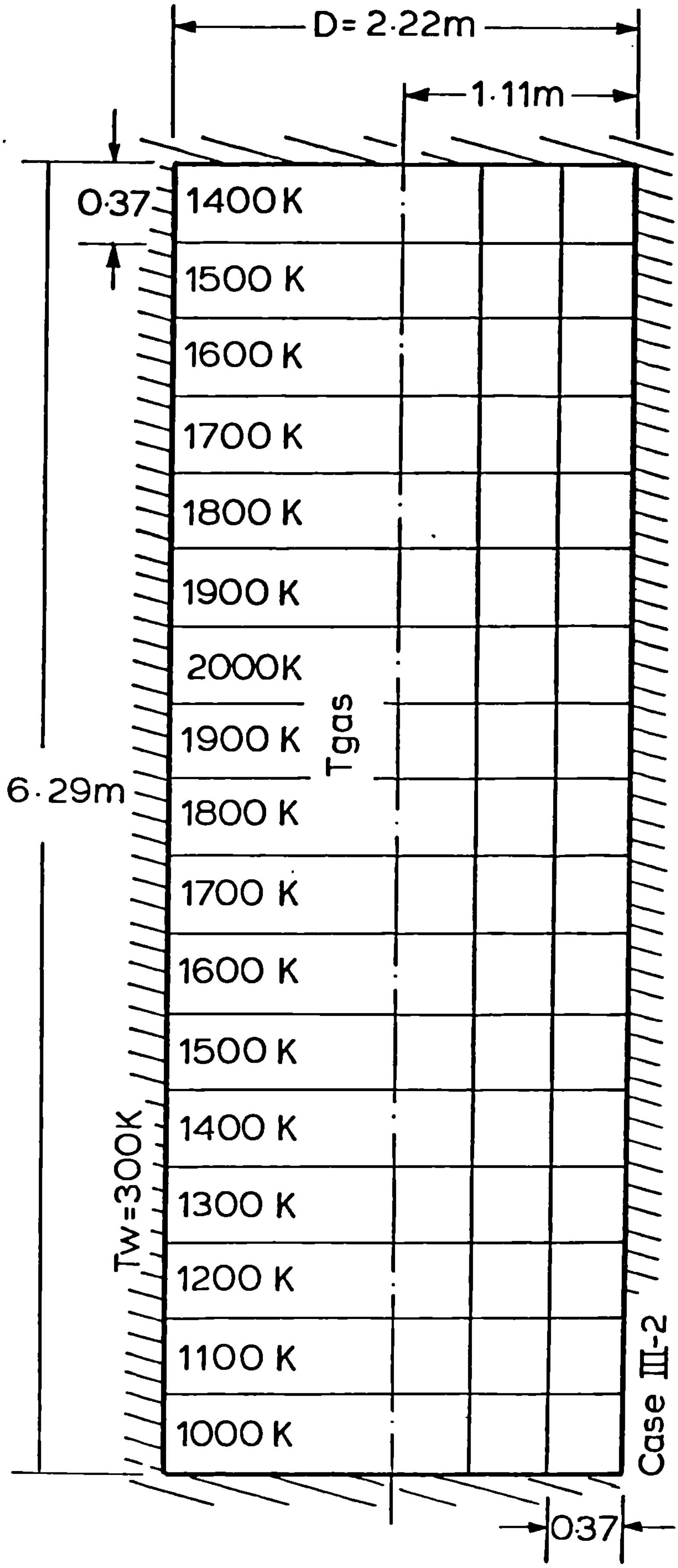

Figure 7.25 The dimensions and specification of conditions on a finite cylindrical enclosure with changing temperatures and non-black walls

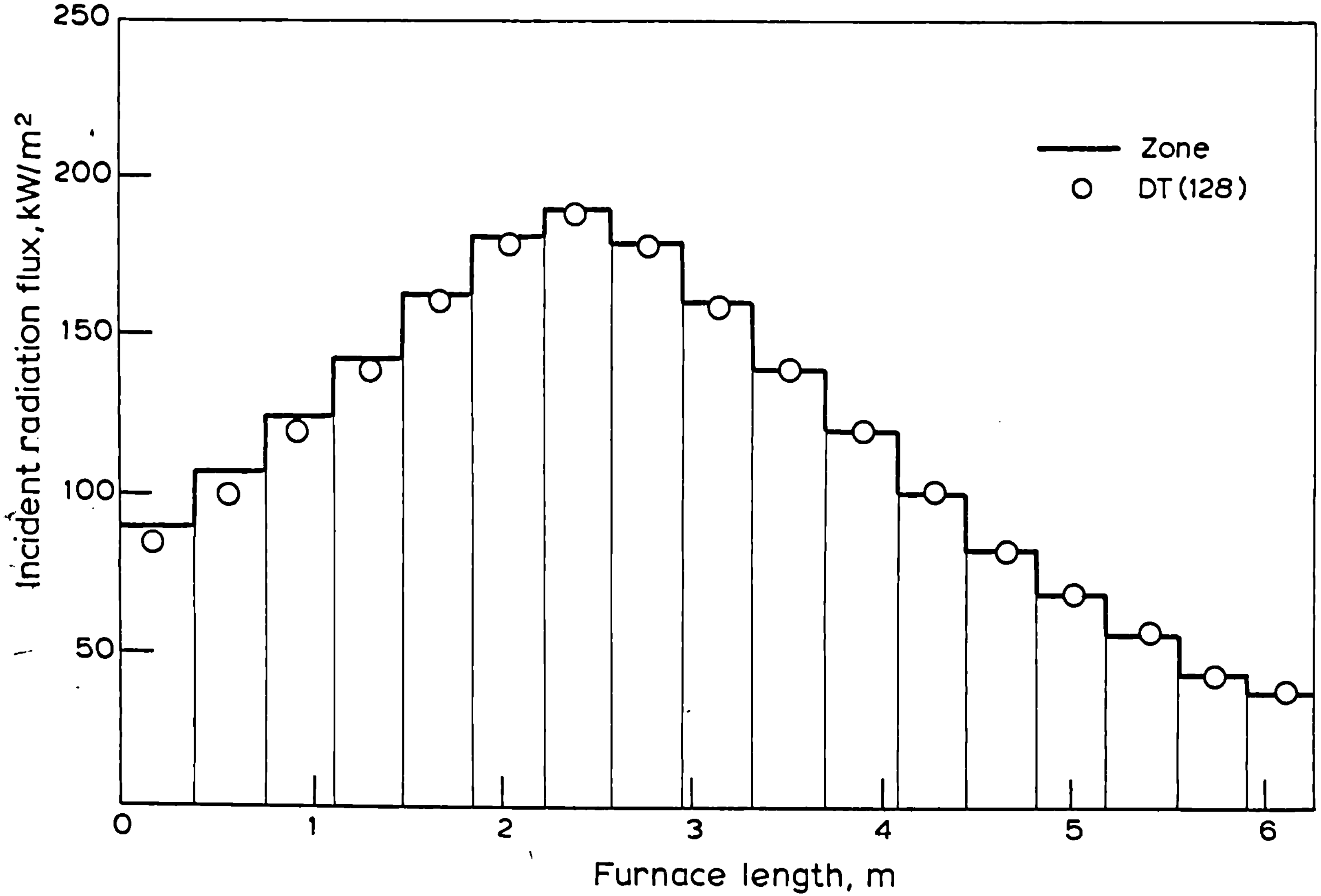

Figure 7.26 Comparison of the incident flux obtained by the zone method (Bartelds, 1976) with the DT method (128 rays) for the case described on Fig. 7.25

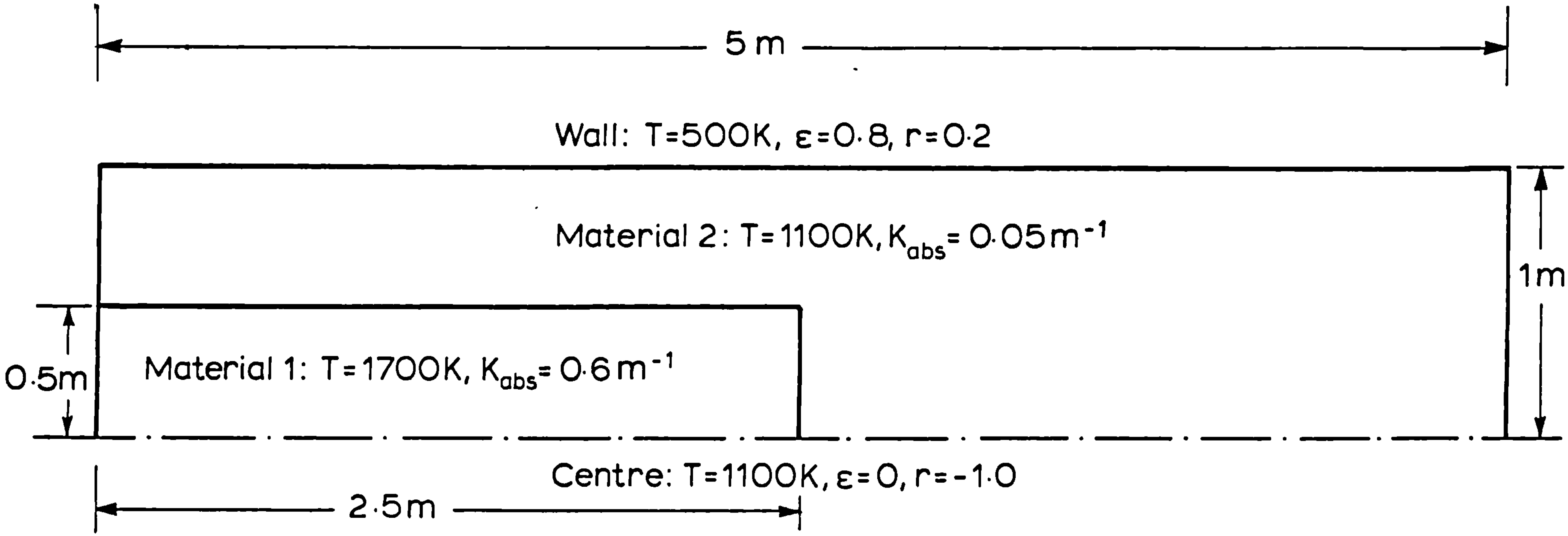

Figure 7.27 The dimensions and specification of the conditions in a finite cylindrical enclosure with non-black walls

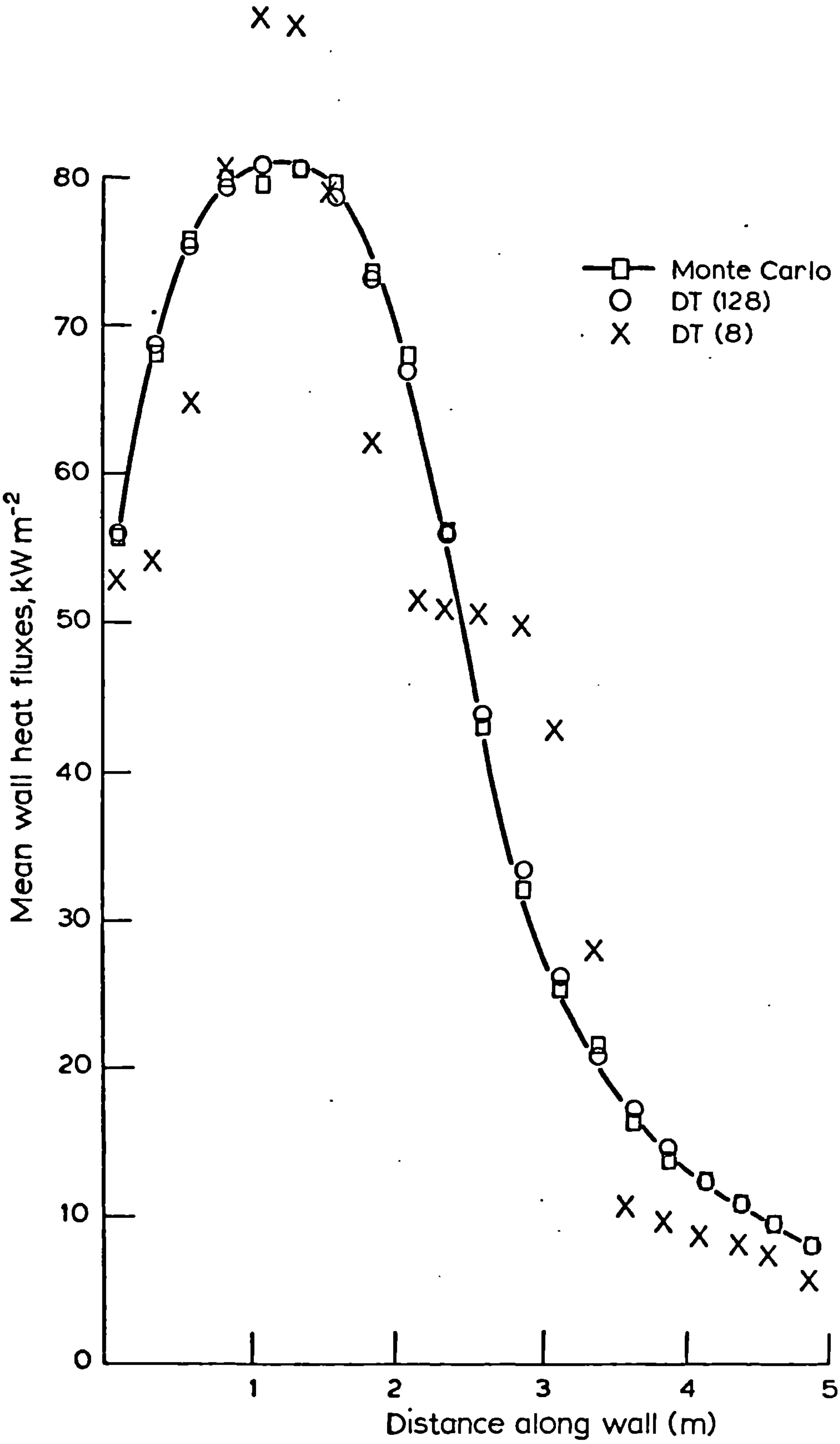

Fig. 7.28 Comparison of the Monte Carlo solution (Gibb, 1974) of the net heat flux through the wall with two solutions using the DT method (128 rays, 8 rays)

7.3 Application to Determination of View Factors

7.3.1 Usage

It is interesting to note that view factors can also be calculated for almost any type of surface using the DT method. Given a surface, it is divided into a grid system such that none of the grid cell subtends an exceptionally large solid angle at the point at which the view factor is being evaluated. The required integrals are then discretised and summed. These view factors so determined were checked against established values for several cartesian cases and good agreement was obtained.

CHAPTER 8

SCATTERING AND NON-GRAY SYSTEMS

8.1 Inclusion of Scattering in the Discrete Transfer Method

8.1.1 Basic Equations

The Discrete Transfer method can be extended to solve a more general form of transport equation (Ozisik, 1973), namely:

$$\frac{dI}{ds'} = -I + S_T \tag{8.1.1}$$

where S_T can be any combination of terms which can be regarded as constant within each cell per iteration as the ray travels through the medium. The analysis done in Chapter 6 can be carried through for eq. (8.1.1) with $\frac{\sigma T_g^4}{\pi}$ term replaced by S_T and K_s by s' where K is here regarded as an extinction coefficient which in general may include the effects of scattering as well as absorption.

Consider the transport equation for an absorbing-emitting-scattering medium. A ray travels through a cell in the medium of temperature Tg and absorption coefficient K_g. Let the scattering coefficient be K_S. Then the change in the intensity of the ray can be related as follows:

$$\frac{dI}{ds} = -(K_g + K_S)I + K_g \frac{\sigma T_g^4}{\pi} + \frac{K_S}{4\pi} \int_{4\pi} P(\underline{\Omega},\underline{\Omega}')I(\underline{\Omega}')d\Omega' \tag{8.1.2}$$

where $P(\underline{\Omega},\underline{\Omega}')$ is a probability function for scattering. (Ozisik, 1973). It is the probability that incident radiation in the direction $\underline{\Omega}'$ will scatter into an element of solid angle $d\underline{\Omega}$ about the direction $\underline{\Omega}$ of the ray. For isotropic scattering, we have $P(\underline{\Omega},\underline{\Omega}') = 1.0$;

a simple anisotropic approximation which often appears in the literature (see for example Dayan and Tien, 1975) is

$$P(\underline{\Omega},\underline{\Omega}') = 1+b(\underline{\Omega}'.\underline{\Omega}) \tag{8.1.3}$$

where b is a constant between +1 and -1. If we define:

$$s' = (K_g + K_S)s \tag{8.1.4}$$

and

$$\omega = \frac{K_S}{K_g+K_S} \tag{8.1.5}$$

then eq. (8.1.2) reduces to the form of (8.1.1) where

$$S_T = (1-\omega)\frac{\sigma T_g^4}{\pi} + \frac{\omega}{4\pi}\left[\int_{4\pi} I(\underline{\Omega}')d\Omega' + b\underline{\Omega}.\int_{4\pi} I(\underline{\Omega}')\,\underline{\Omega}'.d\Omega'\right] \tag{8.1.6}$$

The above expression can often be found in the literature (Beach et al, 1970 for example). Notice if $\omega = 0.0$, S_T then represents a non-scattering medium and $s' = K_g s$.

Since the terms of S_T (eq. 8.1.5) can all be regarded for each ray within a given cell, we can apply the Discrete Transfer method. The quantities in the square brackets, the zeroth and first moments of I, have to be accumulated in separate storage locations.

If there is uniform heat generation S in the interior of a cartesian geometry, eq. (8.1.2) is integrated over the 4π solid angle to yield

$$\frac{S}{4\pi} = -\frac{1}{4\pi}\int I d\Omega + (1-\omega)\frac{\sigma T_g^4}{\pi} + \frac{\omega}{4\pi}\left[\int_{4\pi} I d\Omega'\right] \tag{8.1.7}$$

which can be rewritten as

$$\frac{\sigma T_g^4}{\pi} = \frac{1}{4\pi}\int I d\Omega + \frac{S}{(1-\omega)4\pi} \tag{8.1.8}$$

substituting eq. (8.1.8) into eq. (8.1.5) for T_g, we get

$$S_T = \frac{S}{4\pi} + \frac{1}{4\pi} \int I d\underline{\Omega} + \frac{\omega b}{4\pi}\underline{\Omega} \int_{4\pi} I \underline{\Omega}' d\Omega' \qquad (8.1.9)$$

Replacing eq. (8.1.9) for the S_T term in the transport equation (8.1.1) we may now solve using the procedures described in Chapter 6.

8.1.2 Validation for a One-Dimensional Parallel Plate Case

Consider two parallel cold black plates sandwiching gas at uniform temperature ($\sigma T_g^4 = 1.0$). Let the total optical thickness ($(K_g+K_S)L$) be τ_0. Then for an isotropic scattering gas, a comparison between the DT and exact net fluxes out of the wall is given by table 8.1. The exact solution has been obtained from Beach et al (1970). The DT solutions use 10 rays, the DT energy balance is exact.

Now let us consider two parallel black plates at temperatures $\sigma T_1^4 = 1.0$ and $\sigma T_2^4 = 0.0$ respectively. Let the medium inside be in radiative equilibrium ($S = 0.0$). A comparison between the DT and exact net fluxes out of wall 1 is given by table 8.2 for various optical thicknesses. The exact solution is due to Dayan and Tien (1975).

The disagreement for the larger optical thicknesses is unexpected and represents a source for a further and detailed study.

$q^2/\sigma T_g^4$	$\omega = 0.5$	$b = 0$
τ_0	DT(10)	Exact
0.1	0.0915	0.0911
0.2	0.1704	-
0.3	0.2399	-
0.4	0.3017	-
0.5	0.3562	-
0.6	0.4062	-
0.8	0.4900	-
1.0	0.5575	0.5591
1.5	0.6750	-
2.0	0.7443	-
2.5	0.7853	-
3.0	0.8097	-
10.0	0.8385	0.8535

Table 8.1 Comparison of Discrete Transfer and Exact wall fluxes for: Cold black walls sandwiching a uniform temperature, isotropically scattering medium using the Discrete Transfer Method (10 rays)

τ_0	ωb -0.7		ωb = 0.0		ωb = 0.7	
	DT(10)	exact	DT(10)	exact	DT(10)	exact
0.1	0.899	0.901	0.915	0.916	0.931	0.931
0.2	0.819	-	0.848	-	0.888	-
0.3	0.751	-	0.793	-	0.834	-
0.4	0.693	-	0.745	-	0.797	-
0.5	0.643	0.663	0.704	0.704	0.765	0.750
0.6	0.598	-	0.667	-	0.737	-
0.8	0.522	-	0.604	-	0.690	-
1.0	0.460	0.505	0.553	0.553	0.652	0.611
1.5	0.345	-	0.458	-	0.581	-
2.0	0.267	-	0.391	-	0.534	-
2.5	0.211	-	0.342	-	0.499	-
3.0	0.170	0.260	0.304	0.302	0.473	0.358

Table 8.2 Comparison of Descrete Transfer and exact wall fluxes for: one hot, one cold wall with no heat generation using DT(10 rays)

8.2. Calculation of Radiative Transfer in an Isotropically Scattering Medium with Gas and Particles at Different Temperatures

Consider a control volume containing gas at uniform temperature T_g and absorption coefficient K_g. Let the gas contain particles at temperature T_p, emissivity ε_p, reflectivity r_p, then the transport equation can be written in the following way, if the medium is also isotropically scattering (Gibb,(1975)):

$$\frac{dI}{ds} = K_g\left(\frac{\sigma T_g^4}{\pi} - I\right) + \varepsilon_p K_p\left(\frac{\sigma T_p^4}{\pi} - I\right) + r_p K_p\left(\frac{1}{4\pi}\int I(\underline{\Omega}')d\Omega' - I\right) \tag{8.2.1}$$

where K_p is a temperature and particle size weighted particle surface area, see Gibb (1975).

Next if we define

$$S_T = \left[K_g \frac{\sigma T_g^4}{\pi} + \varepsilon_p K_p \frac{\sigma T_p^4}{\pi} + \frac{r_p K_p}{4} \int I \, d\Omega\right] \Big/ (K_g + \varepsilon_p K_p + r_p K_p) \tag{8.2.2}$$

$$\text{and } s' = (K_g + \varepsilon_p K_p + r_p K_p)s \tag{8.2.3}$$

Then equation (8.2.1) reduces to the form eq. (8.1.1) and can be solved by the Discrete Transfer procedure.

The problem now considered and its Monte Carlo solution have been provided by Gibb (1974). Using his words it is expressed as follows. "Consider a cylindrical furnace chamber (5m long, 1m radius) containing an 'PF flame', approximated as a 5m long cylinder, radius 0.5m, co-axial with the furnace chamber. The first half of the flame contains gas at 1700K and combusting coal particles at a temperature 1750K. The gas (soot) absorption coefficient was assumed to be 0.5m^{-1}. The particle absorption coefficient was estimated by Gibb by assuming a mean particle radius of 25μ and an air/fuel volume ratio of 10^4:1. In this region $\varepsilon_p \approx 1.0$ and $r_p \approx 0.0$ so that $K_p \approx 3m^{-1}$ and $K_s \approx 0.0$. The second half of the flame contains gas at 1400K (K_g = $0.5m^{-1}$) and inactive char particles. In this region ε_p and r_p are taken as 0.5 giving K_p = $1.5m^{-1}$ and K_s = $1.5m^{-1}$. The scattering here is assumed to be isotropic.

The flame is assumed to be surrounded by an annulus of 'clear' gas which was simulated by setting T_g = 1100K, K_g = $0.1m^{-1}$. The furnace chamber has water cooled walls with T_W = 500K, ε_W = 0.8, r_W = 0.2. Fig. 8.1 gives the details of the problem specification.

Fig. 8.2 shows the Monte Carlo solution with the Discrete Transfer method of solution using effectively 64 rays. The agreement is very good along the cylindrical wall. The disagreement at some points is believed mainly due to the statistical scatter of the Monte Carlo solution.

8.3 Method of Solution for Non-Gray Problems

Many different methods and hypothesis are available for solving non-gray systems. (see Ozisik, 1973 for example). For the discrete transfer method we choose to use the band approximations and so reduce the problem to one of solving simultaneously several equations of the type (8.1.1).

Consider a medium with say r frequency bands each thickness $d\nu_i$ and at temperature T_g and absorption coefficient K_{ν_i}. Then the transport equation for the ith band is given by:

$$\frac{dI_{\nu_i}}{ds} = - K_{\nu_i} I_{\nu_i} + \frac{K_{\nu_i} \sigma T^4_{g_i}}{\pi} \tag{8.3.1}$$

for all i's 1 to r. Equation (8.3.1) can be evaluated individually

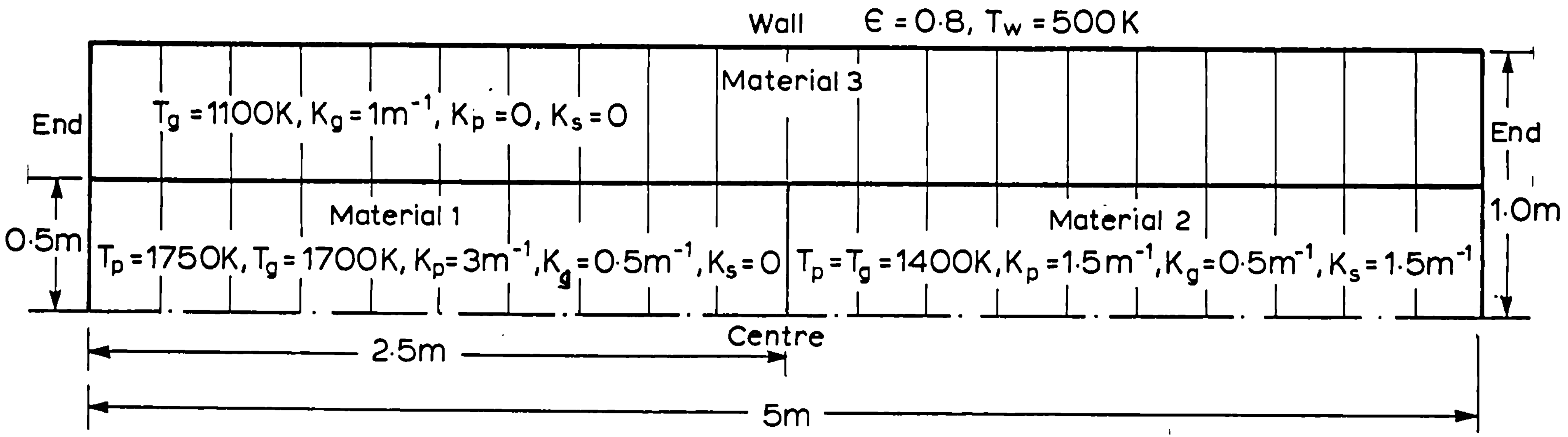

Fig. 8.1 Geometry and physical conditions of a cylindrical enclosure

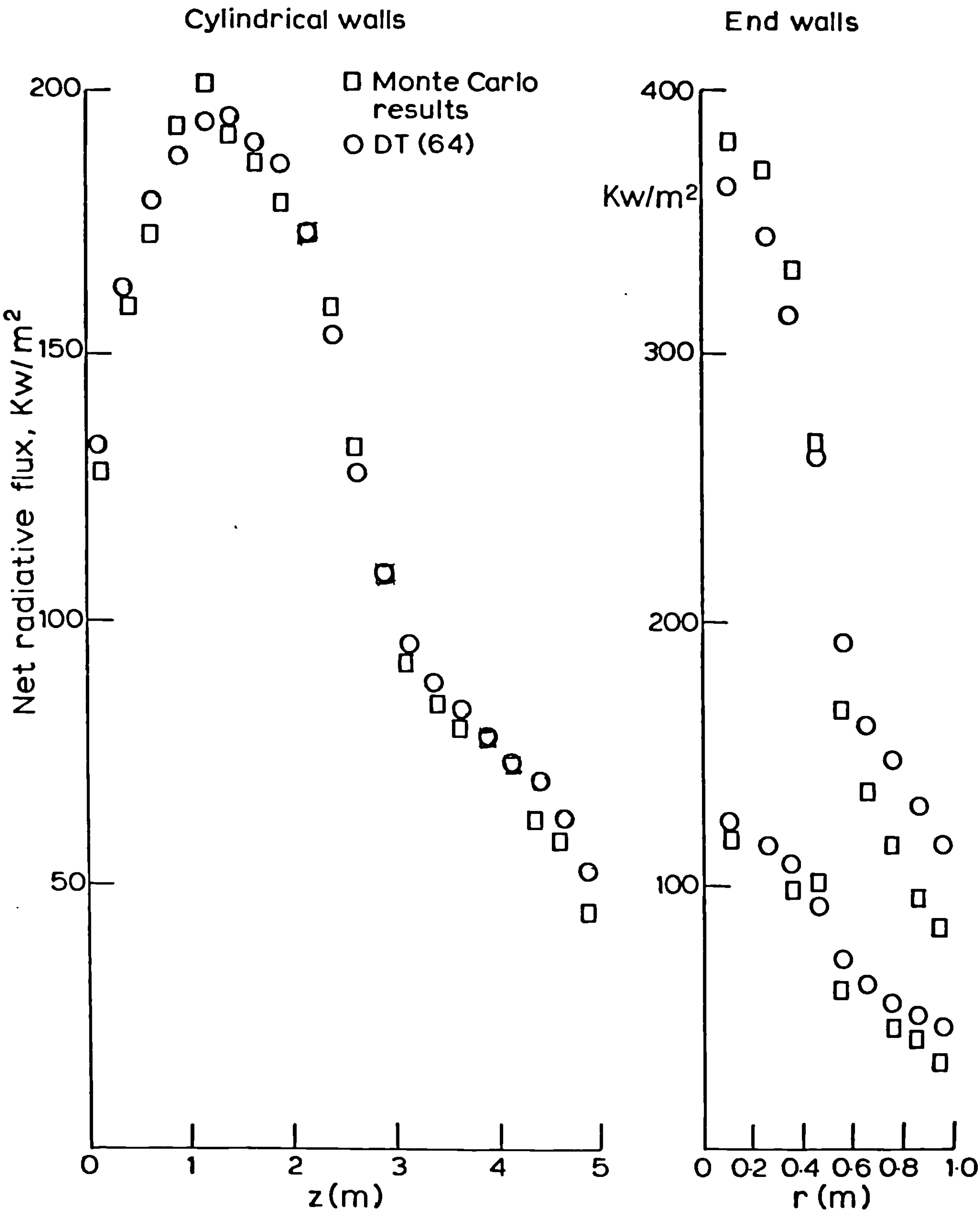

Fig. 8.2 Comparison of Monte Carlo and DT (64 rays) of net radiative flux for conditions as described in fig. 8.1

for every ray since the distances travelled by rays in each cell remains the same.

The intensity I is then evaluated by simply summing the product of each intensity with the band thickness

$$I = \sum_i I_{\nu_i} d_{\nu_i} \tag{8.3.2}$$

All the other quantities can be similarly evaluated.

CHAPTER 9

CONCLUSIONS AND FUTURE RECOMMENDATIONS

9.1 Conclusions

In Chapter 1, we saw that there were basically four methods available to solve for radiative transfer: analytic , zone, Monte Carlo and flux. The analytic methods offer little useful potential because of the complicated integro-differential equations involved, this fact was made evident in Chapter 2. While the zone and Monte Carlo methods can be regarded as numerically exact, the zone method requires considerable storage (Chapter 2) and the Monte Carlo is vulnerable to statistical errors (Chapter 2). This leaves only some kind of flux method as offering a solution to the economic problem posed by engineering calculations.

In Chapters 3 and 4 a flux method was proposed based on the assumption of a special Taylor's Series for the intensity distribution. Three parameters were introduced related to some special surfaces of integration chosen such that the final form of the equations is compact (fig. 3.2). During validation studies, four tables were drawn up recommending relations for these parameters as a function of optical thicknesses for both source and temperature prescribed problems in both Cartesian and cylindrical co-ordinate systems.

Extensions to two dimensional problems revealed that these recommendations did not yield the expected success, especially near the corner regions. Other methods of linking the three parameters with the variables of the problem were therefore investigated in Chpater 5. One of them involved measuring the mean optical depth for every point in the enclosure. Although this gave better results, a small geometric change in one region of the enclosure would cause the mean path lengths for the whole enlcosure to change and not necessarily by a common factor. In practice an extra subroutine would be required and a loss of economy incurred.

The second suggestion involved linking the parameters to the intensity distributions. Since the number of possible intensity distributions is nearly infinite and the amount of data available is very small, this approach was abandoned. With the availability of more data, this method may deserve further investigation. Nevetheless, this particular flux model has been used in its present form at Imperial College with a good degree of success.

After considerable further investigation, it was discovered that the shape of the intensity distribution played a major role in determining the accuracy of any particular flux method. For the typically very discontinuous intensity distribution at a wall boundary, introduction of 'optically thin boundary layers' considerably improved the quality of solutions as was shown in Chapter 5. While the concept of boundary layers gave much insight into the problem, its application in practical problems has very little scope.

In Chapter 6 a new "Discrete Transfer" method was proposed. This may be considered a mixture of the flux, Monte Carlo and zone methods. The statistical dependence of the Monte Carlo method was replaced by discretizing the solid angle 2π. The excessive storage requirements of the zone method was removed. For most flux methods, once the assumptions on the intensity distributions are made, the rest of the solution is buried in a lot of often complex mathematical manipulations while for an engineer, the discrete Transfer method offers a better scope of understanding of the whole concept of radiative transfer. In the discrete transfer method, rays in specific directions are traced and various properties recorded.

Many validation cases were studied in Chapter 7. For all the cases, the predictions were very good. If the accuracy needs to be further improved, a change of a single parameter (no. of rays fired from each surface cell) is all that needs to be done. Crude solutions can be achieved by tracing less rays and a final solution could be calculated by simply increasing the number of rays towards the last few iterations. The computer-storage is small and complicated enclosure geometries can be easily handled.

The extension of the discrete transfer method to scattering and non-gray problems is shown in Chapter 8. Since the transport equations for both these systems can be reduced to a form similar to the original transport equation, no special problems arise except certain new integrals need to be stored. Considering this and all the evidence presented in Chapter 7, we feel that the discrete transfer method holds definite advantages over all other methods.

9.2 Future Recommendations

The flux method described in Chapters 3 and 4 is easy to incorporate with the existing flow procedures so extensions to other co-ordinate systems and also to non-gray, scattering systems are of interest. Whilst not much difference in the general performance is expected for a non-gray system, the flux approach should perform better for scattering systems since the intensity distributions would become more continuous.

Because the discrete transfer method can cope with more complex boundary conditions (part specular, part diffuse surfaces etc.) there is a need in some cases for obtaining more realistic solutions enabling fairer comparisons with experimental data.

The possibility of using the discrete transfer approach to solve other classes of transport equations is worth considering.

The calculation of first and second order moments of intensity at points inside the enclosure needs some further investigation as do problems in scattering and non-gray systems.

There is a need to produce a concise collection of "exact" solutions similar to those of Chapter 7 so that researchers can have a base by which a particular method can be judged for individual cases. The discrete transfer method could prove to be invaluable for such a venture.

Appendix (A2.1)

Analytic Solution of Rectangular Enclosure with Cold Black Walls

Consider an infinitely long rectangular enclosure with cold black walls. The width is a and the height is b. The contained gas is at uniform temperature T_g (fig. A2.1.1). The analysis which is now presented has been provided by Gibb (1977).

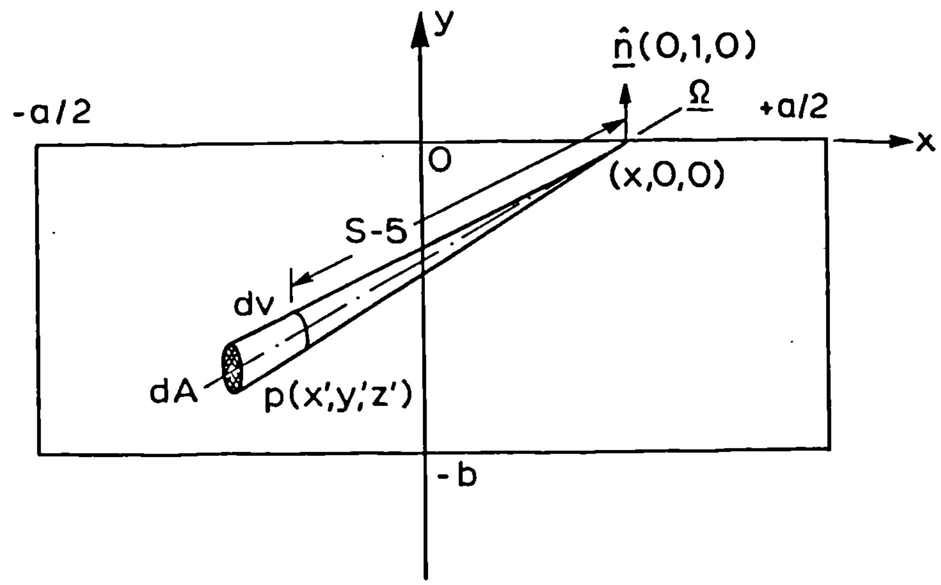

Fig. A2.1.1 A thin pencil of rays in a rectangular enclosure

The following expression can be obtained by integrating the transport equation (1.2.1) along a thin pencil of rays (fig. A2.1.1)

$$I(s) = \frac{\sigma T_g^4}{\pi} \int_0^s Ke^{-K(s-s')} ds' \qquad \text{(A2.1.1)}$$

Substituting this into the definition of flux (1.2.2) and replacing

$$d\Omega = \frac{dA}{(s-s')^2} \tag{A2.1.2}$$

$$d\Omega ds = \frac{dV}{(s-s')^2} \tag{A2.1.3}$$

and $$(\underline{\Omega}.\underline{n}) = -\frac{Y'}{s-s'} \tag{A2.1.4}$$

we obtain

$$q(x) = \frac{\sigma T_g^4}{\pi} \int Ke^{-K(s-s')}\left(-\frac{Y'}{(s-s')^3}\right)dV \tag{A2.1.5}$$

further from geometry

$$r = s-s' = \{(X-X')^2 + Y'^2 + Z'^2\}^{1/2} \quad \text{and } dV = dX'dY'dZ' \tag{A2.1.6}$$

Therefore eq. A2.1.5 reduces to

$$q(X) = \frac{\sigma T_g^4}{\pi} \int_{-\frac{a}{2}}^{\frac{a}{2}} dX' \int_{-b}^{0} (-Y')\, dY' \int_{-\infty}^{\infty} \frac{Ke^{-Kr}}{r^3}\, dZ' \tag{A2.1.7}$$

further if we define

$$\left.\begin{aligned} u &= KX' \\ u_o &= KX \\ v &= -KY' \\ w &= KZ' \\ \rho &= K[(u-u_o)^2 + v^2 + w^2]^{1/2} \\ \text{and} \quad \phi &= \frac{q}{\sigma T_g^4} \end{aligned}\right\} \tag{A2.1.8}$$

the expression A2.1.7 can further be simplified to

$$\phi = \frac{q}{\sigma T_g^4} = \frac{2}{\pi} \int_{-\frac{Ka}{2}}^{\frac{Ka}{2}} du \int_0^{Kb} v\, dv \int_0^{\infty} \frac{e^{-\rho}}{\rho^3}\, dw \tag{A2.1.9}$$

In order to solve the above equation, we put

$$\left.\begin{aligned} a^2 &= (u-u_0)^2 + v^2 \\ \text{and let}\quad J(a) &= \int_0^{\infty} \frac{e^{-\rho}}{\rho^3}\, dw \\ \mu &= \frac{1}{a}(a^2 + w^2)^{1/2} \end{aligned}\right\} \tag{A2.1.10}$$

so that

$$a^2 J(a) = \int_1^{\infty} \frac{e^{-a\mu}}{\mu^2\sqrt{(\mu^2-1)}}\, d\mu$$

$$= \int_a^{\infty} da' \int_{a'}^{\infty} da'' \int_1^{\infty} \frac{e^{-a''\mu}}{\sqrt{(\mu^2-1)}}\, d\mu$$

$$= \int_a^{\infty} da' \int_{a'}^{\infty} da''\, K_0(a'')$$

here K_0 is the modified K bessel function of zeroth order (Abramowity and Stegun (1965), Chapters 9 and 11).

$$a^2 J(a) = K_{i_2}(a)$$

$$= a(K_1(a) - K_{i_1}(a))$$

$$J(a) = \frac{1}{a}(K_1(a) - K_{i_1}(a))$$

Now let

$$j(u,b) = \int_0^{b} vJ((u^2+v^2)^{1/2})dv \tag{A2.1.11}$$

$$U = |u - u_0|, \quad B = Kb.$$

Substituting $\mu^2 = v^2 + U^2$, so that

$$j(U,B) = \int_{U}^{\sqrt{U^2+B^2}} (K_1(\mu) - K_{i_1}(\mu))d\mu$$

$$= K_o(U) - K_o((U^2+B^2)^{1/2}) - K_{i_2}(U) + K_{i_2}((U^2+B^2)^{1/2})$$

$$= L(U) - L((U^2+B^2)^{1/2}) \qquad \text{(A2.1.12)}$$

where $\qquad L(x) = K_o(x) - K_{i_2}(x)$

Therefore, we finally obtain:

$$\phi = \frac{q}{\sigma T_g^4} = \frac{2}{\pi} \int_{-\frac{Ka}{2}}^{\frac{Ka}{2}} \left[L(|u-u_o|) - L(\{(u-u_o)^2 + K^2b^2\}^{1/2})\right] du \qquad \text{(A2.1.13)}$$

The right-hand side of equation (A2.1.13) can now be solved using a simple quadrative formula, Simpson's method for instance.

Appendix A3.1

Integration over the surface surrounding the positive x axis

If Ω is the direction of the ray in a cartesian system with unit normals $\underline{i}$, $\underline{j}$ and $\underline{k}$, the direction cosines can be written as $(\underline{\Omega}.\underline{i})$, $(\underline{\Omega}.\underline{j})$ and $(\underline{\Omega}.\underline{k})$ in the respective coordinate directions. These are represented by X', Y' and Z' respectively in the text. In terms of the spherical angles:

$$X' = (\underline{\Omega}.\underline{i}) = \cos\theta \tag{A3.1.1}$$

$$Y' = (\underline{\Omega}.\underline{j}) = \sin\theta \cos\phi \tag{A3.1.2}$$

$$Z' = (\underline{\Omega}.\underline{k}) = \sin\theta \sin\phi \tag{A3.1.3}$$

$$d\Omega = \sin\theta \, d\theta d\phi \tag{A3.1.4}$$

where the angles θ and ϕ are defined in fig. (A3.1)

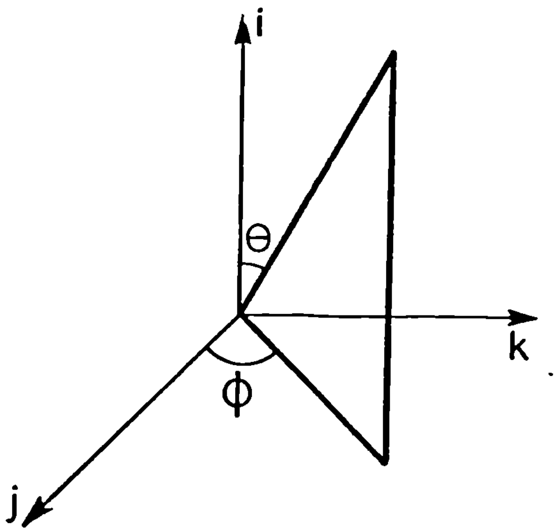

Fig. A3.1 Definition of θ and ϕ angles with respect to i, j, k axis

The limits of integration for the surface are $0 < \phi < 2\pi$ and $0 < \theta < \cos^{-1} X''$. Hence the following results can be easily derived:

$$\int_A d\Omega = 2\pi(1 - X'')$$

$$\int_A X' d\Omega = (1 - X''^2)$$

$$\int_A Y' d\Omega = 0$$

$$\int_A Z' \, d\Omega = 0$$

$$\int_A X'^2 \, d\Omega = \frac{2\pi}{3}(1 - X''^3)$$

$$\int_A Y'^2 \, d\Omega = \left(\frac{2}{3} + \frac{X''^3}{3} - X''\right) \qquad \text{(A3.1.5)}$$

$$\int_A Z'^2 \, d\Omega = \pi\left(\frac{2}{3} + \frac{X''^3}{3} - X''\right)$$

$$\int_A X' \, Y' \, d\Omega = 0$$

$$\int_A X'Z' \, d\Omega = 0$$

$$\int_A Y'Z' \, d\Omega = 0$$

$$\int_A X'^3 \, d\Omega = \frac{\pi}{2}(1 - X''^4)$$

$$\int_A Y'^3 \, d\Omega = 0$$

$$\int_A Z'^3 \, d\Omega = 0$$

$$\int_A X'^2\, Y'\, d\Omega = 0$$

$$\int_A X'^2 Z\, d\Omega = 0$$

$$\int_A Y'^2 X'\, d\Omega = \frac{\pi}{4}\,(1 - X''^2)^2$$

$$\int_A Y'^2 Z'\, d\Omega = 0$$

$$\int_A Z'^2 X'\, d\Omega = \frac{\pi}{4}(1 - X''^2)^2$$

$$\int_A Z'^2\, Y'\, d\Omega = 0$$

Similar integrals can be performed for other surfaces by appropriate rotations of the axis.

Appendix A3.2

The One-Dimensional Optically Thick Solution

We restate equation (3.2.10):

$$\alpha\frac{d^2C_1}{dX^2} = \frac{1}{\alpha}\left(B_1 - \frac{\sigma T^4}{\pi}\right) \tag{A3.2.1}$$

and the boundary condition

$$\frac{2\alpha}{3}\left(\frac{1+X_Q}{\varepsilon_1} - 1\right)\frac{dC_1}{dX} + \frac{\sigma T_1^4}{\pi} = \frac{C_1}{\varepsilon_1} - \left(\frac{1}{\varepsilon_1} - 1\right)\left(\frac{B_1}{2} + \frac{B_2}{4} + \frac{B_3}{4}\right) \tag{A3.2.2}$$

Neglecting terms of $O(\alpha^2)$ from equation (A3.2.1) the outer solution reduces to

$$B_1 = \frac{\sigma T^4}{\pi} \tag{A3.2.3}$$

Thus the flux in the outer region is given by

$$q = -\frac{4}{3K}\frac{d}{dx}(\sigma T^4) \tag{A3.2.4}$$

It is interesting to note that this agrees with the Eddington and Rosseland (1936) approximations. Since the intensity distribution is nearly isotropic the agreement is perhaps not surprising.

For the inner or 'boundary layer' region the sketched coordinate system (3.2.13) and the Taylor's series (3.2.14) are replaced in eq. (3.2.10) to yield:

$$\frac{d^2D_0}{dX_n^2} + O(\alpha) = B_1 - \frac{\sigma T^4}{\pi} \tag{A3.2.5}$$

The boundary conditions are:

$$\frac{2}{3}\left(\frac{1+x_Q}{\varepsilon_1}-1\right)\frac{dD_0}{dX_n}+\left(\frac{1}{\varepsilon_1}-1\right)\left(\frac{B_1}{2}+\frac{\sigma T_0^4}{\pi}\right)+\frac{\sigma T_W^4}{\pi}=\frac{C_1}{\varepsilon_1}$$

at $X_n = 0$, and (A3.2.6)

and

$$C_1 = \frac{\sigma T^4}{\pi} \quad \text{as} \quad X_n \rightarrow \infty \qquad \text{(A3.2.7)}$$

After elminating B_1 using eqs. (3.2.5), (3.2.6) and (3.1.10) from equation (A3.2.5), the final form of the equation is:

$$\frac{d^2D_0}{dX_n^2} = \left[D_0 - \frac{(1-X''^2)}{2}\frac{\sigma T^4}{\pi}\right]\frac{2}{1+X''^2} - \frac{\sigma T^4}{\pi} \qquad \text{(A3.2.8)}$$

The complementary function is

$$D_0 = Ae^{\sqrt{\frac{2}{1+X''^2}}\cdot X_n} + Be^{-\sqrt{\frac{2}{1+X''^2}}\cdot X_n} \qquad \text{(A3.2.9)}$$

where A and B are constants of integration.

The particular integral is

$$D_0 = \left[\frac{1}{D^2 - \frac{2}{1+X''^2}}\right]\left[-\frac{2}{1+X''^2}\frac{\sigma T^4}{\pi}\right] \qquad \text{(A3.2.10)}$$

where D is the differential operator. Evaluating (A3.2.10) and neglecting third and higher order derivatives, D_0 reduces to

$$D_0 = \frac{\sigma T^4}{\pi} - \frac{1+X''^2}{2}\frac{d^2}{dX_n^2}\left(\frac{\sigma T^4}{\pi}\right) \qquad \text{(A3.2.11)}$$

the general solution is the sum of (A3.2.9) and (A3.2.11)

The boundary condition (A3.2.7) implies A = 0, and substituting the general solution into the boundary condition (A3.2.6), and solving for B, the final result is

$$B = \left\{\left[\frac{\sigma T_0^4 - \sigma T_W^4}{\pi}\right] - \frac{2}{3}\left(\frac{1+X_Q}{\varepsilon_1} - 1\right)\frac{d}{dX_n}\left(\frac{\sigma T^4}{\pi}\right) - \frac{1}{2}\left(1 + \frac{X''^2}{\varepsilon_1}\right)\frac{d^2}{dX_n^2}\left(\frac{\sigma T^4}{\pi}\right)\right\}$$

$$\left[-\frac{2}{3}\left(\frac{1+X_Q}{\varepsilon_1} - 1\right)\sqrt{\frac{2}{1+X''^2}} + \left(\frac{1}{\varepsilon_1} - 1\right)\frac{1}{1+X''^2} - \frac{1}{\varepsilon_1}\right]^{-1} \qquad \text{(A3.2.12)}$$

The flux out of the wall is

$$q_0 = -\frac{4\pi}{3}\frac{dD_0}{dX_n} = -\frac{4\pi}{3}\left[\frac{\partial}{\partial X_n}\left(\frac{\sigma T_0^4}{\pi}\right) - B\sqrt{\frac{2}{1+X''^2}}\right] \qquad \text{(A3.2.13)}$$

From the outer solution, the flux is given by eq. (A3.2.4) Substituting (A3.2.4) into (A3.2.13) and replacing B by (A3.2.12) the following temperature slip solution is obtained:

$$\sigma T_0^4 - \sigma T_W^4 = \frac{1}{2}\left(\frac{1+X_Q}{\varepsilon_1} - 1\right)q_0 + \frac{1}{2}\left(1 + \frac{X''^2}{\varepsilon_1}\right)\frac{d^2(\sigma T^4)}{dX_n^2} \qquad \text{(A3.2.14)}$$

Appendix A3.3

The One-Dimensional Optically Thin Solution

The relations (3.2.18) are substituted into (3.2.4) to yield an equation of the flow

$$\frac{d^2C_1}{dX^2} = \alpha^2(B_1 - \frac{\sigma T^4}{\pi}) \qquad \text{(A3.3.1)}$$

The boundary conditions are

$$\frac{2}{3}(\frac{1+X_Q}{\varepsilon_1} - 1)\frac{\partial C_1}{\partial X} + (\frac{1}{\varepsilon_1} - 1)(\frac{B_1}{2} + \frac{B_2}{4} + \frac{B_3}{4})\alpha + \frac{\sigma T_1^4\alpha}{\pi} = \frac{C_1\alpha}{\varepsilon_1} \qquad \text{(A3.3.2)}$$

at the wall X = 0 and

$$-\frac{2}{3}(\frac{1+X_Q}{\varepsilon_2} - 1)\frac{\partial C_1}{\partial X} + (\frac{1}{\varepsilon_2} - 1)(\frac{B_1}{2} + \frac{B_2}{4} + \frac{B_3}{4})\alpha + \frac{\sigma T_2^4\alpha}{\pi} = \frac{C_1\alpha}{\varepsilon_2} \qquad \text{(A3.3.3)}$$

at wall X = L.

Substituting the Taylor's Series eq (3.2.14)

$$C_1 = D_0 + \alpha D_1 + \ldots\ldots \qquad \text{(A3.3.4)}$$

in (A3.3.1), (A3.3.2) and (A3.3.3), and equating terms of equal orders of α, an infinite set is obtained. Equating the term of zeroth order

$$\frac{d^2D_0}{dX^2} = 0 \qquad \text{(A3.3.5)}$$

with boundary condition

$$\frac{2}{3K}(\frac{1+X_Q}{\varepsilon_1} - 1)\frac{\partial D_0}{\partial X} = 0 \qquad \text{(A3.3.6)}$$

at X = 0 and X = L. The solution of this is

$$D_0 = A \tag{A3.3.7}$$

where A is any constant. Equating the first order in α,

$$\frac{d^2D_1}{dX^2} = 0 \tag{A3.3.8}$$

and the boundary conditions

$$\frac{2}{3}\left(\frac{1+X_Q}{\varepsilon_1} - 1\right)\frac{dD_1}{dX} + \left(\frac{1}{\varepsilon_1} - 1\right)\left(\frac{D_0}{1+X''^2} + \frac{X''^2}{1+X''^2}\frac{\sigma T_0^4}{\pi}\right) + \frac{\sigma T_1^4}{\pi} = \frac{D_0}{\varepsilon_1} \tag{A3.3.9}$$

at wall X = 0, and at wall X = L

$$-\frac{2}{3}\left(\frac{1+X_Q}{\varepsilon_2} - 1\right)\frac{dD_1}{dX} + \left(\frac{1}{\varepsilon_2} - 1\right)\left(\frac{D_0}{1+X''^2} + \frac{X''^2}{1+X''^2}\frac{\sigma T_0^4}{\pi}\right) + \frac{\sigma T_2^4}{\pi} = \frac{D_0}{\varepsilon_2} \tag{A3.3.10}$$

Again the solution for D_1 is a general linear function of the form

$$CX + E \tag{A3.3.11}$$

where C and E are constants of integration.

Substituting (A3.3.11) into (A3.3.10) and (A3.3.9) and solving for C, one obtains

$$\frac{2}{3}\left[\frac{1+X_Q-X''^2}{\varepsilon_1} + \frac{1+X_Q-X''^2}{\varepsilon_2} - 2X''^2\left[\frac{1+X_Q}{\varepsilon_1\varepsilon_2}\right]\right] C =$$

$$\frac{\sigma T_1^4}{\pi} - \frac{\sigma T_2^4}{\pi} + X''^2\left[\frac{\sigma T_1^4}{\varepsilon_2} - \frac{\sigma T_2^4}{\varepsilon_1} + \frac{\sigma T^4}{\pi}\,\frac{(1-X''^2)}{(1+X''^2)}\left(\frac{1}{\varepsilon_2} - \frac{1}{\varepsilon_1}\right)\right] \tag{A3.3.12}$$

The flux out of the wall 1 from equation (3.1.20) is given by

$$q_1 = -\frac{4\pi}{3}A_1 = -\frac{4\pi}{3}\frac{\partial C_1}{\partial X} = -\frac{4\pi}{3}C \tag{A3.3.13}$$

Appendix (A3.4)

Solution of flux equations in 1 dimension with prescribed constant source

For this case, the geometry of which corresponds to the circumstances of two infinitely long parallel plates, the eqs. (3.2.1) to (3.2.6) with the boundary conditions 3.2.7 and 3.2.8 are solved. We first re-state eqs. (3.2.13), (1.2.7) and (3.1.20):

$$A_1 = -\frac{1}{K}\frac{\partial C_1}{\partial x} \tag{A3.4.1}$$

$$\nabla.\underline{q} = S \tag{A3.4.2}$$

$$\underline{q} = \frac{4\pi}{3} A_1 \tag{A3.4.3}$$

Substituting (A3.4.1) and (A3.4.3) into (A3.4.2) we get:

$$-\frac{1}{K}\frac{\partial^2 C_1}{\partial^2 x} = \frac{3S}{4\pi} \tag{A3.4.4}$$

Hence the solution of (A3.4.4) is:

$$C_1 = -\frac{3SX^2}{8\pi} + AX + B \tag{A3.4.5}$$

where A and B are constants of integration. Substituting (A3.4.5) into the boundary condition (3.2.7) and (3.2.8) the values for constants A and B are obtained. The equation for flux out of wall 1 reduces to

$$q_{W1} = \frac{4\pi}{3}A. \tag{A3.4.6}$$

Hence the flux out of wall 1 is

$$q_{w_1} = \frac{(\sigma T_1^4 - \sigma T_2^4)(\frac{1}{X_Q} + \frac{3}{4}KL) - \frac{S}{k}\left[\frac{KL}{2} + KL(\frac{1}{\varepsilon_2} - 1)(\frac{1+X_Q}{2})(\frac{1}{X_Q + \frac{3KL}{4}})\right]}{1 + (\frac{1}{\varepsilon_1} + \frac{1}{\varepsilon_2} - 2)(\frac{1+X_Q}{2})(\frac{1}{X_Q + \frac{3KL}{4}})} \qquad (A3.4.7)$$

Here the value of Q can be approximated by

$$Q^* = \frac{1}{X_Q + \frac{3KL}{4}} \quad \text{or} \quad (\frac{1+X_Q}{2})(\frac{1}{X_Q + \frac{3KL}{4}}) \qquad (A3.4.8)$$

depending on whether the wall temperatures differences or the sources are predominant. The difference between the two expressions is small. The solution for temperature is also obtained by substituting the expression for C_1 into 3.2.4, the resulting expression is similar to (eq. 2.2.2) with the following starred approximations for unstarred variables in the equation.

$$Q_s^* = \frac{KL}{2} \qquad (A3.4.9)$$

$$\theta^* = + \frac{3}{4}\frac{(KL-KX)}{(X_Q + \frac{3KL}{4})} + (1 - \frac{X_Q}{2})(\frac{1}{X_Q + \frac{3}{4}KL}) \qquad (A3.4.10)$$

$$\theta_s^* = - \frac{3}{8}K^2X(X-L) + \frac{KL}{4} + \frac{3}{8} + \frac{KL}{4}(X_Q-1) + \frac{3}{8}X''^2 \qquad (A3.4.11)$$

Appendix A4.1

Solution of the Present Flux Model for an Infinitely Long Cylinder with Black Walls and a Constant Heat Source Inside

This is an axi-symmetric problem, therefore the $\frac{\partial}{\partial\theta}$ and $\frac{\partial}{\partial z}$ terms are zero. The system is characterized by eqs (4.1.25) to (4.1.27) and reduces to:

$$\frac{1}{K}\frac{d^2}{dr^2}C_1 = KB_1 - \frac{K\sigma T^4}{\pi} \tag{A4.1.1}$$

$$B_2 = \frac{\sigma T^4}{\pi} \tag{A4.1.2}$$

$$B_3 = \frac{\sigma T^4}{\pi} \tag{A4.1.3}$$

There is no net flux across the symmetry axis hence from eq. (4.1.19) and eq. (4.1.36), the first boundary condition becomes

$$\frac{\partial C_1}{\partial r} = 0 \quad \text{at} \quad r = 0 \tag{A4.1.4}$$

while the second boundary condition from the eq. (4.1.29) for black wall at temperature T_W reduces to

$$-\frac{2r_0}{3K}\frac{dC_1}{dr} + \frac{\sigma T_W^4}{\pi} = C_1 \tag{A4.1.5}$$

Since the sources are required, the relationship (4.1.38) between the sources and temperatures is employed:

$$-\frac{1}{3rK}\frac{dC_1}{dr} + \frac{K\sigma T^4}{\pi} - \frac{K}{3}(B_1 + B_2 + B_3) = \frac{S}{4\pi} \tag{A4.1.6}$$

Using eqs. (A4.1.1) to (A4.1.3) and (A4.1.6) and eliminating B_2, B_3 and T, the final equation reduces to:

$$\frac{1}{K}\frac{d^2C_1}{dr^2} + \frac{1}{Kr}\frac{dC_1}{dr} = -\frac{3S}{4\pi K} \tag{A4.1.7}$$

Multiplying both sides by r, the left-hand side becomes an exact derivative. Integrating both sides with respect to r gives:

$$\frac{rdC_1}{dr} = -\frac{3}{8}\frac{SKr^2}{\pi} + A \tag{A4.1.8}$$

where A is a constant of integration.

The above relation holds for any r, in particular at the centre (r=0). This implies A = 0 so

$$\frac{dC_1}{dr} = -\frac{3}{8}\frac{SKr}{\pi} \tag{A4.1.9}$$

Integrating this relation further with respect to r,

$$C_1 = -\frac{3}{16}\frac{SKr^2}{\pi} + B \tag{A4.1.10}$$

where B is a constant of integration. Applying the outer boundary condition (A4.1.5) to evaluate B, one gets

$$B = (r_Q + \tfrac{3}{4}Kr_2)\frac{Sr_2}{4\pi} + \frac{\sigma T_W^4}{\pi} \tag{A4.1.11}$$

The flux out of the wall is

$$q_Q = \frac{4\pi}{3}A_1 = -\frac{4\pi}{3}\frac{\partial C_1}{\partial r} = \frac{Sr_2}{2} \tag{A4.1.12}$$

For a simple energy check, the sum of the wall fluxes equals the total sum of the internal sources, that is,

$$q.\text{Area} = \frac{Sr_2}{2}.2\pi r_2 = S\pi r_2^2 = \text{Source.Volume} \tag{A4.1.13}$$

Using equation (A4.1.6), the temperature can be evaluated by substituting for $\frac{dC_1}{dr}$. B_1 is evaluated in terms of C_1 using the relation (4.1.16):

$$\frac{\sigma T^4}{\pi} = C_1 + \frac{3S}{16\pi K}(1 + r''^2) \qquad \text{(A4.1.14)}$$

Evaluating eq. (A4.1.14) for the centre and denoting the temperature by T_C, the system reduces to,

$$\sigma T_C^4 - \sigma T_W^4 = \frac{S}{4}\left[\frac{3}{4K}(1 + r''^2) + r_Q r_2 + \frac{3}{4} K r_2^2\right] \qquad \text{(A4.1.15)}$$

Taking the ratio of eq. (A4.1.12) for the flux out of the wall and eq. (A4.1.15), and defining $2Kr_2 = \tau_0$ as the optical diameter, yields;

$$-\frac{q_W}{\sigma T_W^4 - \sigma T_C^4} = \frac{1}{\frac{3}{4\tau_0}(1+r''^2) + \frac{r_Q}{2} + \frac{3}{16}\tau_0} \qquad \text{(A4.1.16)}$$

Appendix A4.2

Solution by the Present Model for Infinitely Long Pair of Coaxial Cylinders with Constant Internal Source

This is an axi-symmetric problem, and the equations governing the radiation are (A4.1.1) to (A4.1.3) of Appendix A4.1. We also use eq. (A4.1.7) of that Appendix:

$$\frac{1}{K}\frac{d^2C_1}{dr^2} + \frac{1}{Kr}\frac{\partial C_1}{\partial r} = -\frac{3S}{4\pi K} \qquad \text{(A4.2.1)}$$

$$B_2 = \frac{\sigma T^4}{\pi} \qquad \text{(A4.2.2)}$$

$$B_3 = \frac{\sigma T^4}{\pi} \qquad \text{(A4.2.3)}$$

The boundary conditions are the same as (4.1.28) and (4.1.29), they too are restated here for convenience.

$$\frac{2}{3K}\left(\frac{1+r_Q}{\varepsilon_1} - 1\right)\frac{\partial C_1}{\partial r} + \left(\frac{1}{\varepsilon_1} - 1\right)\left(\frac{B_1}{2} + \frac{B_2}{4} + \frac{B_3}{4}\right) + \frac{\sigma T_1^4}{\pi} = \frac{C_1}{\varepsilon_1} \qquad \text{(A4.2.4)}$$

and

$$-\frac{2}{3K}\left(\frac{1+r_Q}{\varepsilon_2} - 1\right)\frac{\partial C_1}{\partial r} + \left(\frac{1}{\varepsilon_2} - 1\right)\left(\frac{B_1}{2} + \frac{B_2}{4} + \frac{B_3}{4}\right) + \frac{\sigma T_2^4}{\pi} = \frac{C_1}{\varepsilon_2} \qquad \text{(A4.2.5)}$$

Firstly B_1, B_2 and B_3 are eliminated from condition (A4.2.4) to give the following boundary condition:

$$\left[\frac{2}{3K}\left(\frac{1+r_Q}{\varepsilon_1} - 1\right) + \left(\frac{1}{\varepsilon_1} - 1\right)\frac{r''^2}{2K^2 r}\right]\frac{dC_1}{dr} + \left(\frac{1}{\varepsilon_1} - 1\right)\frac{3r''^2}{8\pi K} S + \frac{\sigma T_1^4}{\pi} = C_1 \qquad \text{(A4.2.6)}$$

The second boundary condition is similarly handled. Then eq (A4.2.1) is multiplied by r and both sides are integrated with respect to r to yield:

$$\frac{dC_1}{dr} = -\frac{3}{8}\frac{SKr}{\pi} + \frac{A}{r} \tag{A.4.2.7}$$

where A is a constant of integration. One further integration yields

$$C_1 = -\frac{3SKr^2}{16\pi} + A\ell nr + B \tag{A4.2.8}$$

B is also a constant of integration. Substituting eqs. (A4.2.7) and (A4.2.8) into the boundary conditions and subtracting the two gives the following expression:

$$A = \frac{\left\{ \begin{array}{l} \dfrac{\sigma T_2^4}{\pi} - \dfrac{\sigma T_1^4}{\pi} + \left(\dfrac{1}{\varepsilon_2} - \dfrac{1}{\varepsilon_1}\right)\dfrac{3r''^2}{8\pi K} S + \dfrac{3SK}{16\pi}(r_2^2 - r_1^2) + \dfrac{3S}{8\pi} \\ \left[\dfrac{2}{3}r_2\left(\dfrac{1+r_Q}{\varepsilon_2} - 1\right) + \dfrac{2}{3r_1}\left(\dfrac{1+r_Q}{\varepsilon_1} - 1\right) + \dfrac{r''^2}{2K}\left(\dfrac{1}{\varepsilon_1} + \dfrac{1}{\varepsilon_2} - 2\right)\right] \end{array} \right\}}{\ell n\dfrac{r_2}{r_1} + \dfrac{1}{r_2}\left[\dfrac{2}{3K}\left(\dfrac{1+r_Q}{\varepsilon_2} - 1\right) + \left(\dfrac{1}{\varepsilon_2} - 1\right)\dfrac{r''^2}{2K^2 r_2}\right] + \dfrac{1}{r_1}\left[\dfrac{2}{3K}\left(\dfrac{1+r_Q}{\varepsilon_1} - 1\right) + \left(\dfrac{1}{\varepsilon_1} - 1\right)\dfrac{r''^2}{2K^2 r_1}\right]} \tag{A4.2.9}$$

The expression for the flux out of wall 1 is given by

$$q_{W_1} = -\frac{4\pi}{3K}\frac{\partial C_1}{\partial r} = \frac{4\pi}{3K}\left[-\frac{3}{8\pi}SKr_1 + \frac{A}{r_1}\right] \tag{A4.2.10}$$

or

$$q_{W_1} = -\frac{Sr_1}{2} + \frac{4\pi A}{3Kr_1} \tag{A4.2.11}$$

Further, the constant B can be evaluated by substituting the value of A into one of the boundary conditions. The second boundary condition is used here for convenience. Substituting equations

(A4.2.8) and (A4.2.7) for C_1 and its derivative, yields

$$B = \left[-\frac{2}{3K}\left(\frac{1+r_Q}{\varepsilon_2} - 1\right) + \left(\frac{1}{\varepsilon_2} - 1\right)\frac{r''^2}{2K^2 r} \right]\left[-\frac{3}{8}\frac{SKr}{\pi} + \frac{A}{r} \right]$$

$$+ \left(\frac{1}{\varepsilon_2} - 1\right)\frac{3r''^2 S}{8K} + \frac{\sigma T_2^4}{\pi} + \frac{3SKr_2^2}{16\pi} + A \ln r_2 \qquad \text{(A4.2.12)}$$

Appendix A5.1

Derivation of new boundary conditions for black walls with interior temperatures prescribed

We need a new boundary condition at an imaginary boundary distance δ from the real black wall bounding gas at constant temperature T_g and absorption coefficient K. (fig. A5.1)

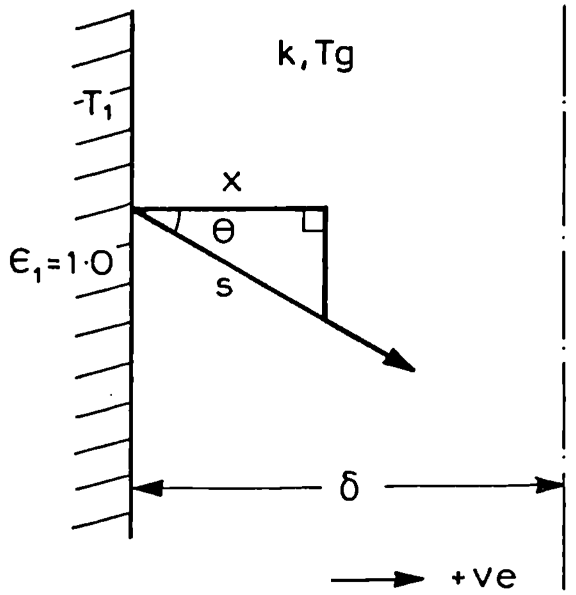

Fig. A5.1 Boundary layer thickness δ near a black wall with normal in positive x direction

The transport equation (1.2.1) can be integrated in this region to

$$I = \frac{\sigma T_g^4}{\pi} + Ae^{-KS} \qquad \text{(A5.1.1)}$$

where A is constant of integration. Wall 1 is a black wall hence the value of intensity in every direction is given by $\frac{\sigma T_1^4}{\pi}$. Letting I_+ indicate intensity in the positive direction (from the wall) we get from equation (A5.1.1)

$$I_+ = \frac{\sigma T_g^4}{\pi}\left(1-e^{-\frac{KX}{\cos\theta}}\right) + \frac{\sigma T_1^4}{\pi}\, e^{-\frac{KX}{\cos\theta}} \qquad \text{(A5.1.2)}$$

The amount arriving in the positive direction in the solid angle of our integration surface is equal to the flux in the same solid angle predicted by the assumed series, that is

$$\frac{2}{3} X_Q A_1 + C_1 = \frac{\sigma T_1^4}{\pi} + \left(\frac{\sigma T_g^4 - \sigma T_1^4}{\pi}\right)\frac{2K\delta}{1+X''} + O(K\delta)^2 \qquad \text{(A5.1.3)}$$

The right-hand side is obtained by expanding the exponentials in equation (A5.1.2) and integrating term by term. The higher order terms are neglected. When there is no boundary layer ($\delta = 0$), equation (A5.1.3) reduces to equation (3.1.24). Similarly for the boundary condition at distance δ from the opposite wall 2 is given by

$$-\frac{2}{3}X_Q A_1 + C_1 = \frac{\sigma T_2^4}{\pi} + \left(\frac{\sigma T_g^4}{\pi} - \frac{\sigma T_2^4}{\pi}\right)\frac{2K\delta}{1+X''} \qquad \text{(A5.1.4)}$$

The negatively-directed intensity distribution at distance δ from wall 1 is given by the assumed series (3.1.1). For any particular direction denote the intensity by I_δ. Then the negative intensity denoted by I_- at any point x from the wall is, from equation (A5.1.1), given by

$$I_- = \frac{\sigma T_g^4}{\pi} + \left(I_\delta - \frac{\sigma T_g^4}{\pi}\right)e^{-\frac{K(\delta-x)}{\cos}} \qquad \text{(A5.1.5)}$$

Substituting the series (3.1.1) for I_δ and substituting equation (A5.1.5) into equation (1.2.4), the negative flux at any point distance x from the wall in the boundary layer is given by

$$-q_- = \left[-\frac{2\pi}{3}A_1 + \frac{\pi}{2}B_1 + \frac{\pi}{4}B_2 + \frac{\pi}{4}B_3\right] + (\delta-x)K\left[\pi A_1 - \frac{2\pi}{3}(B_1+B_2+B_3)\right]$$

$$+ \frac{\sigma T_g^4}{\pi}(\delta-x).\ 2\pi K. \qquad \text{(A5.1.6)}$$

hence using equation (1.2.5) the flux at Wall 1 is given by

$$q_{W1} = \left[-\frac{2\pi}{3}A_1 + \frac{\pi}{2}B_1 + \frac{\pi}{4}B_2 + \frac{\pi}{4}B_3\right] + K\delta\left[\pi A_1 - \frac{2\pi}{3}(B_1 + B_2 + B_3)\right]$$

$$+ 2K\delta\sigma T_g^4 - \sigma T_1^4. \qquad (A5.1.7)$$

Here again terms of order $(K\delta)^2$ have been neglected. Similar expression for wall 2 can be easily derived.

Appendix (A5.2)

One dimensional solution for constant temperature gas using boundary layers

Consider infinity long parallel black plates bounding gas at uniform temperature T_g, The plates are distance L apart and the gas has an absorption coefficient K. The parameter X" is assumed to be uniform for each optical thickness, hence from eq. 3.1.13 to eq. 3.1.18, the governing equations are

$$\frac{d^2C_1}{Kdx^2} = KB_1 - \frac{K\sigma T_g^4}{\pi} \tag{A5.2.1}$$

$$B_2 = \frac{\sigma T_g^4}{\pi} \tag{A5.2.2}$$

$$B_3 = \frac{\sigma T_g^4}{\pi} \tag{A5.2.3}$$

These can be solved to yield

$$C_1 = \frac{\sigma T_g^4}{\pi} + Ae^{\sqrt{\frac{2}{1+X''^2}}\, KX} + Be^{-\sqrt{\frac{2}{1+X''^2}}\, KX} \tag{A5.2.4}$$

using the definition of C_1 (eq. 3.1.10), and A and B are constants of integration.

Substituting the value of C_1 from eq. (A5.2.4) and its derivative in the boundary conditions (A5.1.3) and (A5.1.4) yields the following two simultaneously in A and B:

$$-\frac{2}{3} X_Q X_B (Ae^{X_B K\delta} - Be^{-X_B K\delta}) + \frac{\sigma T_g^4}{\pi} + Ae^{X_B K\delta} + BE^{-X_B K\delta}$$

$$= \frac{2K\delta}{1+X''} \frac{\sigma T_g^4}{\pi} + \frac{\sigma T_1^4}{\pi}(1 - \frac{2K\delta}{1+X''}) \tag{A5.2.5}$$

at $KX = K\delta$, and at $KX = K(L-\delta)$

$$\frac{2}{3}X_Q X_B(Ae^{X_B K(L-\delta)} - Be^{-X_B K(L-\delta)}) + \frac{\sigma T_g^4}{\pi} + Ae^{X_B K(\ell-\delta)}$$

$$+ Be^{-X_B K(\ell-\delta)} = \frac{2K\delta}{1+X''} \frac{\sigma T_g^4}{\pi} + \frac{\sigma T_2^4}{\pi}(1 - \frac{2K\delta}{1+X''}) \qquad \text{(A5.2.6)}$$

where

$$X_B = \sqrt{\frac{2}{1+X''^2}} \qquad \text{(A5.2.7)}$$

Further, let us define

$$BF1 = e^{X_B K\delta}\left[\frac{2}{3}X_Q X_B(e^{X_B K(L-2\delta)} + 1) + e^{X_B K(L-2\delta)} - 1\right] \qquad \text{(A5.2.8)}$$

and

$$BF2 = e^{-X_B K\delta}\left[\frac{2}{3}X_Q X_B(1-e^{-X_B K(L-2\delta)}) + 1 + e^{-X_B K(L-2\delta)}\right] \qquad \text{(A.5.2.9)}$$

Solving eq. (A5.2.5) and eq. (A5.2.6) for A and B, the following relations are obtained:

$$B = \frac{1}{BF2}(1 - \frac{2K\delta}{(1+X'')})(\frac{\sigma T_2^4 - \sigma T_g^4}{\pi}) - (\frac{\sigma T_2^4 - \sigma T_1^4}{\pi})(\frac{2}{3}X_Q X_B + 1)\frac{e^{X_B K(L-\delta)}}{BF1} \qquad \text{(A5.2.10)}$$

$$A = Be^{-X_B KL} + (\frac{\sigma T_2^4 - \sigma T_1^4}{\pi})(\frac{1 - \frac{2K\delta}{1+X''}}{BF1}) \qquad \text{(A5.2.11)}$$

Hence the value of C_1 and its derivative can be evaluated using eq. (A5.2.4). From this, values of A_1, B_1, B_2 and B_3 can be calculated in order to evaluate the flux out of wall 1 using eq. (A5.1.7).

Appendix (A5.3)

Derivation of New Boundary Conditions for Black Walls with Internal Sources Prescribed

To derive a new boundary condition at an imaginary boundary distance δ from a wall with prescribed sources, we need to expand the temperature field in a Taylor's series of the form:

$$\sigma T^4 = \sigma T_W^4 + a_1 KX + O(KX)^2 \qquad (A5.3.1)$$

where a_1 is a constant to be evaluated. In this region, the energy conservation law $\nabla q = S$(eq. 1.2.7) holds. In the present model, in cartesian coordinates it can be restated as follows (see eq. 3.1.23)

$$\frac{S}{4\pi} = -\frac{K}{3}(B_1+B_2+B_3) + \frac{K\sigma T^4}{\pi} \qquad (A5.3.2)$$

Replacing the temperature term by the series (A5.3.1) and rearranging the terms, we get

$$a_1 \frac{KX}{\pi} = \frac{S}{4\pi K} + \frac{1}{3}(B_1+B_2+B_3) - \frac{\sigma T_1^4}{\pi} \qquad (A5.3.3)$$

Now substituting the series (A5.3.1) into the transport equation, eq. (1.2.1), we get,

$$\frac{dI}{ds} = -KI + \frac{K}{\pi}(\sigma T_1^4 + a_1 KX + O(KX^2)) \qquad (A5.3.4)$$

Integrating with respect to s, we get

$$I = \frac{\sigma T_1^4}{\pi} + a_1 . \cos\theta . (Ks-1) + Ae^{-Ks} \qquad (A5.3.5)$$

where A is the constant of integration. At $s = 0$, $I_+ = \frac{\sigma T_1^4}{\pi}$, which gives

$$A = a_1 \cos \theta \qquad \text{(A5.3.6)}$$

Integrating over the integration surface described in section 3.1.2, and replacing a_1 by eq. (A5.3.3), we get

$$q_+ = \frac{\sigma T_1^4}{\pi}(1-X''^2) + K\delta\pi(1-X'')\left(\frac{S}{4\pi K} + \frac{1}{3}(B_1+B_2+B_3) - \frac{\sigma T_1^4}{\pi}\right) \qquad \text{(A5.3.7)}$$

The above expression should match the expression for q_+ derived by integrating the series (3.1.1). Thus the final boundary condition for a black wall with sources prescribed can be written as follows:

$$-\frac{2}{3}\frac{X_Q}{K}\frac{dC_1}{dX} + C_1 = \sigma T_1^4\left(1 - \frac{K\delta}{1+X''}\right) + \frac{K\delta}{1+X''}\left(\frac{S}{4\pi K} + \frac{1}{3}(B_1+B_2+B_3)\right)$$

(A5.3.8)

Similar expressions for non-black walls can be derived.

REFERENCES

Abou Ellail, M.M.M., Gosman, A.D., Lockwood, F.C. and Megahed, I.E.A. "Description and validation of a three-dimensional procedure for combustion chamber flows" Journal of Energy, AIAA, Vol. 2, pp. 71-80 (April, 1978).

Abramowity, M. and Stegun, I.A. "Handbook of mathematical functions" Dover Publications (1965).

Arscott, J.A., Gibb, J. and Jenner, R. "The application of N-E diffusion theory and Monte-Carlo methods to predict the heat transfer performance of a 500 MW power station boiler from isothermal flow data" Heat transfer in furnaces. Proceedings of the Combustion Institute European Symposium 1973, Paper 112, pp. 674-678 (Academic Press 1973).

Baron, J.R., Elgin, J.B. "A variable closure differential approximation for anisotropic radiation" J. Quant. Spec. Rad. Transfer. Vol. 16, pp. 805-818, (1976).

Bartelds, H. "Validity of radiation models" International Flame Research Foundation", Ijmuiden, Holland, Doc. Nr. K. 20/A/91 (Feb. 1976).

Bartelds, H., Heap, M.P., Lowes, T.M., Michelfelder, S. and Pai, B.R. "Prediction of radiant heat flux distribution" Int. seminar, Heat transfer from flames, Trogier, Yugoslavia (1973).

Bauersfeld, G. and Richter, W. "Radiation models for use in complete mathematical furnace models" 25 years International Flame Research Foundation, 3rd Members Conference (1974) Ijmuiden, Holland.

Beach, H.L., Ozisik, M.N. and Siewert, C.E. "Radiative transfer in linearly anisotropic scattering, conservative and non-conservative slabs with reflective boundaries" Int. J. Heat Mass Transfer, Vol. 14, pp. 1551-1565 (1971).

Becker, H.B. "A mathematical solution for gas to surface radiative exchange area for a rectangular parallelepiped enclosure containing a gray medium" J. of Heat Transfer, Vol. 99, pp.203-207 (May 1977).

Beer, J.M., Selcuk, N. and Sidall, R.G., "Two flux modelling of two dimensional radiative transfer in a large-scale experimental furnace". J. Inst. Fuel, Vol. 49, pp.122-126, (1976).

Breig, W.F. and Crosbie, A.L. "Two dimensional radiative equilibrium boundary emissive powers for a finite medium subjected to cosine varying radiation" J. Quant. Spec. Rad. Transfer, Vol. 14, pp. 1209-1237 (1974).

Cess, R.D. "On the differential approximation in radiative transfer" ZAMP Brief reports, Vol. 17, pp. 776-781, (1966).

Cess, R.D. and Sparrow, E.M. "Radiation heat transfer" Brooks/Cole Publishing Company (1966).

Chandrasekhar, S. and Elbert, D. "The X- and Y-functions for isotropic scattering I and II" Astrophysics, J. Vol. 115, pp. 224-278, (1952).

Chandrasekhar, S. "Radiative transfer" Dover Publication, New York, (1960).

Chou, Y.S. and Tien, C.L. "A modified moment method for radiative transfer in non-planar systems" J. Quant. Spec. Rad. Transfer, Vol. 8, pp. 919-933 (1968).

Chu, C.M. and Churchill, S.W. "Numerical solution of problems in multiple scattering of electro magnetic radiation" J. of Physical Chemistry, Vol. 59, pp. 855-863 (1955).

Dayan, A. and Tien, C.L. "Heat transfer in a grey planar medium with linear anisotropicscattering". J. Heat Transfer, Vol. 97, pp. 391-396, (1975).

Deissler, R.G. "Diffusion approximation for thermal radiation in gases with jump boundary condition" Trans. of ASME pp. 240-246 (May 1964).

DeMarco, A.G. "A new flux method for the calculation of radiation heat transfer in three-dimensional combustion chambers" M.Sc. Thesis, Dept. Mech. Eng., Imperial College, London (Sept. 1974).

DeMarco, A.G. and Lockwood, F.C. "A new flux model for the calculation of radiation in furnaces" La Rivista dei combustibili, Vol. 29, pp.184-196 (1975).

Drake, R.M. and Eckert, E.R. "Heat and mass transfer" McGraw-Hill Book Co. New York (1959).

Eddington, A.S. "The internal constitution of stars " Cambridge University Press, London (1926) also Dover Publication, New York (1960).

Gibb, J. "Analytic solution to a two-dimensional cartesian geometry" Private communication (March 1977).

Gibb, J. and Jenner, R. Preliminary note on the Radiant Heat Transfer Program FURDEC CEGB Report MS/C/M646 (1974).

Gibb, J. Private communication and results using the above computer programme (1974).

Gosman, A.D. and Lockwood, F.C. "Incorporation of a flux model for radiation into a finite difference procedure for furnace calculation" Fourteenth Symposium (Int). on combustion, pp. 661-671 (1973).

Goulard, M. and Goulard, R. "One-dimensional energy transfer in radiant media" Int. J. Heat and Mass Transfer, vol. 1, pp. 81-91 (1960).

Grosh, R.J. and Love, T.J. "Radiative heat transfer in absorbing, emitting and scattering media" J. Heat Transfer, vol. 87, pp. 161-166, (1965).

Grosh, R.J. and Viskanta, R. "Heat transfer in thermal radiation in absorbing and scattering medium" Int. developments in Heat Transfer Part IV, ASME, pp. 820-828 (1961).

Heaslet, M.A. and Warming, R.F. "Radiative transport and wall temperature slip in an absorbing planar medium" Int. J. Heat Mass Transfer, Vol. 8, pp. 979-994 (1964).

Hottel, H.C. and Sarofim, A.F. "Radiative Transfer" McGraw-Hill, New York (1967).

Howell, J.R. and Perlmutter, M. "Monte Carlo solution of thermal transfer through radiant media between gray wall" Trans. of ASME pp. 116-122. (Feb. 1964A).

Howell, J.R. and Perlmutter, M. "Radiant transfer through a gray gas between concentric cylinders using Monte-Carlo" Trans. of ASME, pp. 169-179 (May 1964B).

Hyde, D.J. and Truelove, J.S. "The discrete ordinates approximation for multi-dimensional radiant heat transfer in furnaces. AERE R8502 (1977).

Kourganoff, V. "Basic methods in transfer problems", Dover publications, New York (1963).

Krook Max "On the solution of equation of transfer, I" Astrophysics Journal, Vol. 122, pp. 488-497, (1955).

Lockwood, F.C. and Shah, N.G. "A new differential formulation of radiative transfer and its application to the one-dimensional problem". ASME: 76-HT-49, (1976).

Lockwood, F.C. and Shah, N.G. "Evaluation of an efficient radiation flux model for furnace prediction procedure" 6th International heat transfer conference, (1978).

Lockwood, F.C. and Spalding, D.B. "Prediction of a turbulent reacting duct flow with significant radiation". Thermodynamic session, Proc. Colloques d'Evian de la Societe Francaise, (1971).

Ludwig, C.B., Malkmus, W., Reardon, J.E. and Thomson, J.A.L. "Handbook of infrared radiation from combustion gases" NASA, SP3080, (1973).

McCann, R.A. and Whitacre, G.R. "Comparison of methods for the prediction of radiant heat flux distribution and temperature ASME, 75-HT-9, (1975).

Olfe, D.B. "A modification of the differential approximation for radiative transfer" AIAA Journal Vol. 5, pp. 638-643 (1967).

Oppenheim, A.K. "Radiation analysis by network method" Trans. ASME, 78, pp. 725-735, (1956).

Ozisik, M.N. "Radiative transfer and interactions with conduction and convection" A Wiley-Interscience publication (1973).

Richter, W. "Prediction of heat and mass transfer in a pulverised fuel furnace" Letters in heat and mass transfer, Vol. 1, pp. 83-94 (1974).

Rosseland, S. "Theoretical Astrophysics" Oxford University Press, London (1936).

Schuster, A. "Radiation through a foggy atmosphere" Astrophysics Journal, Vol. 21, pp. 1-22 (1905).

Schwarzchild, K. "Veber das Gleichgewicht der Sonneatmosphare" Akad, Wiss Gottigen Math-Phys. KL Nachr., Vol. 1, pp. 41-53, (1906).

Selcuk, N. and Siddall, R.G. "Two-flux spherical harmonic modelling of two-dimensional radiative transfer in a large-scale experimental furnace" Int. Journal of Heat and Mass Transfer (1976A).

Shorin, S.N. "Heat exchange by radiation in the presence of an absorbing medium" Izvestiya Akademi Nauk SSSR, No. 3, pp. 389-406, (1951) (also abridged translation in Engineers Digest, Vol. 12, pp. 324-328 (1951)).

Siddall, R.G. "Flux methods for the analysis of radiant heat transfer" J. Inst. Fuel, Vol. 47, no. 391, pp. 101-109, (June 1974).

Spalding, D.B. "Notes on the two-four and six-flux models of radiation". Private communication (see Gosman and Lockwood 1973) (1972).

Truelove, J.S. "One-dimensional radiative transfer in plane, cylindrical and spherical geometries using the discrete ordinate approximation" AERE R8479 (1976), R 8364.

Truelove, J.S. "An evaluation of the discrete ordinates approximation of radiative transfer in an absorbing, emitting and scattering planar medium-AERE R8478 (1976).

Viskanta, R. "Radiation transfer and interaction of convection with radiation heat transfer", Advances in Heat Transfer Vol. III (Academic Press, New York) (1966).